

DUST AND AEROSOLS IN THE ATACAMA DESERT

Franco Arenas-Díaz^{ab}, Bárbara Fuentes^b, Mark Reyers^c, Stephanie Fiedler^{cd},
Christoph Böhm^c, Eduardo Campos^a, Yaping Shao^c, Roland Bol^{ef*}

a. Universidad Católica del Norte. Departamento de Ciencias Geológicas. Antofagasta, Chile.

b. Universidad Católica del Norte. Departamento de Ingeniería Química. Antofagasta, Chile.

c. University of Cologne, Institute for Geophysics and Meteorology, Cologne, Germany &

d. Hans-Ertel-Centre for Weather Research, Climate Monitoring and Diagnostics,
Cologne/Bonn, Germany.

e. Institute of Bio- and Geosciences, Agrosphere (IBG-3), Forschungszentrum Jülich GmbH,
52425, Jülich, Germany.

f. School of Natural Sciences, Environment Centre Wales, Bangor University, Bangor, United
Kingdom

Abstract

The Atacama Desert is one of the driest and oldest deserts on Earth. The extreme scarcity of rainfall and hence very limited runoff, paired with endorheism, allow sediments and deposited materials to largely remain in the pedosphere and for long periods of time, thereby leading to the generation of thick sediment, salt, and soil deposits. Aerosols are the main inputs of exogenous material to this system. The dominant aerosols deposited in the region are from sea spray, soil and salar playa deflation, volcanic emissions, along with secondary aerosols. The whole Atacama region receives particulate matter (minerals, salts, organic compounds, and microorganisms of variable content) from the Pacific Ocean, the coastal desert, and the Andes Cordillera and Altiplano. Some water may reach the western margin of the Atacama hyper arid core due to fog advection via the Coastal Cordillera.

25 However, despite its aridity, large dust outbreaks from the Atacama Desert are rare.
26 Atmospheric deposition is of great relevance for the landscape evolution of the
27 Atacama Desert. This review summarizes current knowledge on the evolution of the
28 landscape and the climatic conditions that led to it, and the salt and soil deposits,
29 along with other geophysical features, in order to identify the frontier of aerosol
30 research in the Atacama Desert.

31 * Corresponding author: r.bol@fz-juelich.de

32 KEYWORDS: dust; aerosol; deposition; Atacama Desert; hyperarid; fog; soil
33 initiation; salt deposits; nitrates; sulfates; Mars.

34

36 The dust cycle is an integral part of the Earth system (Carslaw et al., 2010; Shao et
37 al., 2011) and the arid zones are of special interest since they are indicated as the
38 main dust sources (Kohfeld et al., 2007). Dust in the atmosphere affects the climate
39 through several ways, e.g. scattering, absorbing and reflecting radiation or serving
40 as nuclei for cloud formation and altering their optical properties and lifetime, and
41 influencing precipitation processes (Andreae and Crutzen, 1997; Mahowald et al.,
42 2014). Dust also has a significant impact on the biosphere, e.g. fertilizing the
43 Amazon rainforest (Yu et al., 2015) and enhancing the marine productivity (Schulz
44 et al., 2012) due to the fact that aerosols carry carbon, iron, phosphorus, among
45 other relevant nutrients (Shao et al., 2011). This supply is of great significance
46 because of the role of dust in the elemental cycling and its influence on the
47 community structures of vegetation (Jiao et al 2018; Jickells et al. 2005; Mahowald
48 et al. 2014).

49 The Atacama Desert, one of the oldest and most arid deserts on Earth, offers a
50 unique view of the importance of atmospheric inputs of elements to soils since the
51 deposited material tends to remain in the pedosphere and not to be leached
52 (Amundson, 2003). This is because large areas of the Atacama Desert experience
53 decades without rainfall, so the arid landscape and its hyper arid core are not
54 subjected to water erosion regularly, except for the few rivers, some of which
55 intermittent, that are fed by highland precipitation. These rivers, especially
56 ephemeral ones produced by rare rainfall events, are important for dust-related
57 processes since their erosive action produce and mobilize fine sediments which can
58 be entrained by wind once they are desiccated. Permanent rivers such as the Loa

River (21.4 °S), for instance, crosses the hyperarid core of the Atacama, and have produced extremely deep canyons in the landscape. To the north, also within the hyper arid core of the Atacama, rivers such as the Lluta (18.4 °S), Vitor (18.7 °S), and the Camarones (19.2 °S) are present. To the south of the Loa, located at 26.4°S, the intermittent Salado River can be found, whereas in the southern margin of the Atacama Desert, the Copiapo River (27.4 °S) is present within the transition zone to a semi-arid conditions according to Ewing et al (2006). Some of these rivers maintain valleys in their path, usually homonymous with the name of the river, and their discharge to the Pacific Ocean produce wetlands. Recently, we have observed the impact of extreme rainfall over the Atacama landscape by flooding, e.g., the 2015 and 2017 events (see Section 1.4).

The variation of water tables of aquifers within the hyperarid core is also relevant since once the water level decreases, sediments may be exposed and suspended by the wind. Conversely, water tables very close to the surface can keep the soil moist, which allows the trapping of atmospheric deposits and prevents their re-suspension. As dust accumulates it reduces the rate of evaporation and increases surface soil moisture, leading to further dust accumulation (Pye, 1987). Moreover, the aquifers recharge produced by rainfall, that are rare and eventually extreme, washes the atmosphere scavenging ions and transferring salts from the atmosphere to soils and also to surface water bodies and aquifers together with salts accumulated in snow and ice glaciers mobilized by melting and the consequent water runoff (Barraza et al., 2021; Gamboa et al., 2019; Houston, 2002; Sepúlveda et al., 2014; Urrutia et al., 2019).

82 Although there are areas of active water erosion in the Atacama Desert, in general
83 the landscape present very low erosion rates (Jungers et al., 2013; Placzek et al.,
84 2010), and a smooth topography (Clarke, 2006; Riquelme et al., 2007) due to the
85 continuing accumulation of the atmospheric deposits (Clarke, 2006), enabled by the
86 hyper-aridity conditions prevalent there for millions of years.

87 Despite its hyper aridity, the Atacama Desert rarely sees strong dust outbreaks.
88 Thus, considering the limited sediment removal, the atmospheric deposition of dust
89 has been suggested as the parent material of the local soil (Ewing et al. 2006; Wang
90 et al. 2014). It is believed that strong dust outbreaks are inhibited in the Atacama
91 because of the local climatic and topographic conditions such as wind regimes and
92 the cordilleras acting as natural barrier (Reyers et al., 2019). Dust emission
93 nevertheless occurs, for instance, as dust devils and non-rotating dust plumes
94 (Jemmett-Smith et al., 2015). Dust devils are driven by the strong thermal instability
95 of the atmospheric boundary layer triggered by the diurnal solar heating of soils and
96 the intrusion of the cold air from the Pacific Ocean into the Atacama (Kurgansky et
97 al., 2011). Wind erosion is also associated with wind gusts, which have a stronger
98 effect in the afternoon when the southerly wind is strongest (Flores-Aqueveque et
99 al., 2010). Ground-based reports on dust aerosol emission and transport are typically
100 restricted to the spatially sparse network of meteorological stations, which is
101 common in uninhabited desert regions (e.g., Shao et al., 2013, Cowie et al., 2014).

102 Once aerosols of marine, lithogenic, biogenic, volcanic, and anthropogenic origin are
103 emitted, the suspended material is mixed and transported by winds and partially
104 deposited dry or wet in the Atacama Desert. These inputs, which may carry nutrients
105 and water (as fog), are of special relevance in the hyperarid core, where plants and

microorganisms have adapted to hyper arid, high UV radiation, and hyper saline environments. Advective fog, a form of liquid aerosol, is deposited in an area from the coast of the Atacama to ca. 90 km inland (Rech et al., 2003) and below 1000 m a.s.l. (Del Río et al., 2018), allowing the formation of microenvironments in soil crusts, sediments, subsoil, and under or inside rocks, such as quartz and halite (Azua-Bustos et al., 2015; McKay et al., 2003; Parro et al., 2011; Valdivia-Silva et al., 2012; Warren-Rhodes et al., 2019; Wierzchos et al., 2011). Such circumstances do facilitate deliquescence and water retention, and act as shelters to microorganisms against the extreme radiation and desiccation.

Hence, the Atacama Desert represents a unique environment due to the extreme climatic conditions and their effects on the landscape and life development. In this paper, we review several studies related to the Atacama Desert landscape, soil surfaces, wind erosion, atmospheric deposition, synoptic conditions, fog occurrence, among others. We analyze the processes of aerosol emission and transport, and the environmental conditions that direct the spatial and temporal dynamics of atmospheric deposition. In addition, we describe the possible sources of dust and their characteristics, along with the characteristics of the soils where they are deposited. Finally, we describe the fog deposition process and its potential consequences for the environment and life.

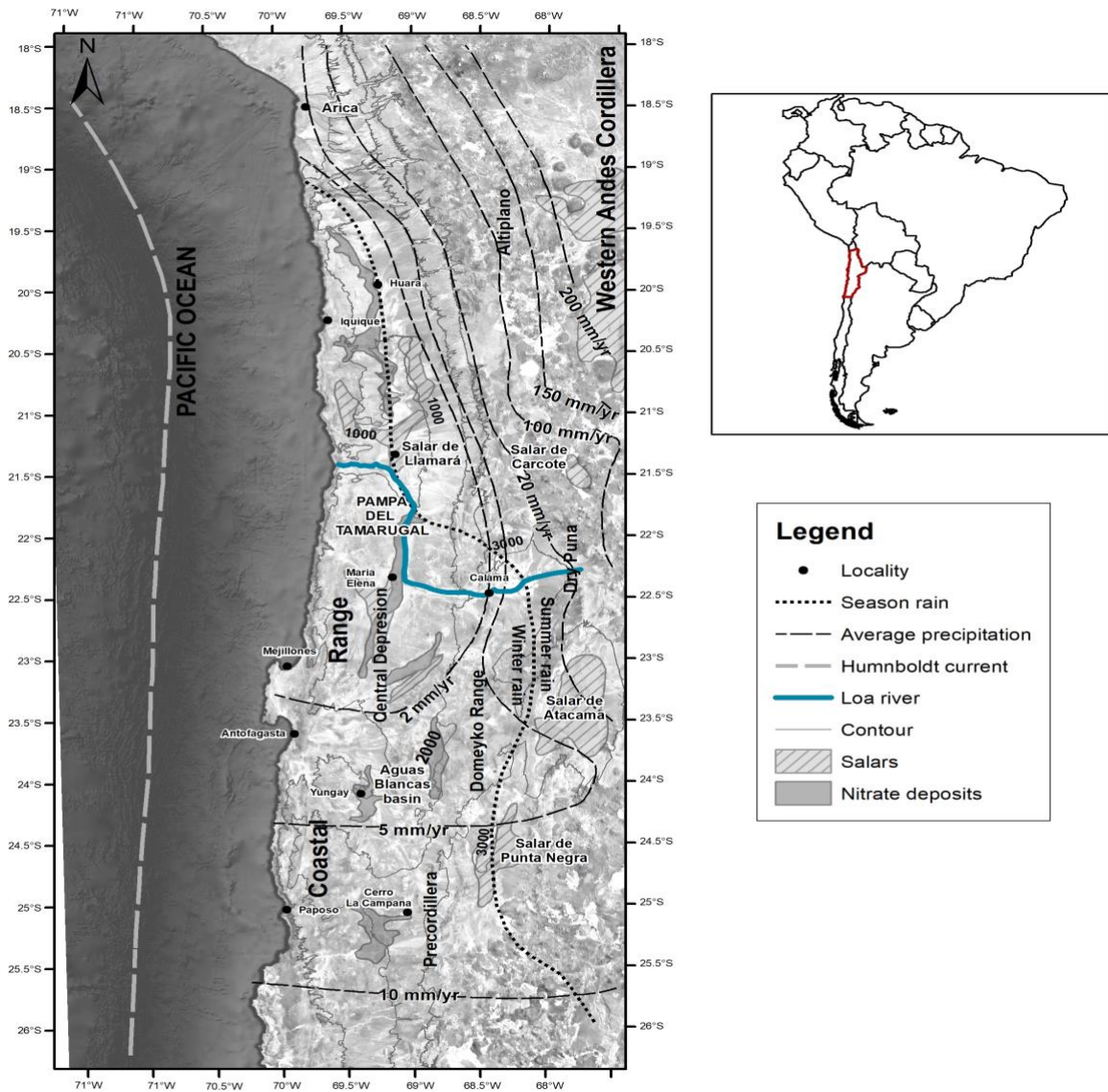
1. Geography and Climate of the Atacama Desert

Landscape evolution theories indicate that the topography inherently records the interaction between climatic, tectonic, and surface processes. Consequently, geological and topographic information can be used to assess erosion and topographic evolution (Bishop, 2013). This is especially relevant when processes such as dust entrainment and atmospheric deposition occur, where the former involves wind erosion of soil surfaces and the latter modifies the topography by dust accumulation.

The Atacama Desert is situated in the western coast of central South America, from northern Peru (5° S) to near La Serena (30° S) (Chile), nevertheless, in Peru, the desert strip is called the Peruvian Desert (or the Sechura Desert) (Goudie, 2013). The Atacama Desert has an extended history that goes back to at least the late Eocene and possibly to the Triassic (Goudie, 2013), and is one of the driest and oldest deserts on Earth (Azua-Bustos et al. 2012; Rech et al. 2003). These main features allow this desert to act as a terrestrial record of climate and landscape evolution since several millions of years, which is a very valuable asset. The aforementioned closed relation between climatic, tectonic, and surface processes are evidenced in the Atacama, e.g., in the relation of the Andes uplift and the Humboldt Current development, the respective consequences of moisture blocking and decreasing air humidity offshore, and the desertification of the Atacama Desert as stated by several authors (Dunai et al., 2005; Garreaud et al., 2010; Hartley and Chong, 2002; Houston and Hartley, 2003; Lamb and Davis, 2003; Rech et al., 2019).

147 The Atacama is bounded to the west by the Pacific Ocean and by the western Andes
148 Cordillera to the east, where the Altiplano and the Puna de Atacama give it continuity
149 (see Fig. 1). Cold waters of the Humboldt Current prevail near the coast preventing
150 precipitation in the coastal areas (Houston and Hartley, 2003), although wetting fogs
151 occur, and occasional high rainfall years associated with El Niño conditions may
152 cause great floods (Goudie, 2013). Besides its hyperaridity, the Atacama Desert is
153 also characterized by its extreme profound diurnal thermal variation, a smooth
154 topography, several mountain ranges, soils with very low concentration of organic
155 matter, and extraordinary deposits of nitrate (among other salts as explained by
156 Michalski et al 2004), salt lakes and playas (salars), among others (see Fig. 1).

157 Regarding dust cycling, the paleoclimate is a relevant topic to address since the
158 availability of dust may be affected by climatic conditions, e.g., arid surfaces are
159 more prone to wind erosion. Thus, knowing the history of the climate in the Atacama,
160 we can outline and suggest areas and/or periods in which dust were more available,
161 especially during dry periods. Moreover, changes in the landscape are registered in
162 the geological record and topography, which have been studied in the Atacama
163 addressing, for instance, denudation and erosion rates.



164

165 **Figure 1.** Geographic map of the Atacama Desert. Main physiographic units of the
 166 Atacama (Tapia et al., 2018), and salars and nitrate deposits distribution are shown
 167 (Finstad et al., 2016). Dashed black lines indicate rainfall rates, and seasonal rainfall
 168 regime is marked by the black dotted line separating west and east areas with the
 169 respective rainfall season predominance (Ritter et al., 2018). Humboldt current is
 170 shown offshore the Atacama and some localities are indicated in the map. (Colors
 171 should be used)

172 **1.1 Geography of the Atacama Desert**

173 The Atacama Desert is associated with the cold Humboldt Current that moves
174 northwards from the Antarctica. The Atacama is classified as “basin and range”
175 desert type, i.e., arid areas dominated by alternating mountains and systems of
176 enclosed drainage, common in areas of tectonic activity such as the south-western
177 United States, the majority of Iran, Afghanistan and Pakistan, parts of central Asia,
178 and the dry coastal deserts of Chile and Peru (Goudie, 2013).

179 The physiography of the Atacama Desert in northern Chile can be divided into five
180 N-S elongated units arranged eastwards: (1) Coastal Cordillera; (2) Central
181 Depression; (3) Pre-Andean Cordillera (or Precordillera); (4) Altiplano, and (5)
182 Western Andes Cordillera (see Fig. 1 and Fig. 2). These units are the result of the
183 active Andean orogeny after the middle Cretaceous and the terrain features
184 produced by the compression and subduction of the oceanic plate below the
185 continental crust (Tapia et al., 2018 and references therein). Thus, from west to east,
186 a very narrow (or non-existent in some areas) Coastal Plain (also known as marine
187 terraces) connects with the Coastal Cordillera, a mountain range (~1500 m;
188 Amundson et al., 2012) that reaches in its peak up to 3000 m a.s.l. (~ 24.5 °S) (Tapia
189 et al., 2018). To the west of this range, vaporized water from the Pacific Ocean is
190 transported as fog and retained by the high coastal summits of the continent. To the
191 east of this range, the situation turns to a dryer landscape, which decreases in
192 elevation and gives way to a longitudinal central valley, locally known as Central
193 Depression. This desert extension, usually referred as the hyper arid core of the
194 Atacama, represents a conjunction of pediment surfaces and longitudinal basins
195 characterized by isolated Cenozoic sedimentation and arid climatic conditions

(Riquelme et al., 2007). This unit, called Pampa del Tamarugal (PdT) from the Loa River to the north, presents a distinctive topography, evidenced by a plateau-like relief formed by sedimentary material, which explains the relative regularity of its topography (Quezada and Cerda, 2003). To the east of the Central Depression, the more prominent relief feature within the hyperarid core of the Atacama rises, the Precordillera also known as Sierra de Moreno in PdT and Domeyko Cordillera to the south of the Salar de Atacama (Tapia et al., 2018). The Domeyko cordillera reaches elevations of up to 5000 m asl, and separates the Central Depression from a narrow, discontinuous pre-Andean depression that contains numerous internally drained salars (Amundson et al., 2012). To the east, in the Western Cordillera, Neogene stratovolcanoes reach 2,000 meters over the Altiplano (average 4000 m a.s.l.) (Jordan et al., 2014), a high plateau composed by a series of intermontane tectonic trenches infilled with sediments (Neogene evaporitic, siliciclastic, and volcanic successions; Jordan et al., 2014), characterized by large basins occupied by salars (Goudie, 2013). The Altiplano contained large bodies of water in the past, e.g., the Salar de Uyuni in the Bolivian Altiplano, that today represent the major source of dust in South America (Goudie, 2013). This general physiography framework exists as far south as Vallenar (~28°S), at which point the Central Depression disappears as a distinct geographical feature, and series of mountain ranges, of increasing elevation, extend from the coast inland (Amundson et al., 2012), the so called Transverse Valleys.

Within the Atacama Desert, it is possible to find several stratigraphic units, which reflect the evolution that the landscape has undergone over millions of years (e.g., Evenstar et al., 2017, 2009; Jordan et al., 2014). It has been suggested that the

220 paleosurface of the Atacama Desert is composed of several paleosurfaces, which
221 were formed by aggradational or degradational processes that occurred from the
222 Miocene (Jordan et al., 2014) to the Pleistocene (Evenstar et al., 2009). In this
223 regard, Evenstar et al (2017) identified six age-based and regionally extensive
224 stratigraphic units distributed at ca. 35-23 Ma; 23-19 Ma; 18-13 Ma; 12-11 Ma; 8-7
225 Ma; and 5-3 Ma. Deposition of each of these units ceased abruptly, marked by
226 hiatuses dated at ~23 Ma, ~19 Ma, ~13 Ma, ~11 Ma, ~7 Ma and ~3 Ma, which may
227 be linked to periods of less erosion due to more arid periods (see 1.3). Just as the
228 (paleo) climate presented spatial and temporal variability, as demonstrated by
229 paleoclimatic records, this variability has been experienced by the processes of
230 aggradation and degradation, so the product of these, i.e., the formation of these
231 surfaces, is not continuous throughout the desert. Moreover, the several surfaces
232 may also have been subjected to post-depositional reworking during wet periods in
233 conjunction with the exfoliation of boulder surfaces according to Evenstar et al
234 (2017).

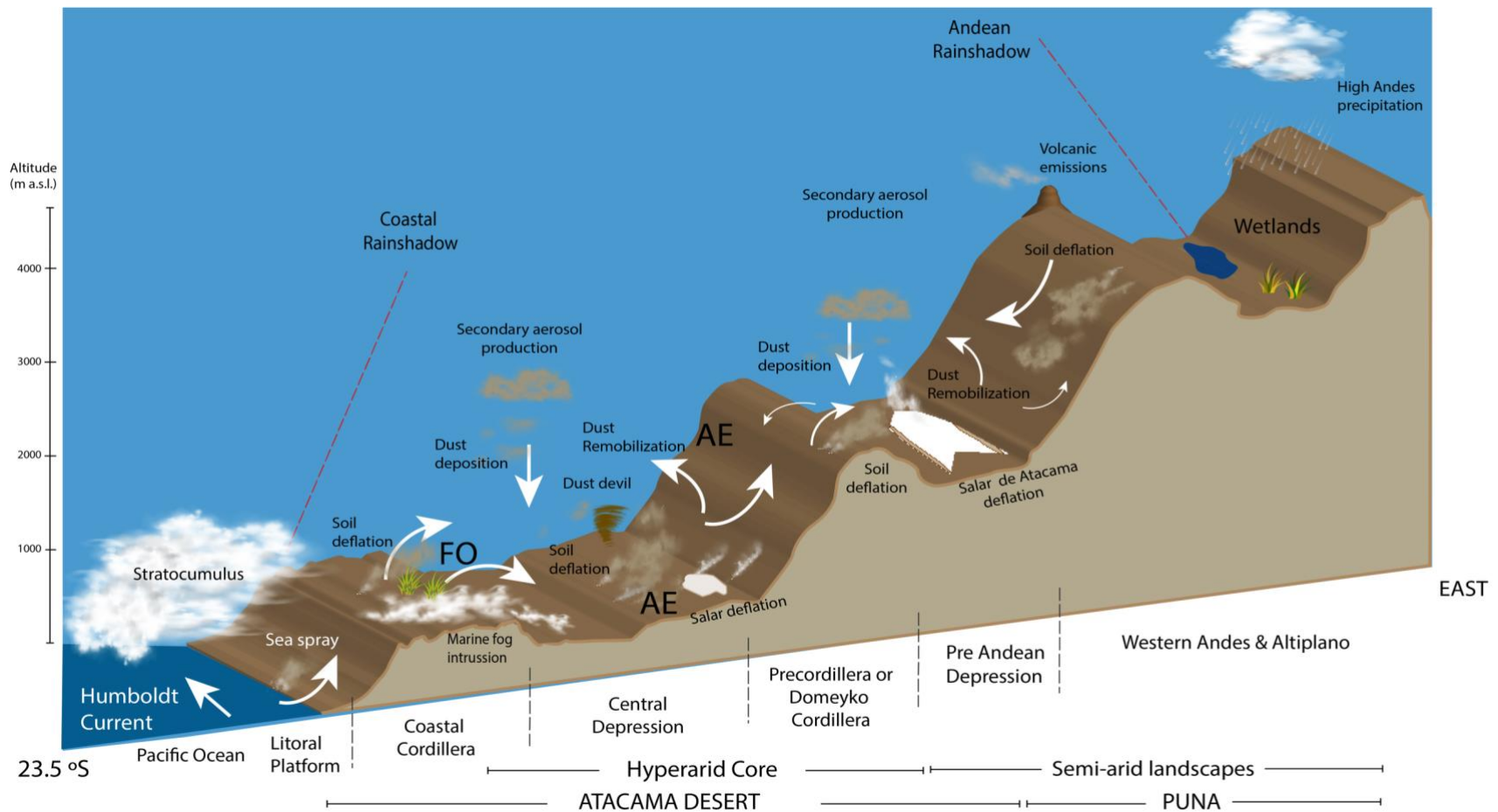


Figure 3. Illustration of dust dynamics in the Atacama Desert. White arrows represent wind mobilization of entrained soils, sediments, and aerosols. Plants are shown in the Coastal Cordillera (FO = fog oases) and over the Precordillera (Wetlands). Marine and volcanic contributions are denoted as well as the secondary aerosol production. AE stands for anthropogenic emissions such as mineral smelters and mining operations. Red dashed lines are a representation of the double rain shadow that affects the Atacama. Objects are not to scale, and the extent of the physiographic units is only for illustrative purposes.

(Colors should be used)

1.2 Atacama Desert Landscape

The current landscape of the Atacama Desert ranges from the less dry areas, mainly represented by fog oases (lomas), and restricted to coastal areas influenced by marine fog (Rundel et al., 1991; Rundel and Mahu, 1976), and few wetlands, located in the dry puna, immediately east of the Atacama (Rech et al., 2002); to the absolute hyperarid desert, a broad expanse of the Atacama Desert almost entirely devoid of precipitation and vascular plants in the Central Depression (Latorre et al., 2002; Maldonado et al., 2005; Squeo et al., 2006). One consequence of the long-term intense aridity to what the Atacama has been subjected is that it contains massive nitrate deposit, likely the most famous and important of the world. Nitrate is a highly soluble salt and can only be accumulated under very dry conditions (Goudie, 2013). It is also possible to find rare iodate and perchlorate salts, as well as abundant chloride, sulfate, and borate salts (Ericksen, 1981a), partially fed by atmospheric deposition (Cosentino et al., 2015; Ewing et al., 2006; Li et al., 2019; Michalski et al., 2004; Rech et al., 2003; Wang et al., 2014), analogously to the salt occurrence on the surface of Mars (Catling et al., 2010; Hecht et al., 2009; Stern et al., 2017). Between Taltal (25 °S) and Chañaral (29 °S), the character of hillslope soils, as well as soils on non-sloping land surfaces, undergoes a fundamental change compared to landscapes to the north. Sulfate in soils of all slope positions declines greatly due to increased rainfall, and carbonates become the dominant secondary mineral in soils as plant density (and resulting soil CO₂ concentrations) increases (Amundson et al., 2012).

Another consequence of hyperaridity is that erosion rates are extremely slow and geomorphic surfaces can survive for long periods of time (Placzek et al., 2010). Morphological features of the Atacama (ancient and modern) are formed mainly by the action of fluvial erosion and deposition generated by the Andean runoff that has formed perennial and many ephemeral rivers which have modified the landscape, e.g., through deep incisions (up to 1200 m) in many sections of these rivers during the Pliocene (1–3 Ma), as a consequence of tectonic uplift and sea-level change, as well as fluctuations in climate (Houston, 2006). Despite of this, only relatively minor subsequent phases of aggradation and incision have taken place (Latorre et al., 2005; Rech et al., 2002) as the fluvial impacts on the landscape became greatly reduced in the late Pliocene to early Pleistocene (Amundson et al., 2012). This almost negligible modification of the landscape during the Quaternary has allowed the preservation of alluvial landforms (Dunai et al., 2005; Ritter et al., 2018) produced from the late Miocene onwards (Amundson et al., 2012).

During the Holocene, short-term but significant fluctuations have also occurred, evidenced by the establishment of temporary wetlands at specific locations (e.g., Quebrada Puripica) and the consequent fluctuating vegetation on the margins of the arid to hyper-arid regions represented by the Domeyko Cordillera. Despite this climatic oscillations, it appears unlikely they would have caused a major overall shift from the generally arid conditions, except locally through supply of both surface and groundwater (Clarke, 2006). Surficial features suggest episodes of increased rainfall during the Quaternary, evidenced e.g., by deposits of a small endorheic basin (Ritter et al., 2019), erosion/ deposition cycles (Jungers et al., 2013), hillslope zebra (stone)

stripes, rills and colluvial deposits on hillslopes (Amundson et al., 2012; May et al., 2020, 2019; Medialdea et al., 2020; Owen et al., 2013), and the presence of pipes that run sub-horizontally below the soil surface (Amundson et al., 2012).

Surficial processes rates are spatially heterogeneous in the Atacama (Evenstar et al., 2009). Placzek et al (2014) analyzed the concentrations of cosmogenic nuclides in more than 100 samples across two east-west transects within the central Atacama Desert (22-26°S). Recent cosmogenic nuclide-based studies suggest that erosion (Placzek et al., 2010), soil (Owen et al., 2011), and fluvial activity (Jungers et al., 2013) are ongoing, but slow in the central Atacama. In relation to this, Kober et al (2007), suggested a relation between erosion rates with elevation and modern precipitation rates. Thus, at the hyperarid Coastal Cordillera and the Western Escarpment along with the northern part of the Atacama Desert, erosion rates are extremely low and of the order of 10–100 cm My⁻¹, whereas at higher altitudes, where the landscape transitions to semi-arid environments due to more frequent rainfall, erosion rates increase at the Western Cordillera and range up to 4600 cm My⁻¹. Sediment production and supply from high altitudes, e.g., the western Andean slope, is very limited (Kober et al., 2007), although it may be variable along watercourses. For instance, sediment generation, transport and deposition in the Rio Lluta catchment is not a simple and continuous (steady-state) process according to the catchment-wide denudation rates and TCN-derived erosion rates from adjacent bedrock hillslope interfluvies obtained by Kober et al (2009). There are similarities in the upper catchment (Western Cordillera) but they differ markedly from each other in the Western Escarpment and the Coastal Cordillera region.

In a previous study, Placzek et al (2010) described the landscape along a transect ca. 23° S. The authors found out that the Coastal Cordillera is one of the more active landscapes in this transect, where active alluvial fans and recent debris flows are prominent features within a few km of the coast. It is also common to find exposed bedrock exposures both on the Coastal Cordillera and along the coastal plain, and gypsum in soil within the Coastal range above ~1000 m, whereas soil carbonate is present closer to the coast. Inland, the Central Depression presents substantially slower erosion rates than its eastern and western margins; however, even the driest part of this transect has erosion rates comparable to those of other deserts, ranging from 0.2–0.4 m My⁻¹. The entire Central Depression is within the hyperarid core (absolute desert) and all landforms here are mantled by a thick cover of loess, gypsum, and in some places nitrate, giving hillslopes a rounded and subdued appearance. Hillslopes often present rocks clusters (boulder fields) which are indicative of some downslope movement of rocks. According to the cosmogenic nuclides assessment carried out by Placzek et al (2010), results indicate that the most stable landscape elements in the hyperarid core are boulder fields, with exposure ages of 1.5–2.6 Ma.

Regarding Central Depression soils, Pfeiffer et al (2021) described both hillslope and alluvial soils in the hyperarid Atacama. About them, the authors evidenced the long-term accumulation of atmospherically deposited salts in a landscape free of vegetation as mentioned by Placzek et al (2010). Hillslope soils develop on weakly fragmented bedrock lacking evidence of chemical weathering and soils become thinner towards the hilltop and thicker towards the footslope. Soil in all the studied

sites have a similar sequence of horizons with a very porous and conductive layer of anhydrite on top of a cemented gypsum layer, which is mostly impermeable except for vertical cracks that penetrate up to ~1.5 m deep. Moreover, Pfeiffer et al (2021) described large scale polygon structures that extend to the surface occurring on 1.5 to m scales, and pipes development on top of the impermeable sulfate layer at several locations. These pipes converge with gullies on hillslopes, and pipe outflows in alluvial fans. Mantling of upper hillslopes depends on the location, and could be soil or rock, whereas zebra stripes commonly develop on the middle slope section, and rills occur more frequently toward the lower slope positions.

About the flanks of the Domeyko Cordillera, Placzek et al (2010) situated them within the absolute desert and described features similar to those of the Central Depression. Although Domeyko hillslopes are thickly mantled in gypsum and loose soils, visible rilling is present and bedrock is occasionally exposed at high elevation, where active alluvial fans and channels are present near the crest. The Andean Flank also present active alluvial fan surfaces along the fringes of salar basins. Incised channels, often with perennial water, transport water and sediment from the highlands. Bedrock is frequently exposed and rocky soils generally contain carbonate, meanwhile the vegetative cover increases up to the 0 °C isotherm.

Moreover, Amundson et al (2012) described the hyperarid basin of Aguas Blancas in the Central Depression (see Fig. 1). There, they found rare surface runoff events that generate sheetwash and rills. In this area, the authors observed two dramatically different landscapes, but they are both still present. The previously active bedrock source areas for Pliocene alluvial fans, and debris flows that are currently “frozen” in

Quaternary salt. Additionally, the authors examined hillslope soils to the south of Antofagasta (23.5°S), and described changes in the soils. In the Pliocene or earlier, hillslopes were mantled with silicate-derived soil but this was stripped off and locally deposited as alluvial fans (late Pliocene to early Pleistocene) that now block or otherwise cause a rearrangement of Pliocene and earlier river channels. The hillslopes have largely accreted a soil mantle of dust and salt since the apparent late Pliocene stripping, suggesting a decline in annual precipitation of at least 125 mm year⁻¹ or more. Moreover, at the latitude of present-day Chañaral (~26.5°S), hillslopes are largely denuded of salts and dust. This suggests that a rainfall threshold has been exceeded, which in turn facilitates fluvial processes capable of removing fine materials from slope surfaces. Finally, the authors calculated rates of soil production (bedrock conversion to a mobile soil mantle) about ≤ 1 m My⁻¹ near Antofagasta, increasing to 2–3 m My⁻¹ at Chañaral, and are up to >20 m My⁻¹ at La Serena (120 mm). Present rates of bedrock conversion to soil are strongly linked to rainfall, and the rates in the Aguas Blancas region are among the lowest rates yet reported on Earth. Moreover, in this basin, a significant amount of soil mass on hillslopes is composed of sulfates and other salts and dust that must be (~50% or more of volume) derived from atmospheric deposition (Amundson et al., 2012).

In environments with limited runoff and scarcity of vegetation as the Atacama Desert, wind erosion may play a major role shaping the landscape, however it is probably the least quantified erosion process worldwide (Carretier et al., 2018). Hillslopes, for instance, are typically shaped by the interplay of sediment production due to bedrock weathering and atmospheric deposition, and sediment loss due to erosion by wind,

677 water (overland flow) and gravity induced processes (Mather et al., 2014; Owen et
678 al., 2011). Hence, the Atacama is a suitable place for wind erosion transport analysis
679 and few studies have taken advantage of this context (e.g. Benison 2017; Flores-
680 Aqueveque et al. 2010). The effect of wind erosion in the Atacama is evidenced by
681 the presence of high winds, high aeolian particle loads and widespread wind
682 erosional features (Wang et al., 2017), e.g. soil deflation (Rech et al. 2003), sand
683 ripples, among others (see Fig. 3). Nevertheless, wind erosion of the landscape can
684 be compensated by the atmospheric deposition of dust and salts (Michalski et al.,
685 2004). This is evidenced in the Central Depression, where the influx of sulfate rich
686 aeolian dust has caused a smoothed appearance of the landscape and hills.
687 Moreover, some quebradas (ravines) have reworked dust and mantled their floors.
688 In pre-Andean basins, such as the Atacama Basin and Salar de Atacama, aerosol
689 deposition is ongoing, which is in contrast to some adjacent areas where deformation
690 processes occur (Clarke, 2006).

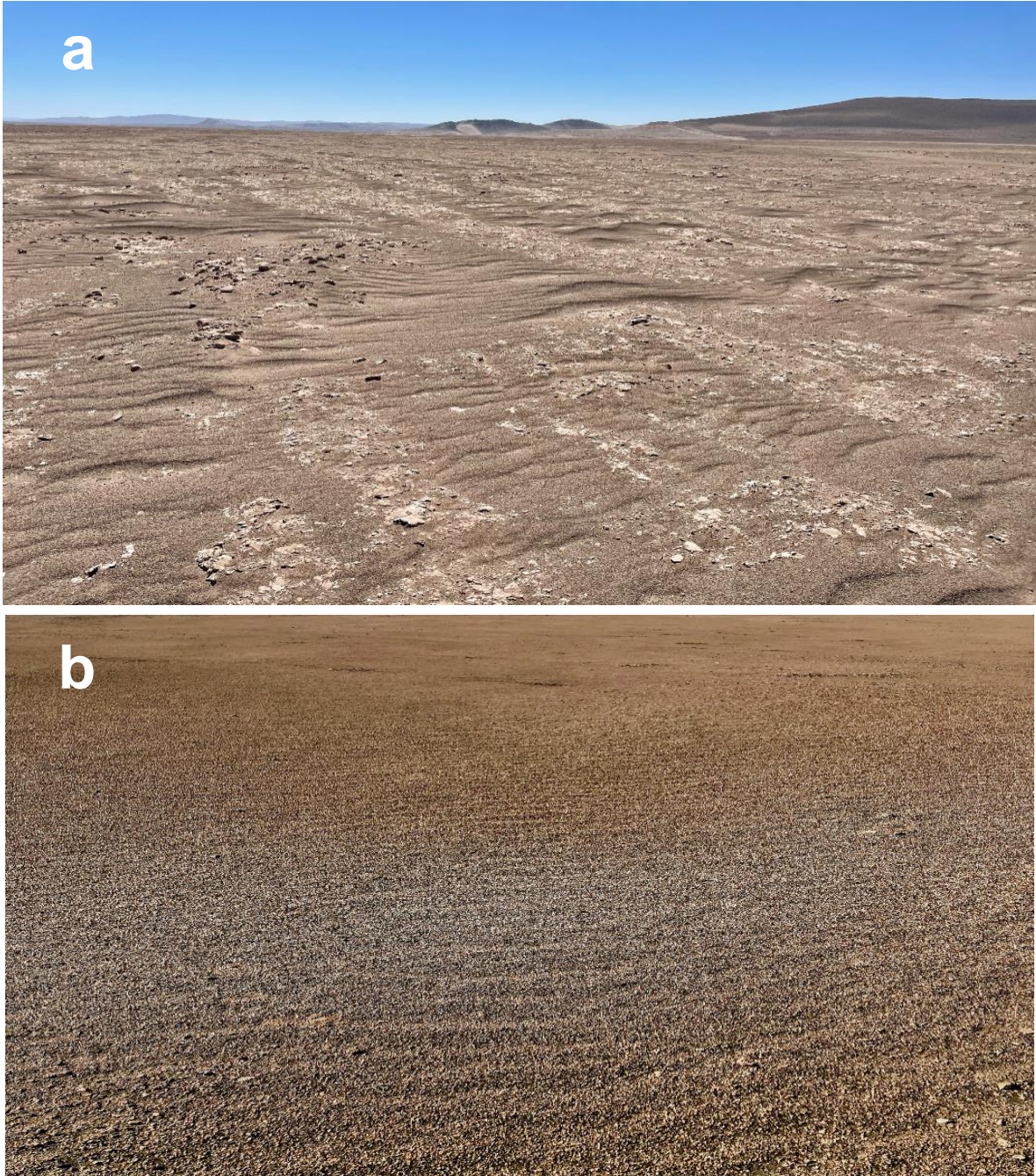


Figure 3. Deflated soil near (a) the Salar de Llamara in the Central Depression showing transverse ripples (N-S oriented) to the wind direction. (b) Smaller E-W oriented ripples in the eastern slope of the Coastal Cordillera are shown.

1.3 Climate and Paleoclimate in the Atacama Desert

The Atacama Desert ranks among the most arid areas of the world (Dunai et al., 2020; Ritter et al., 2018; Rundel and Mahu, 1976), and in consequence represents one of harshest environments on Earth. Aridity is enhanced by the effect of a major two-sided rain shadow projected by the Andes Cordillera to the east and by the Coastal Cordillera to the west, lower but remarkably high mountains that limit the inflow of advective moisture to the Atacama (Bull et al., 2018). Additional factors are the zonal position of the Atacama Desert in relation to the Hadley circulation; its distance from the main Atlantic–Amazonian source of moisture; and its proximity to the Humboldt Current (Houston and Hartley, 2003).

For the modern climate monitoring of the Atacama Desert in Chile, in 2017, a network of 15 permanent weather stations were installed by the Collaborative Research Center (CRC) 1211 (Dunai et al., 2020) within the Atacama Desert in Chile. The weather stations were set along three west-east transect at ca. 19-20°S, 21.4°S, and 25°S, respectively, from the coastal platform to the Precordillera (Hoffmeister, 2018). After more than 30 months of observation, the average annual temperature calculated was 16.1°C with 36.0°C and -3.79°C in Salar de Llamara (in the Central Depression, see Fig. 1) as the maxima and minima recorded, respectively. The annual average incoming radiation was 255.9 W m⁻² peaking in the Central Depression, and winds averaged 3.11 m s⁻¹, with the strongest at Cerro Campana (2550 m a.s.l.), located in the transition between the Central Depression and the Domeyko Cordillera (Precordillera), recording 18.1 m s⁻¹ and NE direction.

Specifically, in the Central Depression, i.e., excluding data from the western slope of the Coastal Cordillera, between 19.5°S and 25°S, winds averaged 3.44 m s⁻¹, where the fastest came from SW, SE and NE. Below ~2600 m a.s.l., a mean annual precipitation of 0.001±0.12 mm year⁻¹ was calculated from the reported data. About potential evapotranspiration (PET), a rate of 1–2 mm day⁻¹ was reported by Mintz and Walker (1993). Hence, with an average annual precipitation lower than 5% of potential evapotranspiration, this area can be classified as hyper-arid (UNEP, 2011).

Arid conditions in the Atacama Desert go back at least from ca. 9 to 37 Ma (Dunai et al., 2005; Evenstar et al., 2009; Kober et al., 2007; Nishiizumi et al., 2005). To assess the age of cessation of erosion, as a consequence of aridification, Dunai et al (2005) analyzed the cosmogenic nuclide concentration on erosion-sensitive landforms in the Coastal Cordillera (~19°35'S and ~70°10'W) in order to reveal the exposure ages of the collected samples. According to their results, the authors proposed an onset of aridity at 37 Ma, with an intensification leading to hyper arid conditions in the Atacama since 25 Ma. Moreover, they considered that the hyper arid conditions favored the uplift of the high Andes (as proposed by Lamb and Davis 2003), which in turn contributed to increase the rain shadow cast by this mountain range, enhancing aridity and allowing the current conditions of hyperaridity. In this sense, Ritter et al. (2018) dated pre-Miocene exposure ages in clasts (~28 Ma and ~34 Ma), which would have required an immobile or less disturbed landscape development during the Oligocene. Also, the authors revealed several episodes of enhanced fluvial erosion and deposition terminated at ~19, ~14, ~9.5 Ma immediately south of the Loa River (~21.5 °S), which implies subsequent more arid

periods with less rainwater, and identified that large scale fluvial modification of the landscape ceased by ~2–3 Ma. Hence, a hypothesis of a singular early and unique aridity onset is refutable and the one supported by the authors, which indicated an early onset of hyperaridity in the core of the Atacama Desert and an aridification process occurring with the interruption of wetter periods (although more or less arid), is more plausible. Wetter periods may produce more sediment due to fluvial erosion and, conversely, drier periods are more favorable to aeolian relocation due to desiccation of sediment deposits and aeolian erosion.

More evidence regarding wetter and variable past in the Atacama Desert has been described by several authors (Diederich et al., 2020; Gayo et al., 2012; Hartley and Chong, 2002; Herrera et al., 2018; Jordan et al., 2020, 2019, 2014; Medialdea et al., 2020; Nester et al., 2007; Placzek et al., 2010; Rech et al., 2019; Ritter et al., 2019, 2018; Sáez et al., 2016, among others). For instance, Rech et al. (2006) evidenced a shift in paleo soils within the Calama basin (~22.5 °S, ~69°W) between 19 and 13 Ma, which was recorded in sediment cores, and thus documenting the change from calcic Vertisols to extremely mature salic Gypsisol, which evidences a reduction in precipitation from $> 200 \text{ mm yr}^{-1}$ to $< 20 \text{ mm yr}^{-1}$. Another piece of evidence of this paleoclimate variability is the one provided by Rech et al (2019), who through the analysis of fossil soils from along an 800-km transect (19–25°S) stated that lower Miocene (24–20 Ma) soils are chemically weathered and contain soil carbonate, indicative of a vegetated landscape and semi-arid climate. In contrast, gypsum dominates massive (2–5 m thick) upper middle Miocene soils that formed on a hyperarid landscape devoid of vegetation. The authors link this change in paleo soils

(to hyperarid conditions) with the rain shadow initiation along the west coast of South America, and inferred a minimum age for the development of the Central Andean rain-shadow of 15 Ma and a strengthening during the late middle Miocene (12–10 Ma). This would be also coincident with the strengthening of the Humboldt Current in the subtropical South Pacific, which may have been crucial to the desiccation of the Atacama from the late Miocene (Garreaud et al., 2010). After the strengthening of the Andean rain-shadow and the Humboldt current establishment, a consequent and extensive arid period is observed, which extends into the Pliocene and upper Pleistocene (Table 1). Concordantly, Jordan et al (2014) assessed the landscape modification through geomorphology, stratigraphy, and pedogenic data and identified four different arid intervals at 11 - 5.5; 4.5 – 4; 3.6 – 2.6; 2.2 – 1 Ma, and repeated intervals during the last 1 Ma. Each of these arid periods were followed by short lived wetter conditions of ca. a million year or less. Moreover, Houston (2006) reported ancient morphological features formed by Andean runoff and its fluvial erosion that formed perennial and many ephemeral rivers which have modified the landscape (deep incisions) during the Pliocene (1–3 Ma), as a consequence of tectonic uplift and sea-level change, as well as fluctuations in climate. Despite of this, only relatively minor subsequent phases of aggradation and incision have taken place (Latorre et al., 2005; Rech et al., 2002) as the fluvial impacts on the landscape became greatly reduced in the late Pliocene to early Pleistocene (Amundson et al., 2012).

From middle to upper Pleistocene, hyperaridity was interrupted by several precipitation events in millennial and orbital time scales. Diederich et al (2020), built

a 68,000 years reconstruction of precipitation variations through the assessment of the sediment infill of the Huara (~20 °S) clay pan basin and other records, and identified several wet periods for the Atacama. The authors indicate wet conditions within the Huara record (ca. 67.8 - 61 ka) following the correlation with the Salar de Uyuni record and its lacustrine phase dated to ca. 60-55 and 70-65 ka. These wetter conditions are followed by dry spells at Huara, Salar Grande, and Salar de Atacama (see Fig. 1 for location). After this, several pluvial phases within the Huara record extents from 58-33.6 ka, interrupted by short-term arid conditions. After this, prolonged moister conditions occurred at the northern edge of the hyperarid core (28.5-16.4 ka). This is consistent with the interpretation of marine sediments from northern Chile, which indicate a low aeolian contribution, implying wet conditions. From 28.8 to 18.0 ka, the Huara record shows a swing back to arid conditions, although the peak wet phase at the Salar de Atacama occurred almost simultaneously (26.7-16.5 ka). Additionally, the Huara clay pan registered a flooding event ~17 ka, which indicates a wet phase synchronous with the first phase of the Central Andean Pluvial Event (CAPE I). This event was responsible for recharge and generate paleo-lakes and wetlands and have been documented by several authors (Diederich et al., 2020; Finstad et al., 2016; Gayo et al., 2012; Herrera et al., 2018; Medialdea et al., 2020; Pfeiffer et al., 2018; Quade et al., 2008; Workman et al., 2020). During the late Pleistocene to mid Holocene (ca. 14-8 ka), the Huara record points to overall dry climate conditions concordant with the Salar Grande records (21°S), where hillslope activity was strongly reduced (Medialdea et al., 2020). A higher aeolian sediment content in the terrigenous fractions of marine sediments offshore northern Chile at 27.5°S (Stuut and Lamy, 2004) and 30°S (Bernhardt et

al., 2017) suggest prevailing arid conditions during the Late Pleistocene and Early Holocene even beyond the hyperarid core. Contrarily to the sites from the Coastal Cordillera, further to the east elevated water levels in the Salar de Atacama (Bobst et al., 2001), wetlands in various parts of the Atacama Desert (Quade et al., 2008; Rech et al., 2002) and formation of rodent middens (Betancourt et al., 2000) highlight a distinct wetter phase between ca. 14 and 10 ka, which is known as the “Central Andean Pluvial Event II” (CAPE II; Quade et al., 2008). Between 12.1-11.4 ka, a wet period in the PdT and upstream was reported by Gayo et al (2012). Within the southern coast of the Atacama, Herrera et al (2018) found that coastal deep wells (at Michilla, 22.75 °S) were recharged ca. 14.5 to 10 ka during CAPE II, which could be associated to past recharge by air masses coming from the Atlantic. In the Altiplano, this wetter period corresponds to the “Coipasa” paleolake phase. The divergent precipitation patterns during this interval, with differing conditions to the north and south of the Loa River, and western parts of the Atacama simultaneous with wetter conditions in the eastern part and the Altiplano, points to a moisture source from the east that could not reach the Huara clay pan and other areas of the coast. Additionally, CAPE II is archeologically important since it facilitated the establishment of Paleo-Indian communities in the Atacama Desert, e.g., in the Quebrada de Mani (Workman et al., 2020).

More recently, Nester et al (2007) identified an important event during the Holocene, which allow phreatophytes trees to grow (*Prosopis* sp.) in Pampa del Tamarugal (PdT) drainages between 1070 and 700 ka (calibrated years before present), which implies higher water tables. This recharge event corresponds to the Medieval

Climatic Anomaly (MCA) and is characterized by its wet impact in the southern portion of the Atacama (northern Chile), opposite to the hydrological dry impact in the coastal Peru, which is consistent with La Niña dominance. This wetter period is also coincident with the reported by Gayo et al (2012), who examined organic material from relict fluvial terraces inserted within four dry and unvegetated valleys (21 °S - 21.5 °S) that also drain into the endorheic basin of PdT, and identified an expansion of the riparian and wetland ecosystems from 1010-710 ka. Additionally, Tully et al (2019) identified several dense paleowetlands within the Calama Basin supported by the Río San Salvador from 11.1 to 9.8, 6.4 to 3.5, 2.8 to 1.3, and 1.0 to 0.5 ka. Finally, according to Herrera et al (2018), spring waters south of the 23°S were recharged by the arrival of moist air masses from the Pacific Ocean 1-5 ka, when the area was already inhabited. The previous periods and dates were gathered and are presented in Table 1.

Table 1. Significant events and periods in the paleoclimate timetable of the Atacama Desert

Epoch	Since kyr	Until kyr	Period significance	Reference
Holocene	1.01	0.71	Expansion of riparian and wetlands ecosystems	Gayó et al., 2012
	1.1	0.7	Increase of water discharge within the Pampa del Tamarugal basin due to the Medieval Climatic Anomaly (MCA)	Nester et al., 2007
	4.7	present	Wetter climate	Saez et al., 2016
	5	1	Coastal aquifers recharge	Herrera et al., 2018
Upper Pleistocene	11		Cessation of carbonate formation	Nester et al., 2007
	11.75		Increase of water discharge within the Pampa del Tamarugal basin	Nester et al., 2007
	12.1	11.4	Expansion of riparian and wetlands ecosystems due to the Central Andean Pluvial Event (CAPE)	Gayó et al., 2012
	12.2	9.8	Wetter climate	Saez et al., 2016
	14.5	10	Recharge of profound aquifer in coastal desert (Michilla) due to the Central Andean Pluvial Event (CAPE)	Herrera et al., 2018
	14.5		Wetter climate	Saez et al., 2016
	17.6	14.2	Expansion of riparian and wetlands ecosystems due to the Central Andean Pluvial Event (CAPE)	Gayó et al., 2012
	17.75	13.75	Increase of water discharge within the Pampa del Tamarugal basin	Nester et al., 2007
Lower Pleistocene	2200	1000	Hyperarid interval within Pampa del Tamarugal basin	Jordan et al., 2014

Table 1. Significant events and periods in the paleoclimate timetable of the Atacama Desert (cont.)

Epoch	Since	Until	Period significance	Reference
	kyr	kyr		
Pliocene	3000	2000	Cessation of fluvial erosion	Ritter et al., 2018
	3600	2600	Hyperarid interval within Pampa del Tamarugal basin	Jordan et al., 2014
	4500	4000	Hyperarid interval within Pampa del Tamarugal basin	Jordan et al., 2014
Upper Miocene	9500		Termination of episodes of enhanced fluvial erosion and deposition	Ritter et al., 2018
	11000	5500	Hyperarid interval within Pampa del Tamarugal basin	Jordan et al., 2014
Middle Miocene	12000		Arid conditions (onset of aridity)	Jordan et al., 2014
	12000	10000	Beginning of aridity between mid and late Miocene	Rech et al., 2019
	12000	10000	Strengthening Andean rain shadow	Rech et al., 2019
	14000		Termination of episodes of enhanced fluvial erosion and deposition	Ritter et al., 2018
Lower Miocene	15000		Central Andes uplift and rain shadow strengthening	Rech et al., 2019
	19000		Termination of episodes of enhanced fluvial erosion and deposition	Ritter et al., 2018
Oligocene	24000	20000	Vegetated soils and semi-arid landscape. Soils chemically weathered with carbonate presence	Rech et al., 2019
	28000		Stagnant landscape development during the Oligocene	Ritter et al., 2018
Eocene/Oligocene	34000		Stagnant landscape development during the Oligocene	Ritter et al., 2018

1.4 Recent Climate Events in the Atacama Desert

In the Atacama Desert, rainfall presents temporal and spatial variability, e.g., in the Calama and Salar de Atacama basins, most of the annual precipitation occurs during the austral summer, while 200 km to the south it occurs during the winter (June to September) (Betancourt et al., 2000). In the Fig. 1 it is possible to observe this distribution as a limit between west and east regions that usually receive precipitations during winter or summer, respectively. Moisture sources of the Summer-rainfall-dominated areas are located east of the Andes, whereas Winter-rainfall sourced in the Pacific Ocean dominates south of the dry core (Houston and Hartley, 2003; Ritter et al., 2018) and are associated with a northward migration of extratropical storm fronts during positive phases of ENSO (Garreaud and Aceituno, 2001), and is sensitive to long-term changes in the sea-surface temperature of the Pacific. This increased rainfall during El Niño-like conditions is evidenced, e.g., by the El Niño-induced extreme rain event in 2015 (Ritter et al., 2018). Moreover, Latorre et al (2011) stated that there is a relationship between rainfall and ENSO in tropical to subtropical northern Chile, which depends on altitude and latitude, e.g., the central Andes receive more summer rainfall during La Niña years, whereas El Niño years, which are dry on the Altiplano, are associated with rare winter rainfall events along the coast of northern Chile.

During the Anthropocene (Ruddiman, 2013) in the Atacama Desert, long-term records of precipitation are rare. This because of the sparse population, and a relatively short duration of settlement (Schween et al., 2020). Pfeiffer et al (2021)

presented a brief summary of the rare pluvial events from 1881 onwards that complement a previous compilation done by Ortlieb (1995), which covers the period between 1796 and 1992. During the last three decades, remarkable rainfall events have occurred in the Atacama Desert. Among these, the 1991 (Garreaud and Rutllant, 1996), 2001 (Houston, 2006), 2015 (Jordan et al., 2020, 2019; Pfeiffer et al., 2021; Scott et al., 2017) and 2017 (Azua-Bustos et al., 2018; Jordan et al., 2020; Schulze-Makuch et al., 2018; Scott et al., 2017) rain events were documented.

On June 18th of 1991, a rainfall that averaged rate of 5-14 mm h⁻¹, with a maximum of up to 24 mm h⁻¹ occurred in Antofagasta city area, which was considered a “hundred-year” rainfall at the time (Garreaud and Rutllant, 1996), and coincided with the development phase of El Niño (Vargas et al., 2006). This wind and rain storm was caused by a winter cold front that migrated northward and reached the coastal desert and part of the interior desert, causing precipitation in Baquedano (17.5 mm) and Aguas Verdes (33.5 mm) but did not extend towards northern or eastern localities as Quillagua, Calama and San Pedro de Atacama. The anomalous northward advance of the cold air and associated frontal disturbance was the result of a blocking SW of the southern cone of the Americas and a weakening of the subtropical anticyclone. This event had catastrophic consequences provoking dozens of deaths (Vargas, 1995), and destructive debris flows on the Coastal Escarpment hillslopes (Vargas et al., 2006).

Another relevant event occurred in February 2001, where widespread flooding occurred throughout the Atacama Desert of northern Chile and southern Peru. Among the effects reported by Houston (2006), the flooding was particularly severe

in the Río Loa basin where several bridges were ruptured and the city of Calama inundated. As far as is known, this is the first recorded historical event in the Atacama Desert of such magnitude and impact. The author also reported considerable erosion, e.g., from the Quebrada de Tuina (pre–Andean Cordillera), where 5 km³ of sediments were redistributed towards the Calama basin, which meant an erosion of 70 mm in the catchment. Some other impacts were incisions of 2-5 meters wide due to the formation of new channels or the growth of others, high sediment concentrations in the Salado and Loa rivers, aggradation of large volumes of sand, gravel bars and crevasse splays. Moreover, overbank flooding and mudflows occurred almost universally within the Atacama (in perennial and ephemeral catchments), and the deposition of fine-grained sediments over large areas (hundreds of km²) and considerable thickness (~1 m). The author also indicated that this type of events in the Atacama Desert, i.e., floods, are generally caused by exogenous rains, provoked by the La Niña phenomenon.

Over a three-year timespan, from 2015 to 2017, there were two extremely uncommon, major precipitation events in the Atacama Desert, as well as several smaller, more typical storms (Jordan et al., 2020). From 24 to 26 March 2015, a warm-season storm brought rain and snow across a major portion of the Atacama (Jordan et al., 2020), which caused rainfall rates and quantities to exceed many historical records (Pfeiffer et al., 2021). Among the precipitation records of this event, Jordan et al (2020) mentioned that 80–90 mm of liquid precipitation fell at some locations in both the mountains and the lowlands. The driver for this event was a synoptic-scale weather system, a cutoff cold upper- level low system that traversed

the Pacific Ocean at a time of unusually warm temperatures of Pacific surface water (Jordan et al., 2019). This led to greater potential for erosion and sediment transport than typical of more common moderate precipitation scenarios which usually include widely distributed snow (Jordan et al., 2019). Here, the results of a reconnaissance from N to S transecting through the plant-free expanse of the Atacama Desert, between 22 and 26 °S, are examined in relation to evidence of past runoff activity coupled with soil architecture and soil hydraulic properties. In order to study the rainfall effects and its potential to activate geomorphic processes, Pfeiffer et al (2021) examined a transect between 22-26 °S, whose results suggest that the rain initiated some minor runoff processes on the upper hillslopes and concluded that the event was too small to reactivate many features that appear to be driven by larger, less frequent storms. Despite this, in some river valleys there was catastrophic damage to property and loss of life, whereas other regions with similar precipitation amounts exhibited little to no surface disturbance (Jordan et al., 2015; Scott et al., 2017). The second significant precipitation event occurred two years later, 6–7 June 2017, with widespread snowfall above 2700 m a.s.l. and rain reported at many lowland gauges (up to 40 mm). A major difference between those two major precipitation events was the role of rain compared to snow: because runoff of surface water is delayed where snow accumulates, streamflow in response to the June 2017 event was delayed and diminished (Jordan et al., 2020).

Other events recorded occurred in 2012, which had landscape consequence near Quebrada de Guatacondo. There, channel walls were plastered with remnants of at least three recent mudflows that occurred in early 2012. The same event in 2012

deposited extensively sediments on a fan that is like-wise characterized by both channelized and overbank flows (Morgan et al., 2014). Jordan et al (2020) add two more minor events. One of them took place between 8–11 August 2015, when a strong winter-season storm impacted the Pacific coastal region, with up to 30 mm of precipitation. This caused infrastructure damage and deaths in cities built at the toe of the steep coastal mountain slope, although most of the interior stations received only trace amounts of rain. The second one occurred on 25–27 June 2016, and brought up to 22 mm rain to coastal communities and snow to the southeastern mountains. Only one interior rain gauge reported a few millimeters of precipitation.

According to their field observations after 2015 rainfall, Pfeiffer et al (2021) suggest that larger scale rainfalls have occurred throughout the Quaternary, and that there are fossilized (or infrequently active) features in various stages of “repair” that provide evidence of rainfall re-occurrence. Thus, the Atacama landscapes largely escaped overland flow alteration due to the high infiltration rate capacity caused by the salt-rich soils, estimated to average 78 mm h^{-1} for hillslopes and 244 mm h^{-1} for alluvial soils. Interestingly, hyperarid landscape within the Atacama are able to provided temporarily favorable conditions for the activity of specialized microorganisms after the rare precipitation event of 2015 until water activity fell again beneath a critical threshold (Schulze-Makuch et al., 2018).

Historical floods, debris and mudflows in the region are mostly associated with rainfall that occurs in the Andean Pre-cordillera and Cordillera such as the Great Atacama floods of 2001 in the Loa River basin (Houston, 2006), flash floods in 2000, and mud/debris-flows in 2012 at the Pampa del Tamarugal (Houston, 2002; Morgan

et al., 2014; Sepúlveda et al., 2014). During these events, rainfall did not occur in the absolute desert or at least was not recorded (Pfeiffer et al., 2021) but their impact through landslides arrived to the Central Depression, for instance, to the Pampa del Tamarugal, which allowed aquifer recharge (Houston, 2002).

2. The Dust cycle in the Atacama Desert

Atmospheric dust constitutes a large portion of the atmospheric aerosol loading (Kohfeld & Tegen, 2007) and here we define it as the set of aerosols of marine, pedogenic, lithogenic, biogenic, volcanic and anthropogenic origin emitted (and mixed) into the atmosphere during surface wind events. Aerosols correspond to the set of solid and liquid particles suspended in the atmosphere that, in fact, include dust. (Pöschl, 2005). The atmospheric dust loadings can be paired with different aerosols sources such as sea spray, volcanic eruptions, industrial emission, fire debris, secondary aerosols and cosmic dust (Pye, 1987), and even microorganisms (Griffin, 2007). Due to the varied origin of these particles, the different processes to which they have been subjected, and the geographic location of sources, dust differ in particle size, grain shape, composition, and mineralogic properties (Choobari et al 2014). With particle diameters in the range of $1 - 10^5$ nm (Pöschl, 2005), these particles include from freshly nucleated clusters containing a few molecules to crustal soil dust particles (McMurry, 2000).

The global dust cycle, e.g., described by Shao et al. (2011), includes five major stages: (1) entrainment of soil particles into the atmosphere, (2) atmospheric transport, (3) eolian transformation, e.g. through mixing with other aerosol types, (4)

deposition, and (5) the particle stabilization, e.g. through chemical binding of clay minerals. This cycle involves a range of processes occurring on spatial scales from local to global and on temporal scales from seconds to millions of years. In South America, dust sources are centered especially to the east of the Atacama Desert (Bolivian Altiplano), the coastal desert of Perú and Chile, and the Andes and Patagonia in Argentina (Marx et al., 2018); the so called arid diagonal (Saukel et al., 2011).

Compared to other regions, the Atacama Desert is a minor contributor to the global dust budget quite unlike North Africa (Ginoux et al., 2012). This may be explained by the topography of the Atacama, which resembles a set of elongated bowls of different sizes, positioned west-east and to different elevations, limited by high mountain ranges that act as natural dust traps, forcing the rework – or remobilization - of the deposited material (see Fig. 2). In consequence, the dust cycle here has mostly a local reach and is almost isolated from the global cycle with some episodic exceptions such as the entrained dust plume from the Atacama Desert occurred in July 2016 and analyzed by Reyers et al (2019).

The dust cycle in the Atacama Desert is represented in the Fig. 2. In this, it is possible to observe that dust entrainment is produced by near surface winds and dust devils (where the latter are frequently observed in the Central Depression, see Fig. 4) that mobilize or suspend particles of soil, salar playas and sediments (see section 2.1 and 2.2). The transport of this material relies on the local wind circulation that generally is from west to east and vice versa (Li et al., 2019; Wang et al., 2014), following more complicate paths in valleys (see section 3). During aeolian transport,

999 dust is mixed with water particles, sea salts and organic compounds contained in the
1000 recurrent coastal fog (see section 3.3), e.g., within the fog influence zone (<1200 m
1001 a.s.l.) and may be deposited wet during the night and early mornings, before fog
1002 evaporates and dissipates. Nevertheless, we infer that dry deposition is the general
1003 mechanism for dust settling because of the limited penetration of fog inland. In
1004 addition to primary aerosols, secondary aerosols are produced and deposited inland,
1005 i.e., particles formed locally by atmospheric chemistry (e.g., nitrate and sulfate
1006 compounds from gaseous oxide precursors; Michalski et al., 2004) that settle and
1007 accumulate in soils. From the east, wind-eroded soils in the Altiplano and Puna
1008 contribute dust, which is likely to have higher concentrations of organic compounds,
1009 nutrients, and microorganisms due to the greater abundance of plants, while the
1010 volcanic contribution is occasional and limited. Also, in this higher zone, wet
1011 deposition of dust is more feasible due to the more recurrent precipitations and the
1012 washout produced by summer showers, the so-called “Altiplanic winter”. Once dust
1013 is deposited, the material is accumulated or remobilized (reworked) by winds usually
1014 within the margins of the Atacama.

1015 The relevance of the deposition process lies in the fact that it is the atmospheric
1016 particulate material that is deposited dry or wet on desert soils that initiate
1017 pedogenesis (Ewing et al., 2006; Wang, 2013; Wang et al., 2014) and has been
1018 indicated as the source of nitrate, sulfate, and chlorides, among others, in the
1019 Atacama Desert (Ericksen, 1981; Rech et al., 2003). Nitrates are probably the result
1020 of the long-term accumulation of secondary aerosols produced in the atmosphere,
1021 while the sulfates would have a component derived from the marine influence

through the fog, the same as for chloride, at least in the zone of marine fog influence, and by the re-mobilization of halite from soils and salars in the Central Depression (Voigt et al., 2020). These salts are long-term accumulated under hyper arid conditions that provide minimum runoff and reduced leaching of the Atacama soils (Ericksen 1981; Ewing et al. 2006; Michalski et al. 2004).

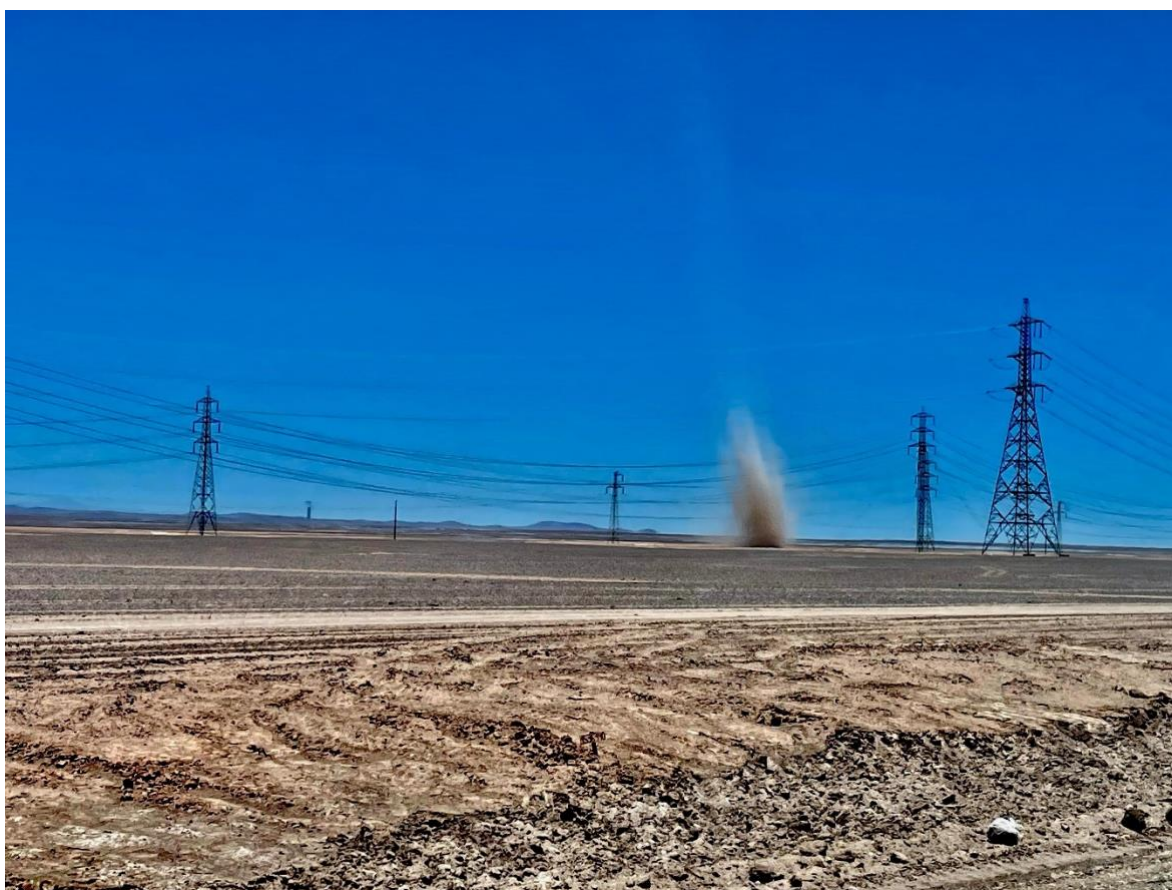


Figure 4. Dust devil spotted in the Central Depression within the Maria Elena district at 13:43 local time. Several dust devils were observed along several kilometers in the area. For reference, electricity towers in the picture are about 25 m high.

2.1. Entrainment of Dust and its Sources in the Atacama Desert

1032 Dust entrainment or emission is the process by which fine particles are emitted from
1033 soil surfaces by strong winds, which typically occurs in regions of sparse or no
1034 vegetation (< 15% vegetation cover) (Kohfeld & Tegen., 2007). Because of water
1035 scarcity, much of the Atacama Desert is almost entirely deprived of plants, making
1036 the surface soils prone to wind erosion. Despite this, dust storms are rare in this
1037 desert (Reyers et al., 2019).

1038 Ginoux et al. (2001) describes potential dust sources in the Atacama Desert. Their
1039 model assumes that in areas with pronounced topographic variations, sediments
1040 available as dust sources are primarily accumulated in valleys and depressions. For
1041 each 1° x 1° grid cell a source function S is obtained which represents the
1042 topographic contrast in the 10° x 10° surrounding area of that grid cell by means of
1043 the maximum and minimum elevation. This source function represents the erodibility
1044 factor at every grid cell, and only land surfaces with bare soil are considered as
1045 possible dust sources. Note that only major valleys are identified as potential dust
1046 sources by this approach, while small-scale features like canyons are not captured
1047 realistically. Fig. 5 shows the results of the potential dust sources in the Atacama
1048 Desert. Due to the topographic features, potential dust sources are restricted to
1049 some areas in the Central Depression and to near coastal plateaus in Northern Chile
1050 and Southern Peru, while Precordillera and the Andes itself are not considered as
1051 dust sources. North of the Loa River, the topography of the area have distinctive
1052 features as the plateau-like relief formed by sedimentary material, which explains
1053 the relative regularity of its topography. Also, this unit is bounded to the west by the
1054 Coastal Cordillera, which appears as a walled cliff at the sea with an approximate

1055 elevation of 300 meters and occasionally connect with the coastal platform, a feature
1056 that is incised by the drainage of large regional ravines in the form of big canyons
1057 (Quezada and Cerda, 2003). Thus, easterlies in this area may face less obstacles
1058 than south of the Loa River to produce dust plumes as the described by Reyes et
1059 al (2019). However, the dust source function is generally low for the area of interest
1060 when compared to other major deserts of the world, like the Sahara or the
1061 Taklimakan Desert, for which values of more than 0.4 are reported (Ginoux et al.,
1062 2001). According to the model results, it is possible to observe that major potential
1063 dust sources are located in northern Atacama, between 17 and 19 °S, where the
1064 (dimensionless) erodibility factor index is 0.1 (out of 1).

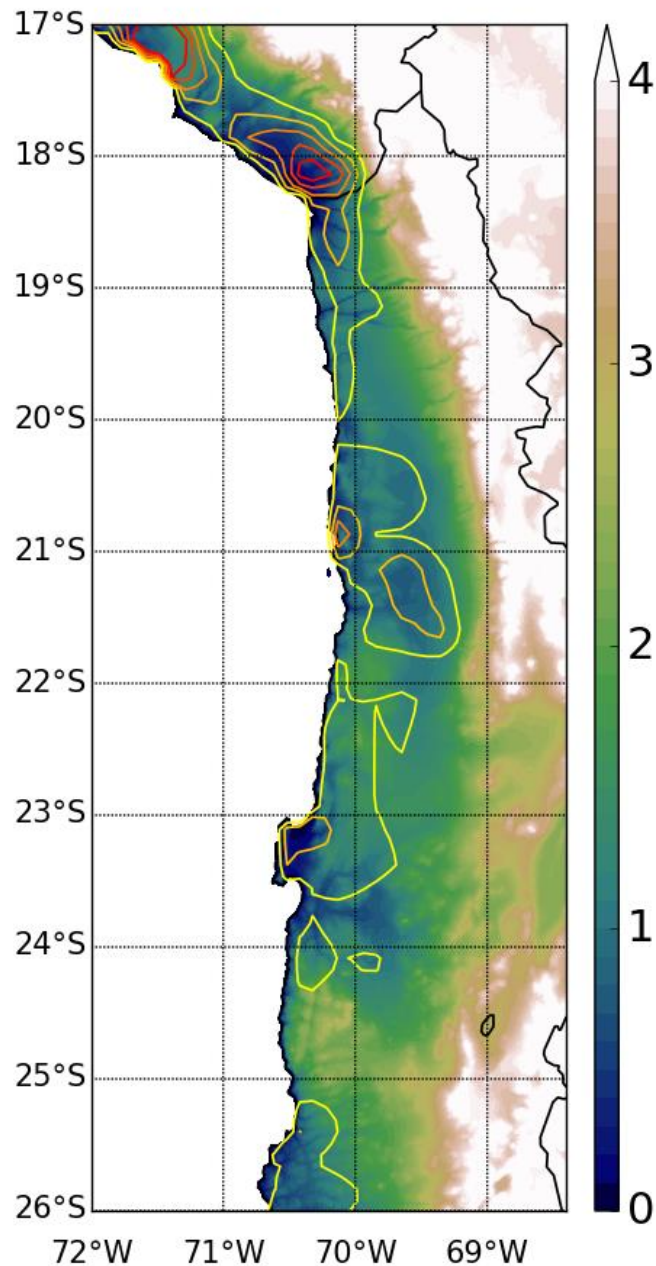


Figure 5. Orography (colored scale at right; in km) from the ETOPO1 Global relief model of the NOAA and the dust source function (S) as obtained by the model of Ginoux et al. (2001). Contours, ranging from 0.02 in yellow to 0.1 in red, represent erodibility factor (0 to 1). For more information see main text. (Colors should be used)

As was mentioned before, the dust source function of Ginoux et al. (2001) only considers topographic features, whereas soil erodibility additionally depends on other factors regarding the landscape and soil properties. The potentially erodible area of a landscape is controlled by the density of plants and other roughness elements such as cobbles or boulders, while soil erodibility is controlled by intrinsic properties of soils, such as the clay fraction, and the combined influence of temporal soil properties of moisture, aggregation, surface crusting and the availability of loose erodible material (Webb and Strong, 2011). The content of clay size particles in a soil (grain size distribution) is a relevant factor since its presence favors the particle cohesion and lead to the formation of aggregates, while the soil organic matter and moisture content affects the aggregates stability (Goudie and Middleton, 2006). Moreover, some other soil surfaces such as desert pavements, soil crusts, and high mass objects arranged on the topsoil can make erodibility even lower. Desert pavements consist of a one- to two-particle-thick layer of closely packed, angular to sub rounded gravel. They are one of the more prominent soil surfaces of arid regions (McFadden et al. 1987) and have developed in the Atacama Desert (Ericksen 1981). For instance, Berger and Cooke (1997) reported well developed stone pavement over alluvial fans across the Atacama Desert: in the Salar de Navidad (600 m a.s.l.), Salar de Atacama (2300 m a.s.l.) and Aguas Calientes Norte (4350 m a.s.l.).

While the full diversity of soils in the Atacama Desert is not fully understood, Finstad et al. (2014) provides an overview of typical features of geomorphic surfaces widespread in this desert. In that research, the authors described two distinctive pedohydrological regimes: (i) alluvial fans and related terraces dominated by sparse

1094 downward soil water movement, and (ii) dry lake beds or nearby environs impacted
1095 by the upward migration of waters driven by evaporation; both cases with salt crust
1096 near the surface.

1097 For alluvial fans, Finstad et al. (2014) selected a well-drained soil in a post-Miocene
1098 alluvial fan in the Yungay area (~24°S) previously reported by Ewing et al. (2006),
1099 considering that rare rainfall events occurred over the past millions of years have
1100 distributed atmospheric-derived salts in the soil profile. Ewing et al (2006) described
1101 the upper 146 cm of the pit as gypsum/anhydrite sequence overlying an indurated
1102 halite zone. In the first 39 cm of the soil profile, the concentration of gypsum exceeds
1103 that of anhydrite, suggesting wetter conditions likely due to fog precipitation, while
1104 below 39 cm and down to the halite profile, anhydrite is dominant.

1105 Along the soil profile, petrogypsic horizons (39-71 cm), followed by gypsic (71-85
1106 cm), gypsic-salic (85-102 cm) and salic (102-122 cm) horizons were found, over the
1107 halite horizon. More recently, Pfeiffer et al (2021) examined the “Ewing’s pit” in
1108 Yungay and described a post-2015-rainfall soil profile consisting of an incomplete
1109 desert pavement overlaying a ~15 cm thick layer of low density (bulk density ~ 0.7 g
1110 cm⁻³), highly porous anhydrite polygons with aeolian dust concentrated in the
1111 polygon interfaces. Below that, gypsum/anhydrite polygons of much higher density
1112 and width extend to a >1 m depth. The porous material can retain the recent
1113 deposited atmospheric dust which add clay-size particles to the soils. XRD analysis
1114 performed by Ewing et al. (2006) indicated that the silicate dust (0.2–2 and 2–20 µm
1115 fractions) in deposition samples contained smectite, chlorite and kaolinite. This
1116 constant input of fine mineral particles, along with the development of desert

pavement (Ewing et al., 2006) and salt crust (Davila et al., 2008) may enhance the stability of the Yungay and analogue regions within the Atacama Desert reducing the wind erosion and, in consequence, dust entrainment. Moreover, hillslope sites within the hyperarid core examined by Pfeiffer et al (2021) tend to have similar features to Yungay soils (pavement, soft porous anhydrite polygons), although the thickness and continuity of the sulfate layers is lower than on level alluvial fan surfaces. Additionally, the development of vesicular (Av) horizons (see Fig. 6) and crack polygons diminishes the available material (salt, silt, coarse sand, volcanic parent material, etc.; Howell 2009) to be entrained by the migration of particles underground. A set of pictures of Yungay soils is given at Figure 6. The second case given by Finstad et al (2014) corresponds to soils from the Salar de Llamara (~21°S), which represent a short chronosequence between Pleistocene and mid-Holocene. Two soils were examined where both have an indurated salic horizon at the surface comprised almost entirely of halite, with thicknesses ranging from 22 to 51 cm. These crusts, formed by the aggregation of soil particles, enhance the surface roughness and in consequence lessen the erodibility of the soil by winds and thus the dust entrainment.

After a rain event in the Atacama Desert in 2015 (see section 1.4), soil surfaces did not collapse and maintained high rates of infiltration, but measurable physical and chemical changes occurred (Pfeiffer et al., 2021). Aguilar et al., (2020) calculated a mean erosion of 1.3 mm caused by the individual extreme storm. According to Pfeiffer et al (2021), after the rain stopped, soil surfaces were harder and more compact, less erodible, and with a higher bulk density. Moreover, a thin layer of

1140 efflorescence salt composed by gypsum, bassanite, and thenardite formed by the
1141 penetration of the rainfall into the surface, and the upward migration of more soluble
1142 NaSO_4 from the large CaSO_4 matrix occurred. Less than a year later of the rain
1143 event, the accumulation of gypsum in soil surface was less, and likely disrupted by
1144 wind deflation and/or fog influences. Gypsum presence is explained by the
1145 conversion from hydrated anhydrite, along with bassanite, and/or through anhydrite
1146 dissolution and reprecipitation as bassanite and gypsum (Shen et al., 2020). These
1147 changes in the gypsum/anhydrite concentrations are also supported by Voigt et al
1148 (2020), who later found gypsum on the surface soil where anhydrite used to
1149 dominate prior the rain event, as shown by several authors (Pfeiffer et al., 2021 and
1150 references therein).

1151 Added to salt crusts, biological soil crusts (BSCs) have been developed in the
1152 Atacama Desert, along with vegetation patches. BSCs are living consortia of pioneer
1153 species in hostile environments such as cyanobacteria, green algae, lichens, and
1154 mosses, whose development provides physical protection against wind erosion,
1155 leading to thickened loose soil profiles beneath the crust (Wang, 2013; Wang et al.,
1156 2017). Widespread BSC communities were identified in a remote valley in the
1157 Atacama Coastal Cordillera, in the southern margin of the Salar Grande ($\sim 21.22^\circ\text{S}$,
1158 69.90°W , ~ 800 m a.s.l.), a basin filled with massive salt mineral deposits. Moreover,
1159 vegetation occurrence is limited in the Atacama, being mainly restricted to fog oases
1160 in the coastal desert, and aquifers and rivers in the Central Depression and pampas,
1161 excluding the Puna vegetation. In the Central Depression, there are established
1162 plant communities such as the tropical thorn forest dominated by *Prosopis tamarugo*

1163 *Phil.* (Garrido et al., 2018) in the Pampa del Tamarugal basin and further plant
1164 communities in the ravines and intermittent waterways around and northwards the
1165 Loa River. Tillandsia vegetation is present over the Coastal Cordillera indicating fog
1166 presence due to their dependence on atmospheric water supply (see section 3.3.1).

1167 Finally, another soil feature of the Atacama that may reduce dust entrainment, and
1168 in consequence dust outbreaks, are the undulating surface (stress) fractures that
1169 also serve as topographic lows that concentrate cobbles/boulders and coordinate
1170 into a polygonal network, i.e., patterns visible at the ground. These cracks of several
1171 tens centimeters of width and few meters of diameter offer natural shelters to salt,
1172 sediment, and surface clasts that fill the voids. The center of the polygons, a few
1173 centimeters below the edges, also exhibits a micro-relief adding microtopographic
1174 complexity to the smooth landscape (Howell, 2009). Fields of boulders are common
1175 around bases of hills in the Atacama Desert and has been suggested that their
1176 transport is triggered mainly by the regular seismic events (Matmon et al., 2015;
1177 Quade et al., 2012; Sager et al., 2020). Several clusters have been reported along
1178 the Atacama Fault, e.g. in Sierra del Buitre (~23.5°S) (Quade et al., 2012); many
1179 clusters in the Yungay area (Matmon et al., 2015; Navarro-González et al., 2003)
1180 and the here reported boulder fields in the Pampa Remiendos; an elongated north
1181 south oriented zone of ca. 1 ha by 24.24°S and 70.28°W. These rock fields represent
1182 obstacles for dust mobilization and may force the fast deposition of material.

1183 In order to characterize the wind erosion process in the coast of the Atacama Desert
1184 around Mejillones Peninsula (23°S), Flores-Aqueveque et al (2010) analyzed data
1185 from sediment traps and from a field experiment performed over the flat

1186 geomorphology of the area. With this data and using the model proposed by
1187 Marticorena and Bergametti (1995), the authors computed a threshold friction
1188 velocity for soil erosion of 0.31 m s^{-1} , which was exceeded only during a small
1189 fraction of the whole measurement period and always during the afternoon when a
1190 peak in the S–SW winds occurred. It should be noted that this research is dedicated
1191 to the study of sand mobilization and used samples from 17 sites representing the
1192 varied soil surfaces from rich gravel soil and partially encrusted to others more prone
1193 to wind erosion, in order to represent the pampa surface heterogeneity. They also
1194 found that the wind-erodible fraction of these soils (particles with diameter < 840
1195 μm) was always a mixture of at most three lognormally distributed populations of
1196 sand grains (Alfaro et al., 2011). The protecting effect of non-erodible elements was
1197 considered by the mean of the overall soil roughness. Complementarily, Alfaro et al.
1198 (2011) proposed a model for the uptake, transport, and deposition towards the bay
1199 of wind-eroded mineral particles in the same area as the Flores-Aqueveque et al.
1200 (2010) study.

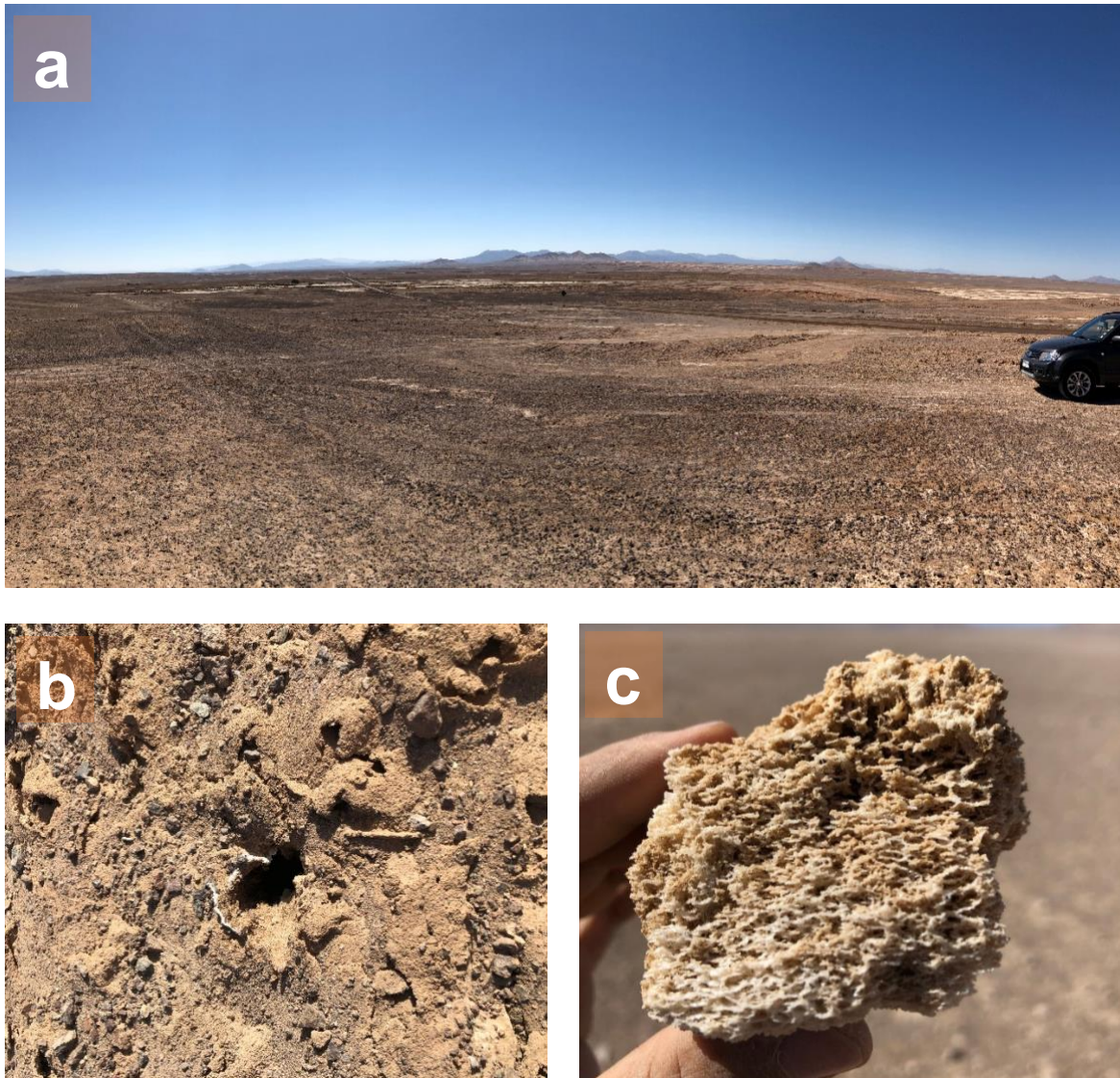


Figure 6. Soils of Yungay area. At the top (a) is shown a panoramic view of Yungay surface soil near the “oasis”. It is possible to see the major development of soil pavement. To the left, at the bottom (b), a photograph of the soil surface with pavement and vesicles development is given. Also note the inflated surface around the central vesicle. To the right (c), a photograph of a salt structure is given. These kind of structures near the surface at 5 cm depth in the Yungay area, near the studied pit by Ewing et al. (2006).

2.2. Origin of aerosols deposited in the Atacama Desert Soils

Due to the size, concentration, and uniqueness of the salt deposits in the Atacama Desert, their origin has been studied for decades, being the deposition of aerosols and their long-term accumulation in the soil suggested as one of the main mechanisms of dust and salt supply to this landscape (Berger and Cooke, 1997; Böhlke et al., 1997; Ericksen, 1983; Ericksen, 1981; Ewing et al., 2006; Grousset et al., 2003; Jiao et al., 2018; Michalski et al., 2004; Pfeiffer et al., 2021; Rech et al., 2003; Reich and Bao, 2018; Voigt et al., 2020; Wang et al., 2017, 2014). Hence, aerosols deposition is closely related to the occurrence of the widespread salt deposits in the Atacama. Moreover, it has been suggested that the local distribution of salt deposits are largely a function of remobilization of existing salts by occasional rainfall (Michalski et al 2004), aeolian transport (Berger and Cooke, 1997), capillary action (Mueller, 1968), groundwater discharge, possibly hydrothermal reworking (Pueyo et al., 1998), and sedimentation (Michalski et al 2004).

Among the main atmospheric salt inputs, the following have been suggested: aerosols with extra-local origin (nitrate, iodate, perchlorate) (Böhlke et al., 1997; Claridge and Campbell 1968; Ericksen 1981), direct volcanic emissions (sulfates) (Berger and Cooke, 1997; Oyarzun and Oyarzun, 2007), and marine aerosols coming from the Pacific Ocean (nitrates, sulfates chlorides and iodates) (Ericksen 1981, Rech et al. 2003). In addition, anthropogenic emission sources have also been identified such as copper smelters and other industries in the desert (Voigt et al., 2020; Wang et al., 2014).

1223 The atmospheric circulation helps to understand the spatial and temporal
1224 precipitation composition in the regional and local hydrological cycle (Valdivielso et
1225 al., 2020). Therefore, the presence and composition of aerosols entrained in the rain
1226 drops influence both surface and groundwater. In this sense, recently, it has been
1227 found that in the hyper-arid core, the deflation of the local salts from the Central
1228 Depression (sulphate rich paleosoils and highly soluble salts accumulation)
1229 contributes to the precipitation composition, and certainly in the groundwater
1230 composition, in the highest parts of the Domeyko Cordillera, over 3400 m a.s.l. and
1231 to the east of the Central Depression, discarding the marine aerosols contribution at
1232 this distance inland (Gamboa et al., 2019). To the north of the Salar de Atacama,
1233 the scarce precipitation comes from the north and northeast via the Amazon basin,
1234 and from the southeast via the Gran Chaco in summer. Whereas, the winter
1235 precipitation is largely sourced by frontal systems originating from the Pacific in form
1236 of snow, their effect on aquifer recharge has been discussed (Valdivieso et al., 2020
1237 and references therein). Urrutia et al (2019) estimated that snow is an important
1238 input flow to the hydrological system in winter, while Moran et al (2019) considered
1239 that aquifers are not recharged, because there is sublimation (between 20 and 30%),
1240 and there are no permanent seasonal ice fields. However, as will be discussed later
1241 in this section, snow and glacier ice from the Andes are capable of accumulating
1242 salts and thus recharging water bodies. The transport and deposition of the local salt
1243 aerosols also contribute to the chemical composition of the rain and watercourses in
1244 other hyper-arid regions (Jódar et al., 2020).

According to Michalski et al. (2004), the major part of nitrates and other soluble salts found in soils of the Atacama Desert are the result of the aerosol deposition produced by photochemical conversion of gas-to-particles processes, i.e., secondary aerosols, and as a minor contribution, marine aerosols and local land sources. Other studies using stable isotope supported this idea (Bao and Gu, 2004; Böhlke et al., 1997). For instance, Rech et al (2003) and Cosentino et al., (2015) using S and Sr isotopes demonstrated a strong influence of marine aerosols on soil gypsum/anhydrite development, although this effect was limited to areas where sea spray penetrates 90 km inland (Rech et al., 2003), below 1000 m a.s.l. (Del Río et al., 2018) (see section 3.3). For higher lands, where soils contain higher levels of nitrate, perchlorate, and iodate, the authors stated that these were produced by the extensive aeolian reworking of salar flats in the Atacama and the Altiplano, and were indicated as the main source for Ca and S. Additionally, these authors support the idea of a tropospheric N input since the spatial distribution of high-grade nitrate deposits appears to correspond with areas that receive the lowest fluxes of local marine and salar salt. Marine aerosols may be comprised by sea salt constituents, inorganic S (Rech et al., 2003) and N (Michalski et al., 2004), organic C and N, as well as Ca and inorganic C from degradation of marine invertebrates shells (Moore and Blough, 2002). Michalski et al (2004) estimated that the larger deposits of salts in the Atacama Desert have been accumulated from atmospheric depositions in a period of 200,000 to 2 million years under similar arid conditions to present-day.

Regarding the deposition of aerosols in the Central Depression, several authors have indicated that hillslopes and soils within the hyperarid core tend to

accumulate salt and dust from atmospheric depositions (e.g., Cosentino et al., 2015; Ewing et al., 2006; Medialdea et al., 2020; Owen et al., 2013; Pfeiffer et al., 2021). Furthermore, active aeolian deposits were documented south of Pica (20.5°S, 69.3°W), around Quebraba Infiernillo, and Longacho and Chintaguay Flexura (20.6 °S), where Blanco and Tomlinson (2013) reported well-sorted sands in unconsolidated condition, medium to coarse-grained, composed mainly of sub-spherical volcanic and plutonic detritic grains, and monominerals of delphosphate, quartz, pyroxene, amphibole and epidote, rich in magnetite (5-10%). Among these deposits, crescentic, mantle, longitudinal, and transverse dunes were observed. Another modern dunes were reported by Cosentino and Jordan (2017) between 20 and 21.5 °S within the Central Depression (PdT) and at the Coastal Cordillera. Besides, Vásquez et al (2018) reported siliciclastic alluvial playa sediments from aeolian and evaporitic processes around the Salar de Llamara area. Some old aeolian deposits were also reported in the same geological location, usually more to the east of 69.20°W but also close to the Central Depression. These Upper-Miocene to Pliocene deposits were described by the authors as medium to coarse, well-sorted, rounded sandstones, with planar or trough cross-stratification, in metric-scale sets. They are intercalated in the piedmont deposits or are located at their base.

Another work on aerosol deposition is from Pfeiffer et al (2019) reporting hydrated CaCl₂-rich soils that formed ~ 50-cm-thick aeolian material deposits over a layer of indurated halite in a narrow gorge between the Cerro Soledad and Cerro Salar to the west of the Salar de Llamara. Soils were relatively moist in this region, with a

1291 measured surface water content of 12.6 wt% (mass percentage concentration),
1292 decreasing to 5.9 wt% at 40 cm depth. The authors suggested that probably fog is
1293 responsible for these wetter conditions, which causes a vertical gradient in the
1294 available water in the soil profile. The wet surface stabilizes the soil surface and acts
1295 as a dust trap, allowing dust deposits to accumulate.

1296 To the west of the Central Depression, an interesting phenomenon occurs in the
1297 west of the Salar de Carcote (or Salar de San Martín) at 21.36°S. Ericksen and Salas
1298 (1990) reported the existence of gypseous ramparts in this salar, which consist of
1299 low ridges formed by nodular gypsum of 50-100 cm high, formed by the deposition
1300 of wind-borne aerosols and the subsequent evaporation of water. Additionally, they
1301 found gypsum dunes on the lee side of several salars in the Andean Highlands,
1302 produced by wind deflation of newly deposited saline material on the salar surfaces.

1303 Analyzing soils of the Atacama Desert to study atmospheric particles and the
1304 atmospheric deposition phenomenon has uncertainties due to the scarce knowledge
1305 of (1) aerosol deposition rates in this desert, (2) transformations of dust particles and
1306 salts once deposited on the soil, (3) concentrations in the atmosphere of colloids or
1307 very fine particles difficult to settle, (4) impacts of ongoing human activities that
1308 generate aerosols, (5) processes across geological time scales including
1309 paleoclimate, and others. One difficulty is that material forming the soils and
1310 transported to the region by the atmosphere has been accumulated over long time
1311 periods. For instance, Ericksen (1981) suggested that the accumulation of saline
1312 materials from the atmosphere in soils may have started in the middle Miocene (10-
1313 15 Ma), and continued until today.

Modern aerosol depositions in the Atacama Desert can be directly observed, but there is no dense measurement network for routine observations of aerosol deposition. This is not specific to the Atacama Desert, but a typical limitation for largely uninhabited desert regions worldwide. Deposition measurements rather stem from field campaigns and instruments installed for a limited time period (Zheng et al., 2017; Figgis et al., 2018; Wang et al., 2020). To date, there is no systematic dust deposition data acquisition or available datasets that allow for more exact representation of the deposition rates in the different seasons of the year and for periods of climatic variations in relation to for example ENSO events. A few studies collected and analyzed the atmospheric depositions in the Atacama Desert (Li et al., 2019), with Ewing et al. (2006) being the first one describing depositions in the Atacama . The authors quantified the deposition rates of major ions (Na^+ , Ca^{2+} , NO_3^- , Cl^- and SO_4^{2-}) at three sites along a 300 km north-south transect in the Central Depression, and observed significant spatial variations in ion depositions. From north to south, the sampling locations were Yungay (24°S) within the hyperarid core, Altamira (25.5°S), and the southernmost location nearby Copiapo (27.3°S), where the latter represented the semi-arid transition. In Yungay, a deposition rate of $4 \pm 2 \text{ g m}^{-2} \text{ year}^{-1}$ was measured by the authors and at all sites. They found evidence of both marine and salar-derived solutes in atmospheric depositions to the soils, as well as silicate dust inputs containing clay minerals. In this case, water-soluble salts comprised $44 \pm 15\%$ of total airborne particle mass. Moreover, Na and Cl accounted for 10–15% of total mass in air and dust samples, suggesting a significant sea salt component in soils (20– 30%).

Although the Coastal Cordillera works as a barrier that limits the entry of marine primary and secondary aerosols into the Central Depression, aerosols pass through ravines that connect the hyper arid core with the coast, and eventually settles in the desert. It was considered by Michalski et al. (2004) that the main component of marine aerosols reaching the desert surface were likely particles roughly 1 μm in diameter or smaller, where the submicron fraction was readily entrained into the free troposphere. Once there, smaller particles can be transported over great distances, and can grow during cloud processing to micron size particles that are then removed by deposition. Considering this, Ewing et al (2006) took air samples at a coastal site and compare it with the inland sampling locations. The authors found that coastal airborne particles had about 10-fold more Na and Cl in the coarse fraction, which suggests that 90% of coarse sea salt may be deposited during the transport of airborne particles inland. Close to Yungay, Owen et al (2013) set three passive collectors at Oficina Rosario, 70 km to the southeast of Yungay. After two years of dust collection, they calculated a mean deposition rate of $3.6 \pm 0.4 \text{ g m}^{-2} \text{ year}^{-1}$. Moreover, deposition rates of NO_3^- , Cl^- , and SO_4^{2-} were significantly lower than the calculated by Ewing et al (2006) at Yungay, with the rate of sulfate deposition ($0.554 \pm 0.013 \text{ g m}^{-2} \text{ year}^{-1}$) being the largest. In contrast, the ratio of silicate material to soluble material was larger than Yungay's, but still comparable. This difference, explained the authors, is due to different geographic settings which control fog movement inland, as Yungay is a valley that crosses the Coast Range and provides a route for fog advection, whereas Oficina Rosario is located on the lee side of a laterally-continuous section of the Coast Range which blocks fog from moving inland.

Another study by Wang et al. (2014) set up ten dust traps along a west-east transect (23°S) (MT) from the Mejillones Peninsula (~23°S, 70.5°W) to the Andean plateau (~23°S, 67.5°W). The authors reported the chemical, mineral, and nitrate isotopic compositions of atmospheric deposition, and found an abrupt decline in the Na⁺ or Cl⁻ deposition between the first and second trap located at the west and east of Coastal Cordillera, respectively. Nevertheless, they found no clear trends for Na⁺ distribution inland showing that Na inputs were not exclusively from marine origin. In addition, the authors underline the importance of anthropogenic sources due to industrial activities related to the production of NO_x and the erosion of soils produced by off-road vehicles and surface mining in the case of CaSO₄. At the coast, SO₄²⁻ came not only directly from seawater but also likely from atmospheric transport. They also explain that it is associated with the oxidation of SO₂ in the atmosphere into sulfate by OH radicals, H₂O₂ and O₃. Furthermore, Li et al. (2019) supported Wang et al (2014) results and also found greater deposition rates of insoluble particles ranging from 3.8 to 149.0 g m⁻² year⁻¹, and a high interannual variability on soluble salts and insoluble particles which was attributed to changes in winds. A recent study by Voigt et al. (2020) focused on the spatial distribution of sulfates, chlorides, and nitrates in the Atacama Desert soils, along three west-east transects at 19.5°S, 21°S and 24.5°S. The authors indicated that chloride derived from sea sprays are the main natural source of Cl and Na, although wind erosion and salt re-deposition from salars are also included as a minor and local source for Na and Cl. Additionally, they suggested a large impact of anthropogenic emissions regarding exceptionally high Na/Cl ratios in present-day aerosols analyzed by Wang et al. (2014) and Li et al. (2019). Li et al. (2019) determined changes in aerosol depositions in the Atacama

between two periods of sampling, 2007–2009 (Wang et al., 2014) and 2010–2011, where the deposition of dust (insoluble particles) increased by 3.6 times over time in the Andes, emphasizing the importance of a long-term monitoring of insoluble dust fluxes.

A latter experiment were performed by Azua-Bustos et al., (2019), who evaluated aerosol deposition along two west-east transects starting near Iquique (20°S) and Tocopilla (22°S), and ca. 63 and 51 km long, respectively. Each transect considered three sampling points, and the Iquique transect (IT) had three sampling dates, while the Tocopilla (TT) only two. At each sampling point, ten empty Petri dish plates were left to assess the amount of dust arriving at each site/date. From the published results, it is possible to observe that within both transects, mean dust mass captured was larger than 4 g m⁻² during the sampling period of one day on June 30th and August 30th, and October 27th in IT and TT, respectively. Although, an important intra-plate variability was reported, the authors found that the amount of dust arriving at each site of the IT was up to four times higher in the afternoon hours, which is coincident with the time of the day at which winds have been reported to be stronger in the hyperarid core. These results indicate differences in calculated atmospheric deposition rates in the Atacama Desert from those reported by Wang et al., (2014) and Li et al (2019) (MT), with annual deposition rates above 5 g m⁻² year⁻¹ and 4 g m⁻² year⁻¹, respectively, at similar sampling sites. Moreover, Ewing et al (2006) reported a deposition rate of 4 ± 2 g m⁻² year⁻¹ within the hyper arid core, 50 km far from the coast (at Yungay, 24.1 °S), and Owen et al (2013) indicated a 3.6 g m⁻² year⁻¹. These apparent discordances can be explained by several reasons. Firstly,

the method of collection differs. All mentioned works, excepting Azua-Bustos (2018), stated the use of metal passive dust traps mounted in a distance of at least 1 m from the ground surface, in order to avoid the accumulation of saltating sand. It is not clear whether Azua-Bustos et al (2018) collected dust at ground level or higher. Also, the location of TM is further south (>50 km) than TT, as well as Yungay and Of. Rosario, and the relief conditions are different in the 3 transects (IT, TT, MT) and at Of. Rosario. For example, the IT is located on a plateau-like area, due to the change of topography south and north of the Loa as explained in section 1.2, with a cliff facing the Pacific, while in the TT, a ravine connects the coast and the inland desert, and finally, the MT sites are located behind the coastal range. These topographic differences may influence aeolian dynamics and consequently atmospheric deposition. Furthermore, there may be differences also in the availability of material to be suspended, in addition to the year-to-year changes indicated by Li et al (2019). Further research is needed to better understand these differences.

The chemical composition of the dust particles is very varied and contains both organic and inorganic compounds which are of natural and anthropogenic origin (Azua-Bustos et al., 2019; Barraza et al., 2021; Ewing et al., 2006; Li et al., 2019; Wang et al., 2014). In the case of the Atacama Desert, it would be expected that the inorganic components would mostly be of natural origin related to the mineralogical components of the soil, and to a lesser extent comprise of organic compounds due to the scarcity of vegetation, with also some type of anthropogenic contribution due to the significant mining activity in the region. However, the content of salts in deposited aerosols has a greater relevance since it has been proven that it can be

transferred to groundwater via atmospheric washing and thus recharging aquifers because of rains and snow melting (Gamboa et al., 2019; Voigt et al., 2020). The composition of atmospheric deposition was studied by Wang et al (2014) (among others) who indicated that the major mineral (>5% by mass) assemblage in atmospheric bulk deposition in a transect from the coast to the Andes sites was anorthite–quartz–albite–gypsum. Moreover, the atmospheric load deposited along the same ten dust traps was rich in Cl^- , NO_3^- , SO_4^{2-} , Na^+ , and Ca^{2+} , which totaled over 90% of the dissolvable salt mass, with small amounts of NH_4^+ , Mg^{2+} and K^+ cations. Complimentary, Li et al (2019) obtained coincident results where deposition rates of soluble salts ranging from 0.2 to 6.0 g m⁻² yr⁻¹ and displayed a general decreasing trend from the coast to the Andes. Further south, Barraza et al (2021) studied the aerosol deposition in the Tapado Glacier. Their results showed that in this point of the Andes Cordillera, the sources of major soluble ions were still aeolian dust (38%) from the Atacama Desert (including mining sites), together with natural weathered sulphates (27%), anthropogenic nitrates (25%), and coastal aerosols (10%). The major ion load of the winter snowpack is dominated by Ca^{2+} (60%), SO_4^{2-} (16%) and NO_3^- (13%), and there is little influence from marine air masses at the site, with most SO_4^{2-} , Mg^{2+} , Ca^{2+} and Na^+ , derived from non-sea salt sources (Sinclair and MacDonell, 2016)

3. Transport and Deposition of Dust and Aerosol in the Atacama Desert

The transport of materials driven by wind action plays an important role in desert systems where it represents the predominant input of exogenous material (Wang 2013; Wang et al. 2014). Once deposited, soluble salts accumulate due to the hyper aridity that affects this area along with insoluble dust, together generating soil deposits. In the following subsections transport mechanism and conditions that allow these phenomena are described in large and local scale, and finally the role of fog and the effect over the landscape and life are discussed.

3.1. Large-scale atmospheric processes driving aerosol transport and deposition.

The synoptic conditions in Northern Chile are dominated by a stable surface anti-cyclone over the subtropical Southeast Pacific (Garreaud et al., 2010) and a rather zonal westerly flow in the troposphere aloft due to a gentle south-to-north geopotential height gradient. However, different large-scale circulation patterns can disturb these dominating features. Using two-year wind measurements from a station at Sierra Gorda (~23°S), Jacques-Coper et al (2015) demonstrate that synoptic-scale winds connected with mid-tropospheric circulation patterns can influence or superpose the local near-surface wind systems. For example, the 5 % highest mean diurnal wind speeds and the 5 % lowest mean nocturnal wind speeds at Sierra Gorda are associated with mid-tropospheric geopotential height anomalies which are centered off the Atacama coast north of 30°S. These results indicate that the northwesterly flow at the foreside of troughs occurring far north over the subtropical Southeast Pacific reinforce the diurnal near-surface westerly winds and distinctly reduce the nocturnal easterly winds. Weakest westerlies during day, in

1474 contrast, occur in case of undisturbed synoptic conditions. A more complex picture
1475 is revealed when near-surface winds at different sites of the Atacama Desert are
1476 taken into account, as was done by (Reyers and Shao, 2019) who analyzed mid-
1477 tropospheric cutoff lows off the coast of the Atacama Desert. Cutoff lows are
1478 segregated troughs which form from deepening negative geopotential height
1479 anomalies. While for the near-surface wind at a station close to Sierra Gorda the
1480 impact of cutoff lows on the diurnal and nocturnal wind regime is similar to the
1481 findings of Jacques-Coper et al. (2015), an opposite synoptic forcing is found for the
1482 local wind system at a station located in a plain further south ($\sim 23.8^{\circ}\text{S}$), i.e. wind
1483 speeds are lower during day and slightly higher during night. At a station located at
1484 $\sim 25^{\circ}\text{S}$ cutoff lows facilitate reduced wind speeds throughout the day. Despite this
1485 heterogeneous forcing, it can nevertheless be concluded that upper-level cyclonic
1486 anomaly patterns over the subtropical Southeast Pacific may influence dust-emitting
1487 winds and deposition of aerosols in the Atacama Desert.

1488 In the morning hours of July 8, 2016, an unusual dust storm occurred over the
1489 Atacama Desert. To the authors' best knowledge, it is the only strong dust event that
1490 has ever been reported for the Atacama Desert. It turned out that this event was
1491 triggered by a particular temporal evolution of a mid-tropospheric trough west of the
1492 Atacama Desert (Reyers et al., 2019). When the trough approached the Andes it
1493 zonalised, thus leading to upper-level horizontal convergence over the Northern
1494 Atacama. Owing to mass conservation, these processes finally lead to a strong
1495 acceleration of the easterly downslope winds (for more details see Reyers et al.
1496 2019), which usually prevail during this daytime. At a near-coastal station in Northern

1497 Atacama (~18.8°S) wind speeds of more than 12 m s⁻¹ were observed during the
1498 event, whereas the average wind speed during winter is less than 3 m s⁻¹ at this site.
1499 Consequently, a dense dust plume was released and transported hundreds of
1500 kilometers west- and southwestwards. This event clearly shows that upper-level
1501 circulation patterns may be very important for landscape evolution and dispersion of
1502 microbial life via massive dust translocation. However, many questions are still open.
1503 For example, it is unclear where the emitted dust was deposited after this event, and
1504 there is large uncertainty about the frequency of occurrence of such events in the
1505 recent and the paleoclimate.

1506 The impact of the El Nino Southern Oscillation (ENSO) on near-surface winds in the
1507 Atacama Desert is found to be rather low. While for Central Chile strongly reduced
1508 and slighter increased wind speeds occur during El Nino and La Nina events,
1509 respectively, the effect of ENSO on wind velocities at stations north of 23°S is only
1510 weak (Watts et al., 2017). According to these findings, ENSO only marginally
1511 influences the dust cycle in the hyper-arid core of the Atacama Desert.

1512 North of the Atacama Desert, along the Pisco-Ica desert in Southern Peru (14°S),
1513 eventual dust storms develop 4 or 5 times per year, usually in the afternoons towards
1514 the end of austral winter (Escobar Baccaro, 1993; Quijano, 2013). These events are
1515 locally known as “Paracas” events and occur over the extremely dry coastal desert
1516 due to strong southerly winds along southern Peru, with typical speeds exceeding
1517 10 to 15 m s⁻¹, blowing from the South –Southeast (S-SE) (Briceño-Zuluaga et al.,
1518 2017). Using daily MODIS images, Briceño-Zuluaga et al (2017) identified 15
1519 emission days and more than 21 polygonal probable source-areas. The authors

reported 65 widespread independent plumes from different sources, suggesting that emission processes vary within a wide range of extension and intensity. As observed in MODIS images by Briceño-Zuluaga et al (2017), the coastal region of the Ica desert proved to contribute the most to active emission, with transport of this material northwestward towards the ocean, although a significant fraction of entrained material is transported into the continent over the Pisco-Paracas area (Gay, 2005). Briceño-Zuluaga et al (2017) results showed that dust loads follow alongshore equatorward trajectories according to the used model, and fine particles (3-10 μm) plumes spread northwestward (up to 300 km for the finer ones) from the emission sources. Moreover, they indicate that coarsest 90 μm particles reach up to 50 km downwind from the sources. According to the research results, the authors concluded that dust fluxes during Paracas wind events originate over the coastal zone, where strong winds forced by steep Alongshore (sea-level) Pressure Gradient (APG) develop. Synoptic-scale meteorological composites from NCEP/NCAR reanalysis data show that Paracas wind events (steep APGs) are mostly associated with the strengthening of anticyclonic conditions in northern Chile, that can be attributed to cold air advection associated with an incoming trough.

In order to evaluate directly the importance of recent wind-transported material in the eastern equatorial Pacific and its sources, Prospero and Bonatti (1969) sampled atmospheric dust during a cruise of RV Pillsbury in 1967, between 10°N and 15°S, and 115-80°W, in front of the coasts of Ecuador and Peru. The authors identified two sources of the collected material due to differences in the mineralogy of two groups of samples and wind regimes. They concluded that the supply of aeolian dust to

ocean sediments south of the intertropical convergence zone (ITCZ) is less than on its northern side. For the samples collected south of the ITCZ, they identified the Peruvian coastal desert and the Atacama Desert as the source regions. As low-level winds in these regions flow parallel to the coast, they are not conducive to the transport of dust far out to sea, which accounts for the lower collection rates ($0.14 \mu\text{g m}^{-2}$) when compared to the domain north of the ITCZ. A possible pathway of the Atacama depositions over the Pacific Ocean relates to the entrainment of dust produced by southern winds and their east (and upslope) inland components (Alfaro et al., 2011; Flores-Aqueveque et al., 2015, 2010; Garreaud et al., 2003; Muñoz et al., 2018, 2013; Reyers et al., 2019; Reyers and Shao, 2019) paired with the local relief, which allow dust incorporation in the atmosphere and then transported by the SE trade winds and distribute it above the ocean (Saukel et al., 2011).

A modern spatial pattern of aeolian-derived marine sediments in the eastern equatorial and subtropical Pacific (10°N to 25°S) was presented by Saukel et al (2011). The authors found that the two source areas for marine sediments in the Southeast Pacific Ocean, the coastal desert of Peru and the Atacama Desert in northern Chile, distinctly differ in the amounts of feldspars and chlorite. While quartz and feldspars, which are products of weathered volcanic rocks and physically weathered metamorphic rocks, are delivered from both source areas, feldspars are reduced off northern Peru, pointing to the Atacama as the major source. Another marker used by the authors is related to clay-mineral composition of sediments, in which illite is a robust indicator that continuously decreases in a northern direction, indicating that dust transport from the Atacama Desert dominates.

3.2. Local atmospheric processes driving aerosol transport and deposition.

In the Atacama Desert, wind erosion is associated with wind gusts (Flores-Aqueveque et al., 2010; Kurgansky et al., 2011). Field studies using dust traps along a west-east transect in the Atacama Desert (~23°S) reveal that atmospheric depositions in the inland region are mainly controlled by the local entrainment of insoluble dust and soluble salts (Wang et al. 2014; Li et al. 2019). This is because marine inputs are strongly reduced due to the blocking by the Coastal Cordillera (Rech et al. 2003), and the input from the Andes is low due to an upslope air flow which prevails at large parts of the daytime (Li et al. 2019). The primary local driver controlling the dust transport and deposition in the Atacama Desert is thus the near-surface thermally driven wind system, which is a result of the interplay of extreme insolation and the local topography, revealing a strong diurnal cycle. During daytime, the strong heating of inland surfaces generates a sea breeze with westerly winds in the hyper-arid Atacama Desert and upslope air flows at the Andes Cordillera (e.g. Jacques-Coper et al., 2015; Muñoz et al., 2018). These winds are further accelerated by the strong insolation effects at the western slopes of the Andes (“Andean pumping”; Rutllant et al., 2013). Consequently, strong near-surface westerly flows with wind speeds of up to 20 m s⁻¹ may be generated, not only at the Andes Cordillera but also in the Central Depression and in coastal valleys (Muñoz et al. 2018) and are thus potentially important for the entrainment of surface dust particles. At night, when the land surfaces are rapidly cooling, the wind regime shifts to easterly downslope winds. These downslope winds are particularly strong in broad valleys extending from the Andes to the lower plains of the Atacama Desert (Muñoz et al. 2018), where

they form down-valley low-level jets with hourly averaged wind speeds of up to 20 m s⁻¹ in the cold season. The jets are concentrated along the central axes of the valleys and are driven by the pressure gradient resulting from the near-surface cooling along sloping valley axes (Muñoz et al., 2013).

Another mechanism generating dust-emitting winds are dust devils. These rotating plumes of dust aerosols are caused by thermal instability are frequently observed in the Atacama Desert (Kurgansky et al., 2011; Metzger et al., 2010; Saukel et al., 2011). According to Kurgansky et al. (2011), one of the few studies on dust devils in the Atacama Desert, they mainly occur between 11:30-16:30 local time, when the air temperature is highest, reaching mean wind speeds of 2–8 m s⁻¹. Towards the afternoon, when westerly winds develop, the number and diameter of the dust-devils increase with vortex diameters of a few meters to about 20 m. Moreover, gypsum dust devils have been reported in the Atacama as well. Benison (2017) observed whirling air columns moving large gypsum crystals entrained from saline pan surfaces, transported a few kilometers away (ca. 5 km) and deposited in large dune-like mounds.

The relative importance of wet and dry deposition fluxes varies with the seasons, with rainfall amounts and with location. Considering the arid climate of the Atacama Desert, dry deposition might be the general rule, at least in the central hyper-arid areas. According to Pye (1987) conditions for dry deposition are: (i) a reduction in wind velocity and turbulence allowing aerosols to sink, (ii) the aerosols are 'captured' by collision with rough, moist or electrically charged surfaces, and/or (iii) the particles become charged and form aggregates which sink faster to the ground. In large parts

of the Atacama Desert wind speeds are distinctly reduced at nighttime, with velocities hardly exceeding 5 m s^{-1} at most sites of the hyper-arid core (e.g., Muñoz et al., 2018). Furthermore, observations from wind towers reveal that even lower wind speeds may occur during the transition between the diurnal and nocturnal wind regimes (Jacques-Coper et al., 2015; Muñoz et al., 2018), also in the aforementioned valleys with strong nocturnal low-level jets (Muñoz et al., 2013). Hence, conditions for dry deposition of dust and aerosols are particularly beneficial during these transition periods.

3.3. Fog as water provider and sea spray mobilizer inland the Atacama Desert

Fog corresponds to liquid water particles suspended in the atmosphere, i.e., liquid aerosols mixed with salts and organics (Cereceda et al., 2002). Due to the scarcity of rainfall and rivers in the Atacama Desert, fog is considered one of the main inputs of water and salts to local ecosystems and landscape, particularly for those established on the Coastal Cordillera and the west portion of the Central Depression (see section 3.3.1). Convective fog found along the coast of the Atacama Desert correspond to a massive cloud named stratocumulus formed over the Pacific Ocean and moved hundreds of kilometers onshore by westerly winds towards the Atacama (Cereceda et al., 2002) (see Fig. 7). The thermal inversion produced by the subsidence of warm air, typical of these latitudes, generates a first humid and cold marine layer, intensified by the Humboldt Current and the deep-sea upwelling (Osses et al., 2017). Thus, stratocumulus is found between 500 and 1000 m a.s.l. and present ca. 300 m thickness average. Once it gets inland, the cloud contacts

1635 the continent plains and the Coastal Cordillera, remarkably in coastal mega cliffs,
1636 being considered then as fog or “Camanchaca” as it is locally known. Alternatively,
1637 orographic fog is formed near the coast, in situ on the first windward slope facing the
1638 sea, and where higher mountains or special forms of the relief and coastline work as
1639 obstacles that oblige the incoming air mass to ascend and cool by expansion,
1640 condensing the water vapor and generating fog, as explained by Cereceda et al
1641 (2002). According to this latter study, a third type -radiation fog- was noted in the
1642 Pampa del Tamarugal (PdT) in the Central Depression. Radiation fog occurs due to
1643 the condensation of atmospheric vapor as a result of the strong temperature
1644 decrease at night (Cereceda et al., 2008; Farias et al., 2005).

1645 In the coast the stratocumulus cloud deck frequently moves onshore into the desert
1646 and thus generates advective fog (Cereceda et al., 2008). The transport of fog inland
1647 is able to reach the east slope of the Coastal Cordillera and the western portion of
1648 the Atacama Desert using corridors in the Coastal Cordillera, where plants are
1649 episodically seen (see Fig. 9). The amount of fog on the coast of the Atacama Desert,
1650 both in Chile and Peru, presents seasonal variations throughout the year, with the
1651 minimums being recorded during the summer months (Osses et al., 1998), which
1652 adds to the interannual variability that can vary between 15-19% according to data
1653 published by Cereceda et al. (2008) for the period 1998-2005 for Alto Patache and
1654 Cerro Guatalaya, respectively. The Southeast Pacific (SEP) acts as an ocean–
1655 atmosphere interconnected system that determines the fog water variability through
1656 the year. The inter-annual variability of fog water content measured at the coast of

1657 the hyperarid Atacama Desert is closely related to the local and meso-scale sea
1658 surface temperature and low cloud cover inside the SEP realm. (Del Río et al., 2018)

1659 Wet deposition of aerosols can occur either below a cloud, when raindrops,
1660 snowflakes or hail-stones scavenge dust as they fall, or within a cloud when dust
1661 particles are captured by water droplets and descend to the ground when the
1662 precipitation falls (Goudie and Middleton, 2006). For the Atacama Desert, wet
1663 deposition is typically restricted to the western region below altitudes of 1300 m a.s.l.
1664 (due to fog) and to the Altiplano and Andes Cordillera (due to rain- and snowfall).
1665 The spatial extend of the stratocumulus peaks in winter and at night, and accordingly
1666 the fog water flux reveals a maximum at the coastal cliff in altitudes between 750
1667 and 850 m a.s.l. during the cold season (Cereceda et al., 2008).

1668 To assess the mean spatial distribution of the coastal fog, we utilize satellite remote
1669 sensing data. The Moderate Resolution Imaging Spectroradiometer (MODIS)
1670 onboard the Aqua satellite provides a Level 2 Cloud Mask product (Ackerman et al.,
1671 2017) which assigns the categories “confident cloudy”, “probably cloudy”, “probably
1672 clear” and “confident clear” to grid points at a 1 km resolution. From this product, we
1673 derive the mean total cloud cover (TCC) by dividing the number of all cloudy cases
1674 by the total number of available overpasses for a 16-year period (2003–2018) for
1675 each grid point. The TCC can be considered a proxy for the frequently occurring
1676 marine stratocumulus clouds. By only considering July, August and September, we
1677 focus on the main fog season (austral winter). Furthermore, daily overpasses at
1678 around 14:00 and 02:00 local time are distinguished so that the daytime and
1679 nighttime situations can be visualized (Fig. 8).

During the nocturnal maximum, the cloud advection reaches the coastal mountain range leading to fog formation. Fog corridors can be identified for regions with lower topographic heights allowing the stratocumulus to penetrate the coastal mountain range, e.g., at Punta Chomache (21.13°S), Punta Chipana, Punta Patache (20.81°S), Punta Chucumata, and Punta Gruesa (20.21°S). Through some of these corridors between Iquique and the mouth of the Rio Loa (21.4°S), fog can reach even into the PdT. These coastal and interior corridors have been described previously by Farias et al (2005) and are visualized here at a higher resolution (Fig. 8). Furthermore, the extended region of our analysis allows identification of additional corridors farther North, e.g., around Arica, and farther South, e.g., to the North of the Mejillones Peninsula in Morro Moreno (23.46°S), and around Antofagasta (23.65°S). The latter one also allows penetration into the Central Valley.

The water quality of coastal fog in northern Chile has been examined by Schemenauer and Cereceda (1992) for coastal sites north of La Serena (~29.30 °S) and Sträter et al. (2010) at the Alto Patache fog oasis (~20.85). These studies reported chemistry of advective fog captured in traps, indicating pH value means of 4.99 ± 0.86 and 4.65 ± 0.89 (Schemenauer and Cereceda, 1992) and between 2.9 and 3.5 (Sträter et al., 2010). Also, both studies report high ionic concentrations coming from sea salt.

Fog is one of various sources for salt deposits within the Atacama Desert (Cosentino et al., 2015; Ewing et al., 2006; Owen et al., 2013; Rech et al., 2003; Voigt et al., 2020; Wang et al., 2014), with the importance of fog decreasing inland due to the reduction of its occurrence (Rech et al., 2003; Wang et al., 2014). Interested in

understanding fog impact on atmospheric deposition in soils, Wang et al (2014) compared ionic composition of passively collected dust samples near Mejillones (MT) (see section 2.2) , a Salar Grande fog sample (SGF), and an El Tofo (29.26°S, 71.15°W) fog sample (ETF) which has been collected and analyzed previously by Schemenauer and Cereceda (1992). When comparing the samples from MT dust samples and the ETF, Wang et al (2014) found a similar ionic composition, despite small discrepancies in Ca^{2+} , Mg^{2+} and Cl^- . Furthermore, the SGF sample was considerably more enriched in Ca^{2+} than ETF (67-fold), and had a $\text{Ca}^{2+}/\text{SO}_4^{2-}$ molar ratio of ~ 1 similar to gypsum minerals found on the surface of Salar de Grande, near where the fog was collected, indicating that local dust sources are involved. Enhanced NO_3^- concentration by a factor of 25.4 compared to the ETF, and a factor of six compared to the MT suggests that the SGF may have been subject to anthropogenic NO_x emissions from the nearby Tocopilla city and power plants to the north. Thus, SGF ion content was considerably impacted by dust from Salar Grande and anthropogenic emissions.

Besides dust, fog may also carry pollutants as indicated by Farias et al (2005) and the aforementioned situation. In this sense, Sträter et al (2010) sampled fog in the fog oasis Alto Patache (20.82°S, 70.82°W) in July and August 2008. The authors found that pH of convective fog varied between 2.9 and 3.5, whereas orographic fog exhibited a pH of 2.5. Moreover, high percentages of sulfate and very high enrichment factors (versus sea salt) of heavy metals were found. According to this, the authors concluded that anthropogenic activity caused high concentrations of

1725 heavy metals and contributed to the low pH of fog. In this case, specifically mineral
1726 processing facilities, ship traffic, and power plants are the main responsible.

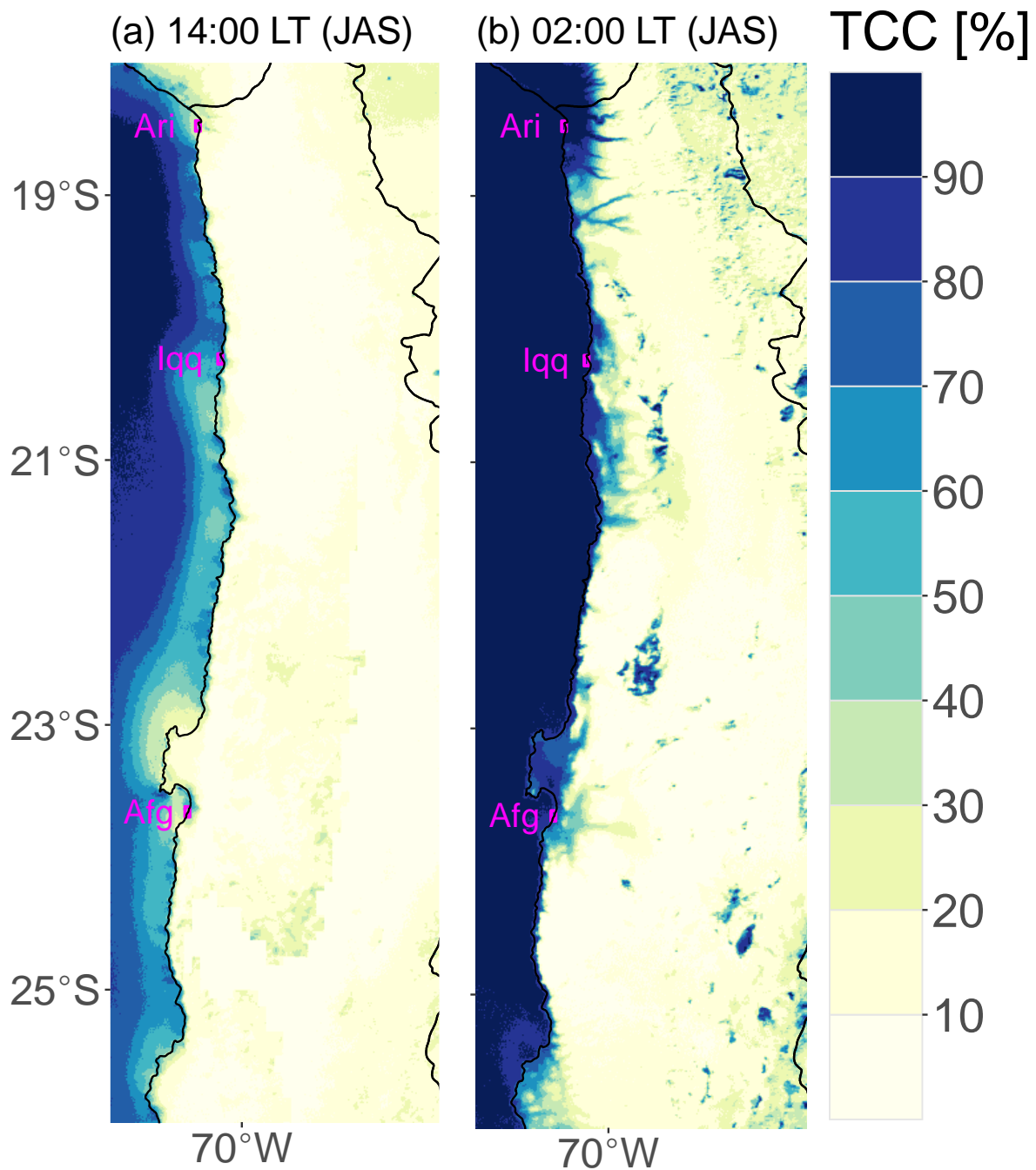
1727 Wang et al (2014) suggested that fog was an important driver of atmospheric
1728 deposition at MT (~20%). Fog water droplets efficiently scavenge gaseous species
1729 from the atmosphere, enhancing coastal deposition of large marine aerosols.
1730 However, fog may not significantly impact inland transport of small particles (sea
1731 salts, non-sea salt Ca^{2+} , and secondary NO_3^- and SO_4^{2-}). Thus, fog water droplets
1732 carry salts into the Atacama which crystallize once water is vaporized (Wang et al.,
1733 2014). Cosentino et al (2015) suggested that calcium sulfate crystals recently formed
1734 within the hyperarid core after wet deposition from marine aerosols. Fog also
1735 modifies the landscape and impacts the dust cycle, as salt inputs could contribute to
1736 surface soil crusting and thereby minimize wind erosion (Owen et al., 2013).







Figure 7. Set of pictures showing the cycle of fog close to the coast near the Loa river canyon within the Atacama Desert at 8.00 (a), 12.00 (b), 16.00 (c) and 20.00 (d) local time. Pictures were taken from a camera trap located in Cerro de Calate at 1148 m ASL (May and Hoffmeister, 2018). During the morning, fog is dissipating due to solar heating. After completely disappearing at noon, fog moves back inland during the afternoon covering the landscape by the sunset.



1737

1738 **Figure 8.** MODIS mean total cloud cover (TCC) for austral winter seasons (July,
 1739 August, September) within a 16-year period (2003–2018). TCC is used as a proxy
 1740 for the coastal stratocumulus over ocean and for fog over land in winter at 14:00 (a)

and at 02:00 (b) local time. Magenta points represent the locations of the coastal cities Arica (Ari), Iquique (Iqq) and Antofagasta (Afg). **(Colors should be used)**

3.3.1. Life and atmospheric deposition in the Atacama Desert

As water is an extremely scarce resource in the Atacama Desert, life faces extreme environmental conditions that have forced highly specialized adaptation of organisms to thrive (Azua-Bustos et al., 2012). Thus, plants and microorganisms are distributed in patches across this desert, particularly in places with higher relative water availability. The vegetation is restricted mainly to a narrow belt along the coast that receives water from fog, deep valleys that cross the desert, and the western flank of the Andes (Moreira-Muñoz, 2011) (see Fig. 2). Something similar happens with microorganisms in the hyper arid core, whose distribution in soil is defined by fog presence, being the wet deposition of marine aerosols the most important source of water for native plants, biological soil crusts (Cáceres et al., 2007), and microbial communities (e.g., Azúa-Bustos et al., 2011; Gómez-Silva, 2018a; McKay et al., 2003) in the hyperarid Atacama.

On the coastal cliff along the Atacama Desert, fog oases and Tillandsia fields are representative of the island-like plant formations. Among them, 4 ecosystems may be differentiated according to the predominance: cacti, shrub formation, Bromeliaceas (tillandsias) and annual plants, being the latter supported by the rare rains (Cereceda et al., 2002), and hence ephemeral. Lomas or fog oases are phytogeographic units that generally contain a high number of endemic genera and species (Mostacero et al 1996; Rundel et al. 1991), and have more established

1763 communities. A complete map for fog oases location was published by Rundel et al.
1764 (1991). Among other plant communities in the Atacama, *Tillandsia* fields are present
1765 to the north of the Loa River and in southern Peru (see Fig. 9). These plants have
1766 colonized the coastal desert and the Central Depression, being an indicator of fog
1767 reach since they obtain water from it. Curiously, *Tillandsia* facilitate not only the local
1768 atmospheric water deposition to the soil beneath, but also the mineral dust
1769 deposition. According to Latorre et al. (2011), *Tillandsia landbeckii* plants act as sand
1770 traps, which is accumulates downwind from these plants in near-horizontal layers.
1771 They spread over the sand, thereby maximizing their profile toward the wind and fog,
1772 and creating a small incipient dune-like structure. Successive stages of growth,
1773 dieback and colonization explain the unusual stratigraphy (and increased height with
1774 age) seen in these dunes. Some other plants population that captures mineral dust
1775 and possibly fog are Saltgrass *Distichlis spicata*. These plants usually grow in salar
1776 (salt lakes) margins and get water from aquifers. When it is possible, these plants
1777 grow in columns trapping the circulating dust, using it as accretion material.

1778 The Atacama Desert contains regions that represent the most extreme hyperarid
1779 soils known. Considering that water availability is the primary controlling factor for
1780 microbial activity, biomass and diversity in desert soils (Connon et al., 2007), the
1781 distribution of soil microorganisms is defined by the occurrence of fog in the
1782 hyperarid Atacama. As the air humidity decreases from the coast towards to the east,
1783 so does the density of biological soil crust (Cáceres et al., 2007). Despite of this, in
1784 places with extreme dry conditions which are used as analog to the Martian surface
1785 (Gómez-Silva et al., 2007; McKay et al., 2003b; Navarro-González et al., 2003),

1786 microorganisms still can be found in the hyper arid core of the desert and have been
1787 reported, e.g. in Altamira, Yungay station, Lomas Bayas, Maria Elena, Salar Grande,
1788 Salar Soronal, Pozo Almonte, and Humberstone; all locations between 700 and 2000
1789 m a.s.l. (Contador et al., 2020). Moreover, soil microorganisms present a relative
1790 fast response to fog water presences, as shown by (Jones et al., 2018).
1791 Nevertheless, fog is not distributed uniformly and extremely dry soils (Navarro-
1792 González et al., 2003) occur in locations where fog is blocked by high coastal
1793 mountains (Rech et al 2003). A distribution map of microorganisms is available in
1794 the Atacama Database (<http://www.atacamadb.cl>).

1795 Due to the new knowledge generated regarding the microbiology of the Atacama
1796 Desert is that today we understand this region not as a barren soil but as a territory
1797 colonized by a rich microbiota that includes extremophiles and extreme-tolerant
1798 microorganisms (Gómez-Silva, 2018b). These organisms have been found in soil
1799 crusts (biological soil crusts) (Wang et al., 2017), soil subsurface and sediments
1800 (Parro et al., 2011; Warren-Rhodes et al., 2019) and as lithobiontic life (Gómez-Silva,
1801 2018b), excluding of course the aquatic microbial life. These terrestrial
1802 microorganisms rely on the collection of liquid water from incoming fog and/or water
1803 vapor condensation and deliquescence on or within halite and quartz rock surfaces.
1804 In the case of microbial endolithic communities from halites exposed to coastal fogs
1805 and high relative humidity, Robinson et al. (2013) concluded that these were more
1806 diverse and that their archaeal and bacterial assemblages were accompanied by a
1807 novel algae related to oceanic picoplankton of the Mamiellales. In contrast, they
1808 found no algae in the Yungay pinnacles. The same was stated by Warren-Rhodes

et al. (2006) for hypolithic cyanobacteria, whose diversity decreases progressively along an aridity transect (south-north) between Copiapo and Yungay. Moreover, they determined that hypolithic cyanobacteria are rare and exist on small, spatially isolated areas in the middle of microbiologically unpopulated bare soil. Azúa-Bustos et al. (2011) reported complex associations of cyanobacteria, archaea, and heterotrophic bacteria along the coast of the Atacama, 1.5 km from the Pacific Ocean, inhabiting the undersides of translucent quartz stones. They concluded that colonization rates in these areas, which receive virtually no rain but mainly fog, are significantly higher than those reported inland in the Central Depression at the same latitude and in consequence, the Coastal Cordillera offers a more benign sites for the development of microbial life.

The more robust microbial life inhabiting the ocean and the coastal desert is prone to be transported inland through wind mobilization using passages in the Coastal Range. This was proven by Azua-Bustos et al. (2019) who, using Petri dishes exposed to atmospheric deposition in the coast, Coastal Cordillera and the Central Depression of the Atacama Desert, were able to cultivate and identify different strains of microorganisms, some of them native of the oceans (e.g. *Oceanobacillus oncorhynchi*, *Bacillus oceanisediminis*, *Brachybacterium paraconglomeratum* and *Bhargavaea cecembensis*) and from plant rhizosphere (e.g. the bacterial specie *Bacillus simplex* and the fungal specie *Ophiosphaerella herpotricha*) coming possibly from the sparse plant-covered areas of fog oases on top of the hills of the Coastal Cordillera. Also, airborne bacteria were reported possibly coming from further and unknown places (*Kocuria flava*, an actinobacteria and *Bacillus*

1832 *altitudinis*). Authors also studied the daytime when more microorganisms were
1833 collected revealing that late afternoon transport is more abundant and, in
1834 consequence, a wet deposition due to fog is more feasible. This timetable is
1835 coincident with faster coastal winds coming from south and southwest that
1836 penetrates into the desert and displace towards the Andes.

1837 Nevertheless, the arrival of organic compounds and microorganisms may be
1838 affected and oxidized by the chemical reactivity of surface soils in the Atacama. The
1839 production of secondary aerosols and oxidative agents occurs due to atmospheric
1840 chemistry from gaseous oxide precursors such as NH_3 , NO_2 , NO_3 , SO_2 and their
1841 reaction with O_3 and OH radicals powered by the extreme solar radiation to which
1842 the Atacama is subjected (Ewing et al., 2006; Quinn et al., 2005). Some hyper arid
1843 environments such as Yungay in the Atacama Desert are rich in highly oxidative dust
1844 (Quinn et al., 2005), which is produced by these reactions and is capable of produce
1845 sulphuric and nitric acid. The presence of these acids in soils is important because
1846 during nighttime, when water is more available due to fog and humidity penetration,
1847 may react oxidizing the deposited organic compounds and microorganisms arrived
1848 to the Atacama, especially after the sunset, affecting the availability of nutrients and
1849 toxins for plants, diversity of microbial life, activity and colonization, and the
1850 mechanisms for organic compounds degradation and cycling. Relevantly, it is likely
1851 that oxidants are formed by photochemical reactions among the interfaces
1852 soil/dust/atmosphere in an analog way to that suggested for Mars and be responsible
1853 for the presence of iodates chromates, perchlorate, among others detected in that
1854 planet (Quinn et al., 2005).

1855





Figure 9. At the top (a), a field of Tillandsias over the south-western slope of the Cerro de Calate is shown, to the north the Loa river canyon (visible in the picture). At the bottom (b), several alive specimens of tillandsias are shown next to a buried dead mat of tillandsias.

1856

1857

1858

4. Concluding remarks

1859 The scientific literature indicates that the Atacama Desert is (one of) the oldest and
1860 driest deserts on Earth and, in consequence, the scarce leaching and run off
1861 associated with precipitation affecting soils and salt deposits are typically negligible.
1862 These characteristics makes the Atacama Desert an ideal environment to study and
1863 constraint the temporal and spatial dynamics of atmospheric depositions and their
1864 long-term accumulation in the soils.

1865 In the last two decades several efforts characterized atmospheric depositions
1866 including measurements of deposition rates in the Atacama Desert. Based on
1867 reviewing the past research, we conclude that the aerosols deposited in the Atacama
1868 Desert, both from local and remote aerosol sources, play an important role in the
1869 formation of soil and salt deposits, and vary in aerosol deposition amount and
1870 chemical composition in space and time. For instance, the western Atacama is
1871 strongly influenced by fog and sea spray on soil gypsum/anhydrite with depositions
1872 of soluble salts (Rech et al., 2003), while the eastern margin has more insoluble
1873 material components from the Andes and further eastern deflated soils (Li et al.,
1874 2019). Moreover, the redistribution of salts from deflated salars (playas) was also
1875 denoted being very important in the Central Depression (Ewing et al., 2006; Rech et
1876 al., 2003). All of the above mentioned processes correspond to the aeolian
1877 redistribution of particles but contributions from (secondary) aerosols produced
1878 directly in the atmosphere have also been suggested, e.g., nitrate and sulfate
1879 deposits (Ericksen, 1983; Ewing et al., 2006; Rech et al., 2003; Wang et al., 2014).

1880 The examination of the deposited aerosols has been done by setting several series
1881 of passive dust traps arranged in west-east and north-south oriented transects in
1882 order to ponder the influence of sea sprays (W-E) and aridity (N-S), along with the
1883 examination of soils (Ewing et al., 2006; Li et al., 2019; Wang et al., 2014). To the
1884 west of the Atacama, the Humboldt Current flows northwards from Antarctica.
1885 Consequently, the marine upwelling of colder waters develops immediately offshore
1886 and leads to a high biological productivity in the coastal ocean (Marín and Olivares,
1887 1999; Moore et al., 2002). As a result, it would not be rare to find Na, Cl (Ewing et
1888 al., 2006), inorganic S (Rech et al., 2003) and N (Michalski et al., 2004) in the
1889 Atacama soils transported by westerly winds from the Pacific Ocean. Thus, the
1890 aerosol loading may be rich in inorganic compounds and also supply organic C and
1891 N, as well as Ca (Wang et al., 2014) and inorganic C from marine organisms (Moore
1892 et al., 2002), water and even microorganisms (Azua-Bustos et al., 2019). From the
1893 Andes and Altiplano, easterly winds can carry mineral dust, volcanic emissions,
1894 organic compounds from the more vegetated areas, and alluvial sediments
1895 mobilized by the summertime rains. These easterlies are not uncommon as they are
1896 related to a southward shift of the Bolivian High, an upper-level feature that
1897 frequently develops in austral summer (e.g., Reyes et al., 2020).

1898 Aside from the natural aerosol sources, aerosols associated with anthropogenic
1899 activity must be considered. The Atacama Desert is affected by industrial mineral
1900 exploitation, because of the massive salt and metal deposits harbored within. These
1901 aerosol-producing activities comprise not only the mining activity itself but for
1902 instance also the mineral and manpower transport, fossil fuel burning, and smelting

processes. Several authors have suggested that nitrate, sulfate, Na and Ca loads in the atmosphere may be emitted by anthropogenic sources in the Atacama Desert (Ewing et al., 2006; Voigt et al., 2020; Wang et al., 2014). Moreover, exceptionally high Na/Cl ratios were found in present day aerosol samples (Wang et al., 2014; Li et al., 2019), along with an excess of Cl in the Atacama soils which can be confirmed to represent a large impact of anthropogenic emissions (Voigt et al., 2020).

Despite the hyper aridity and deprivation of plants in much of the Atacama Desert, making the surface soils, anhydrite dust and gypsum, prone to wind erosion, dust storms are rather rare and less intense in comparison to North Africa. In principle, this may be explained by low erodibility of the soil, low emissivity of the prevailing winds, or a combination of the two. Our review suggests a low erodibility of the undisturbed soils in the Atacama Desert in the present climate due to (1) the hyper aridity leading to low fluvial activity and hence the extremely low rates of erosion, (2) the typical presence of non-erodible objects, such as boulders and cobbles, and (3) the occurrence of desert pavements, soil crusts, salt nodules and crusts, and soil vesicular surface horizons. These characteristics reduce or inhibit the mobilization and entrainment of desert-dust particles, even when there are strong winds. Case studies of past dust storms indicate that a sufficient erosivity of winds can occur, but the typically prevailing weather in the present climate seem unfavourable for generating sufficiently strong and persistent winds. Further research is needed to fully understand the occurrence and long-term changes of dust storms in the Atacama Desert in the context of the geological and anthropogenic changes of the local soils.

1926

Acknowledgements

1927 This project was funded by the Chilean National Agency for Research and
1928 Development (ANID)/ Beca Doctorado Nacional/ 2018 – 21181718, the Deutsche
1929 Forschungsgemeinschaft (DFG, German Research Foundation) through the
1930 Collaborative Research Centre 1211: Earth -Evolution at the Dry Limit (CRC 1211,
1931 Project-ID 268236062), and CONICYT MEC 80180018 project.

1932

References

1933 Ackerman, S., 2017. MODIS Atmosphere L2 Cloud Mask Product.
1934 https://doi.org/http://dx.doi.org/10.5067/MODIS/MYD35_L2.061

1935 Aguilar, G. n., Cabré, A., Fredes, V., Villela, B., 2020. Erosion after an extreme storm
1936 event in an arid fluvial system of the southern Atacama Desert: An assessment
1937 of the magnitude, return time, and conditioning factors of erosion and debris
1938 flow generation. Nat. Hazards Earth Syst. Sci. 20, 1247–1265.
1939 <https://doi.org/10.5194/nhess-20-1247-2020>

1940 Alfaro, S.C., Flores-Aqueveque, V., Foret, G., Caquineau, S., Vargas, G., Rutllant,
1941 J.A., 2011. A simple model accounting for the uptake, transport, and deposition
1942 of wind-eroded mineral particles in the hyperarid coastal Atacama Desert of
1943 northern Chile. Earth Surf. Process. Landforms 36, 923–932.
1944 <https://doi.org/10.1002/esp.2122>

1945 Amundson, R., Dietrich, W., Bellugi, D., Ewing, S., Nishiizumi, K., Chong, G., Owen,

1946 J., Finkel, R., Heimsath, A., Stewart, B., Caffee, M., 2012. Geomorphologic
 1947 evidence for the late Pliocene onset of hyperaridity in the Atacama Desert. Bull.
 1948 Geol. Soc. Am. 124, 1048–1070. <https://doi.org/10.1130/B30445.1>

1949 Andreae, M.O., Crutzen, P.J., 1997. Atmospheric Aerosols: Biogeochemical
 1950 Sources and Role in Atmospheric Chemistry. Science (80-.). 276, 1052–1058.
 1951 <https://doi.org/10.1126/science.276.5315.1052>

1952 Azua-Bustos, A., Caro-Lara, L., Vicuña, R., 2015. Discovery and microbial content
 1953 of the driest site of the hyperarid Atacama Desert, Chile. Environ. Microbiol.
 1954 Rep. 7, 388–394. <https://doi.org/10.1111/1758-2229.12261>

1955 Azua-Bustos, A., Fairén, A.G., González-Silva, C., Ascaso, C., Carrizo, D.,
 1956 Fernández-Martínez, M., Fernández-Sampedro, M., García-Descalzo, L.,
 1957 García-Villadangos, M., Martín-Redondo, M.P., Sánchez-García, L., Wierzchos,
 1958 J., Parro, V., 2018. Unprecedented rains decimate surface microbial
 1959 communities in the hyperarid core of the Atacama Desert. Sci. Rep. 8.
 1960 <https://doi.org/10.1038/s41598-018-35051-w>

1961 Azua-Bustos, A., González-Silva, C., Fernández-Martínez, M.Á., Arenas-Fajardo,
 1962 C., Fonseca, R., Martín-Torres, F.J., Fernández-Sampedro, M., Fairén, A.G.,
 1963 Zorzano, M.P., 2019. Aeolian transport of viable microbial life across the
 1964 Atacama Desert, Chile: Implications for Mars. Sci. Rep. 9, 1–11.
 1965 <https://doi.org/10.1038/s41598-019-47394-z>

1966 Azúa-Bustos, A., González-Silva, C., Mancilla, R.A., Salas, L., Gómez-Silva, B.,

1967 McKay, C.P., Vicuña, R., 2011. Hypolithic Cyanobacteria Supported Mainly by
 1968 Fog in the Coastal Range of the Atacama Desert. *Microb. Ecol.* 61, 568–581.
 1969 <https://doi.org/10.1007/s00248-010-9784-5>

1970 Azua-Bustos, A., Urrejola, C., Vicuña, R., 2012. Life at the dry edge: Microorganisms
 1971 of the Atacama Desert. *FEBS Lett.* 586, 2939–2945.
 1972 <https://doi.org/10.1016/j.febslet.2012.07.025>

1973 Bao, H., Gu, B., 2004. Natural perchlorate has a unique oxygen isotope signature.
 1974 *Environ. Sci. Technol.* 38, 5073–5077. <https://doi.org/10.1021/es049516z>

1975 Barraza, F., Lambert, F., MacDonell, S., Sinclair, K., Fernandoy, F., Jorquera, H.,
 1976 2021. Major atmospheric particulate matter sources for glaciers in Coquimbo
 1977 Region, Chile. *Environ. Sci. Pollut. Res.* 28, 36817–36827.
 1978 <https://doi.org/10.1007/s11356-021-12933-7>

1979 Benison, K.C., 2017. Gypsum gravel devils in Chile: Movement of largest natural
 1980 grains by wind? *Geology* 45, 423–426. <https://doi.org/10.1130/G38901.1>

1981 Berger, I.A., Cooke, R.U., 1997. The Origin and Distribution of Salts on Alluvial Fans
 1982 in The Atacama Desert, Northern Chile. *Earth Surf. Process. Landforms* 22,
 1983 581–600. [https://doi.org/10.1002/\(SICI\)1096-9837\(199706\)22:6<581::AID-](https://doi.org/10.1002/(SICI)1096-9837(199706)22:6<581::AID-ESP714>3.0.CO;2-4)
 1984 [ESP714>3.0.CO;2-4](https://doi.org/10.1002/(SICI)1096-9837(199706)22:6<581::AID-ESP714>3.0.CO;2-4)

1985 Bernhardt, A., Schwanghart, W., Hebbeln, D., Stuut, J.B.W., Strecker, M.R., 2017.
 1986 Immediate propagation of deglacial environmental change to deep-marine
 1987 turbidite systems along the Chile convergent margin. *Earth Planet. Sci. Lett.*

- 1988 473, 190–204. <https://doi.org/10.1016/j.epsl.2017.05.017>
- 1989 Betancourt, J.L., Latorre, C., Rech, J.A., Quade, J., Rylander, A., 2000. A 22 , 000-
- 1990 Year Record of Monsoonal Precipitation from Northern Chile ' s Atacama
- 1991 Desert. *Science* (80-.). 289, 1542–1546.
- 1992 Bishop, M.P., 2013. Remote Sensing and GIScience in Geomorphology:
- 1993 Introduction and Overview, *Treatise on Geomorphology*. Elsevier Ltd.
- 1994 <https://doi.org/10.1016/B978-0-12-374739-6.00040-3>
- 1995 Blanco, N., Tomlinson, A.J., 2013. Carta Guatacondo, Región de Tarapacá., in: Wall,
- 1996 R., Espinoza, F., Gajardo, A., Lara, L., Tomlinson, A., Jordan, T., Mpodozis, C.,
- 1997 Jefa, J.U. de P.S.A.N. (Eds.), *Servicio Nacional de Geología y Minería, Carta*
- 1998 *Geológica de Chile*. Santiago, p. 109.
- 1999 Bobst, A.L., Lowenstein, T.K., Jordan, T.E., Godfrey, L. V., Ku, T.L., Luo, S., 2001.
- 2000 A 106 ka paleoclimate record from drill core of the Salar de Atacama, northern
- 2001 Chile. *Palaeogeogr. Palaeoclimatol. Palaeoecol.* 173, 21–42.
- 2002 [https://doi.org/10.1016/S0031-0182\(01\)00308-X](https://doi.org/10.1016/S0031-0182(01)00308-X)
- 2003 Böhlke, J.K., Ericksen, G.E., Revesz, K., 1997. Stable isotope evidence for an
- 2004 atmospheric origin of desert nitrate deposits in northern Chile and southern
- 2005 California, U.S.A. *Chem. Geol.* 136, 135–152. [https://doi.org/10.1016/S0009-](https://doi.org/10.1016/S0009-2541(96)00124-6)
- 2006 [2541\(96\)00124-6](https://doi.org/10.1016/S0009-2541(96)00124-6)
- 2007 Briceño-Zuluaga, F., Castagna, A., Rutllant, J.A., Flores-Aqueveque, V., Caquineau,
- 2008 S., Sifeddine, A., Velazco, F., Gutierrez, D., Cardich, J., 2017. Paracas Dust

2009 Storms: Sources, trajectories and associated meteorological conditions. *Atmos.*

2010 *Environ.* 165, 99–110.

2011 Bull, A.T., Andrews, B.A., Dorador, C., Goodfellow, M., 2018. Introducing the

2012 Atacama Desert. *Antonie Van Leeuwenhoek* 111, 1269–1272.

2013 <https://doi.org/10.1007/s10482-018-1100-2>

2014 Cáceres, L., Gómez-Silva, B., Garró, X., Rodríguez, V., Monardes, V., McKay, C.P.,

2015 2007. Relative humidity patterns and fog water precipitation in the Atacama

2016 Desert and biological implications. *J. Geophys. Res. Biogeosciences* 112, 1–

2017 11. <https://doi.org/10.1029/2006JG000344>

2018 Carretier, S., Tolorza, V., Regard, V., Aguilar, G., Bermúdez, M.A., Martinod, J.,

2019 Guyot, J.L., Hérail, G., Riquelme, R., 2018. Review of erosion dynamics along

2020 the major N-S climatic gradient in Chile and perspectives. *Geomorphology* 300,

2021 45–68. <https://doi.org/10.1016/j.geomorph.2017.10.016>

2022 Carslaw, K.S., Boucher, O., Spracklen, D. V., Mann, G.W., L. Rae, J.G., Woodward,

2023 S., Kulmala, M., 2010. A review of natural aerosol interactions and feedbacks

2024 within the Earth system. *Atmos. Chem. Phys.* 10, 1701–1737.

2025 <https://doi.org/10.5194/acp-10-1701-2010>

2026 Catling, D.C., Claire, M.W., Zahnle, K.J., Quinn, R.C., Clark, B.C., Hecht, M.H.,

2027 Kounaves, S., 2010. Atmospheric origins of perchlorate on mars and in the

2028 atacama. *J. Geophys. Res. E Planets* 115, 1–15.

2029 <https://doi.org/10.1029/2009JE003425>

2030 Cereceda, P., Larrain, H., Osses, P., Farías, M., Egaña, I., 2008. The spatial and
 2031 temporal variability of fog and its relation to fog oases in the Atacama Desert,
 2032 Chile. Atmos. Res. 87, 312–323.
 2033 <https://doi.org/10.1016/j.atmosres.2007.11.012>

2034 Cereceda, P., Osses, P., Larrain, H., Farías, M., Lagos, M., Pinto, R., Schemenauer,
 2035 R.S., 2002. Advective, orographic and radiation fog in the Tarapacá region,
 2036 Chile. Atmos. Res. 64, 261–271. [https://doi.org/10.1016/S0169-](https://doi.org/10.1016/S0169-8095(02)00097-2)
 2037 [8095\(02\)00097-2](https://doi.org/10.1016/S0169-8095(02)00097-2)

2038 Choobari, O.A., Zawar-Reza, P., Sturman, A., 2014. The global distribution of
 2039 mineral dust and its impacts on the climate system: A review. Atmos. Res. 138,
 2040 152–165. <https://doi.org/10.1016/j.atmosres.2013.11.007>

2041 Claridge, G.G.C., Campbell, I.B., 1968. Origin of nitrate deposits. Nature 217, 428–
 2042 430.

2043 Clarke, J.D.A., 2006. Antiquity of aridity in the Chilean Atacama Desert.
 2044 Geomorphology 73, 101–114. <https://doi.org/10.1016/j.geomorph.2005.12.035>

2045 Connon, S.A., Lester, E.D., Shafaat, H.S., Obenhuber, D.C., Ponce, A., 2007.
 2046 Bacterial diversity in hyperarid atacama desert soils. J. Geophys. Res.
 2047 Biogeosciences 112, 1–9. <https://doi.org/10.1029/2006JG000311>

2048 Contador, C.A., Veas-Castillo, L., Tapia, E., Antipán, M., Miranda, N., Ruiz-Tagle,
 2049 B., García-Araya, J., Andrews, B.A., Marin, M., Dorador, C., Asenjo, J.A., 2020.
 2050 Atacama Database: a platform of the microbiome of the Atacama Desert.

2051 Antonie van Leeuwenhoek, *Int. J. Gen. Mol. Microbiol.* 113, 185–195.
 2052 <https://doi.org/10.1007/s10482-019-01328-x>

2053 Cosentino, N.J., Jordan, T.E., 2017. $^{87}\text{Sr}/^{86}\text{Sr}$ of calcium sulfate in ancient soils of
 2054 hyperarid settings as a paleoaltitude proxy: Pliocene to Quaternary constraints
 2055 for northern Chile (19.5–21.7°S). *Tectonics* 36, 137–162.
 2056 <https://doi.org/10.1002/2016TC004185>

2057 Cosentino, N.J., Jordan, T.E., Derry, L.A., Morgan, J.P., 2015. $^{87}\text{Sr}/^{86}\text{Sr}$ in recent
 2058 accumulations of calcium sulfate on landscapes of hyperarid settings: A bimodal
 2059 altitudinal dependence for northern Chile (19.5°S–21.5°S). *Geochemistry,*
 2060 *Geophys. Geosystems* 16, 4311–4328. <https://doi.org/10.1002/2015GC005954>

2061 Davila, A.F., Gómez-Silva, B., de los Rios, A., Ascaso, C., Olivares, H., McKay, C.P.,
 2062 Wierzchos, J., 2008. Facilitation of endolithic microbial survival in the hyperarid
 2063 core of the Atacam Desert by mineral deliquescence. *J. Geophys. Res.*
 2064 *Biogeosciences* 113, 1–9. <https://doi.org/10.1029/2007JG000561>

2065 Del Río, C., Garcia, J.L., Osses, P., Zanetta, N., Lambert, F., Rivera, D., Siegmund,
 2066 A., Wolf, N., Cereceda, P., Larraín, H., Lobos, F., 2018. ENSO influence on
 2067 coastal fog-water yield in the atacama desert, Chile. *Aerosol Air Qual. Res.* 18,
 2068 127–144. <https://doi.org/10.4209/aaqr.2017.01.0022>

2069 Diederich, J.L., Wennrich, V., Bao, R., Büttner, C., Bolten, A., Brill, D., Buske, S.,
 2070 Campos, E., Fernández-Galego, E., Gödickmeier, P., Ninnemann, L., Reyers,
 2071 M., Ritter, B., Ritterbach, L., Rolf, C., Scheidt, S., Dunai, T.J., Melles, M., 2020.

2072 A 68 ka precipitation record from the hyperarid core of the Atacama Desert in
 2073 northern Chile. *Glob. Planet. Change* 184, 103054.
 2074 <https://doi.org/10.1016/j.gloplacha.2019.103054>

2075 Dunai, T.J., González López, G.A., Juez-Larré, J., 2005. Oligocene-Miocene age of
 2076 aridity in the Atacama Desert revealed by exposure dating of erosion-sensitive
 2077 landforms. *Geology* 33, 321–324. <https://doi.org/10.1130/G21184.1>

2078 Dunai, T.J., Melles, M., Quandt, D., Knief, C., Amelung, W., 2020. Whitepaper: Earth
 2079 – Evolution at the dry limit. *Glob. Planet. Change* 193.
 2080 <https://doi.org/10.1016/j.gloplacha.2020.103275>

2081 Ericksen, G.E., 1983. The Chilean nitrate deposits. *Am. Sci.* 71, 366–374.

2082 Ericksen, G.E., 1981a. Geology and Origin of the Chilean Nitrate Deposits. *Geol.*
 2083 *Surv. Prof. Pap.* 42. <https://doi.org/10.2113/gsecongeo.15.3.187>

2084 Ericksen, G.E., 1981b. Geology and origin of the Chilean nitrate deposits. *US Geol.*
 2085 *Surv. Prof. Pap.* 1188. <https://doi.org/10.3133/pp1188>

2086 Ericksen, G.E., Salas, O.R., 1990. Geology and resources of salars in the Central
 2087 Andes. *Geol. Andes its Relat. to Hydrocarb. Miner. Resour.* 11, 151–164.

2088 Escobar Baccaro, D.F., 1993. Evaluacion climatologica y sinoptica del fenómeno de
 2089 vientos Paracas. Universidad Nacional Agraria La Molina.

2090 Evenstar, L.A., Hartley, A.J., Stuart, F.M., Mather, A.E., Rice, C.M., Chong, G., 2009.
 2091 Multiphase development of the Atacama Planation Surface recorded by

2092 cosmogenic ^3He exposure ages: Implications for uplift and Cenozoic climate
 2093 change in Western South America. *Geology* 37, 27–30.
 2094 <https://doi.org/10.1130/G25437A.1>

2095 Evenstar, L.A., Mather, A.E., Hartley, A.J., Stuart, F.M., Sparks, R.S.J., Cooper, F.J.,
 2096 2017. Geomorphology on geologic timescales: Evolution of the late Cenozoic
 2097 Pacific paleosurface in Northern Chile and Southern Peru. *Earth-Science Rev.*
 2098 171, 1–27. <https://doi.org/10.1016/j.earscirev.2017.04.004>

2099 Ewing, S.A., Sutter, B., Owen, J., Nishiizumi, K., Sharp, W., Cliff, S.S., Perry, K.,
 2100 Dietrich, W., McKay, C.P., Amundson, R., 2006. A threshold in soil formation at
 2101 Earth's arid-hyperarid transition. *Geochim. Cosmochim. Acta* 70, 5293–5322.
 2102 <https://doi.org/10.1016/j.gca.2006.08.020>

2103 Farias, M., Cereceda, P., Osses, P., Núñez, R., 2005. Comportamiento espacio-
 2104 temporal de la nube estratocúmulo, productora de niebla en la costa del desierto
 2105 de Atacama (21° lat. S., 70° long. W.), durante un mes de invierno y otro de
 2106 verano. *Investig. Geogr.* 43–61.

2107 Finstad, K., Pfeiffer, M., Amundson, R., 2014. Hyperarid Soils and the Soil
 2108 Taxonomy. *Soil Sci. Soc. Am. J.* 78, 1845–1851.
 2109 <https://doi.org/10.2136/sssaj2014.06.0247>

2110 Finstad, K., Pfeiffer, M., McNicol, G., Barnes, J., Demergasso, C., Chong, G.,
 2111 Amundson, R., 2016. Rates and geochemical processes of soil and salt crust
 2112 formation in Salars of the Atacama Desert, Chile. *Geoderma* 284, 57–72.

2113 <https://doi.org/10.1016/j.geoderma.2016.08.020>

2114 Flores-Aqueveque, V., Alfaro, S., Muñoz, R., Rutllant, J.A., Caquineau, S., Le Roux,
2115 J.P., Vargas, G., 2010. Aeolian erosion and sand transport over the Mejillones
2116 Pampa in the coastal Atacama Desert of northern Chile. *Geomorphology* 120,
2117 312–325. <https://doi.org/10.1016/j.geomorph.2010.04.003>

2118 Flores-Aqueveque, V., Alfaro, S., Vargas, G., Rutllant, J.A., Caquineau, S., 2015.
2119 Aeolian particles in marine cores as a tool for quantitative high-resolution
2120 reconstruction of upwelling favorable winds along coastal Atacama Desert,
2121 Northern Chile. *Prog. Oceanogr.* 134, 244–255.
2122 <https://doi.org/10.1016/j.pocean.2015.02.003>

2123 Gamboa, C., Godfrey, L., Herrera, C., Custodio, E., Soler, A., 2019. The origin of
2124 solutes in groundwater in a hyper-arid environment: A chemical and multi-
2125 isotope approach in the Atacama Desert, Chile. *Sci. Total Environ.* 690, 329–
2126 351. <https://doi.org/10.1016/j.scitotenv.2019.06.356>

2127 Garreaud, R., Rutllant, J., 1996. Análisis meteorológico de los aluviones de
2128 Antofagasta y Santiago de Chile en el periodo 1991-1993. *Atmosfera.*

2129 Garreaud, R., Vuille, M., Clement, A.C., 2003. The climate of the Altiplano: Observed
2130 current conditions and mechanisms of past changes. *Palaeogeogr.*
2131 *Palaeoclimatol. Palaeoecol.* 194, 5–22. [https://doi.org/10.1016/S0031-](https://doi.org/10.1016/S0031-0182(03)00269-4)
2132 [0182\(03\)00269-4](https://doi.org/10.1016/S0031-0182(03)00269-4)

2133 Garreaud, R.D., Aceituno, P., 2001. Interannual rainfall variability over the South

2134 American Altiplano. *J. Clim.* 14, 2779–2789. <https://doi.org/10.1175/1520->
 2135 0442(2001)014<2779:IRVOTS>2.0.CO;2

2136 Garreaud, R.D., Molina, A., Farias, M., 2010. Andean uplift, ocean cooling and
 2137 Atacama hyperaridity: A climate modeling perspective. *Earth Planet. Sci. Lett.*
 2138 292, 39–50. <https://doi.org/10.1016/j.epsl.2010.01.017>

2139 Garrido, M., Silva, H., Franck, N., Arenas, J., Acevedo, E., 2018. Evaluation of
 2140 Morpho-Physiological Traits Adjustment of *Prosopis tamarugo* Under Long-
 2141 Term Groundwater Depletion in the Hyper-Arid Atacama Desert. *Front. Plant*
 2142 *Sci.* 9, 453. <https://doi.org/10.3389/fpls.2018.00453>

2143 Gay, S.P., 2005. Blowing sand and surface winds in the Pisco to Chala Area,
 2144 Southern Peru. *J. Arid Environ.* 61, 101–117.
 2145 <https://doi.org/10.1016/j.jaridenv.2004.07.012>

2146 Gayo, E.M., Latorre, C., Jordan, T.E., Nester, P.L., Estay, S.A., Ojeda, K.F., Santoro,
 2147 C.M., 2012. Late Quaternary hydrological and ecological changes in the
 2148 hyperarid core of the northern Atacama Desert (~21°S). *Earth-Science Rev.*
 2149 113, 120–140. <https://doi.org/10.1016/j.earscirev.2012.04.003>

2150 Ginoux, P., Chin, M., Tegen, I., Prospero, J.M., Holben, B., Dubovik, O., Line, S.,
 2151 2001. Sources and distributions of dust aerosols simulated with the GOCART
 2152 model. *J. Geophys. Res.* 106, 20255–20273.

2153 Ginoux, P., Prospero, J.M., Gill, T.E., Hsu, N.C., Zhao, M., 2012. Global-scale
 2154 attribution of anthropogenic and natural dust sources and their emission rates

2155 based on MODIS Deep Blue aerosol products. *Rev. Geophys.* 50, 1–36.
 2156 <https://doi.org/10.1029/2012RG000388>

2157 Gómez-Silva, B., 2018a. Lithobiontic life: “Atacama rocks are well and alive.” *Antonie*
 2158 *van Leeuwenhoek, Int. J. Gen. Mol. Microbiol.* 111, 1333–1343.
 2159 <https://doi.org/10.1007/s10482-018-1033-9>

2160 Gómez-Silva, B., 2018b. Lithobiontic life: “Atacama rocks are well and alive.” *Antonie*
 2161 *van Leeuwenhoek, Int. J. Gen. Mol. Microbiol.* 111, 1333–1343.
 2162 <https://doi.org/10.1007/s10482-018-1033-9>

2163 Gómez-Silva, B., Rainey, F.A., Warren-Rhodes, K.A., McKay, C.P., Navarro-
 2164 González, R., 2007. *Atacama Desert Soil Microbiology* 117–132.
 2165 https://doi.org/10.1007/978-3-540-74231-9_6

2166 Goudie, A.S., 2013. *Arid and Semi-arid Geomorphology*, 1st ed. Cambridge
 2167 University Press, Oxford.

2168 Goudie, A.S., Middleton, N.J., 2006. *Desert Dust in the Global System*. Springer
 2169 International Publishing.

2170 Griffin, D.W., 2007. Atmospheric movement of microorganisms in clouds of desert
 2171 dust and implications for human health. *Clin. Microbiol. Rev.* 20, 459–477.
 2172 <https://doi.org/10.1128/CMR.00039-06>

2173 Grousset, F.E., Ginoux, P., Bory, A., Biscaye, P.E., 2003. Case study of a Chinese
 2174 dust plume reaching the French Alps. *Geophys. Res. Lett.* 30, 23–26.

2175 <https://doi.org/10.1029/2002GL016833>

2176 Hartley, A.J., Chong, G., 2002. Late Pliocene age for the Atacama Desert:
2177 Implications for the desertification of western South America. *Geology* 30, 43–
2178 46. [https://doi.org/10.1130/0091-7613\(2002\)030<0043:LPAFTA>2.0.CO;2](https://doi.org/10.1130/0091-7613(2002)030<0043:LPAFTA>2.0.CO;2)

2179 Hecht, M.H., Kounaves, S.P., Quinn, R.C., West, S.J., Young, S.M.M., Ming, D.W.,
2180 Catling, D.C., Clark, B.C., Boynton, W. V., Hoffman, J., DeFlores, L.P.,
2181 Gospodinova, K., Kapit, J., Smith, P.H., 2009. Detection of perchlorate and the
2182 soluble chemistry of martian soil at the phoenix lander site. *Science* (80-.). 325,
2183 64–67. <https://doi.org/10.1126/science.1172466>

2184 Herrera, C., Gamboa, C., Custodio, E., Jordan, T., Godfrey, L., Jódar, J., Luque,
2185 J.A., Vargas, J., Sáez, A., 2018. Groundwater origin and recharge in the
2186 hyperarid Cordillera de la Costa, Atacama Desert, northern Chile. *Sci. Total*
2187 *Environ.* 624, 114–132. <https://doi.org/10.1016/j.scitotenv.2017.12.134>

2188 Hoffmeister, D., 2018. Meteorological and soil measurements of the permanent
2189 weather stations in the Atacama desert, Chile. CRC1211 Database
2190 (CRC1211DB). <https://doi.org/10.5880/CRC1211DB.1>

2191 Houston, J., 2006. The great Atacama flood of 2001 and its implications for Andean
2192 hydrology. *Hydrol. Process.* 20, 591–610. <https://doi.org/5555555555>

2193 Houston, J., 2002. Groundwater recharge through an alluvial fan in the Atacama
2194 Desert, northern Chile: Mechanisms, magnitudes and causes. *Hydrol. Process.*
2195 16, 3019–3035. <https://doi.org/10.1002/hyp.1086>

2196 Houston, J., Hartley, A.J., 2003. The central andean west-slope rainshadow and its
 2197 potential contribution to the origin of hyper-aridity in the Atacama Desert. *Int. J.*
 2198 *Climatol.* 23, 1453–1464. <https://doi.org/10.1002/joc.938>

2199 Howell, M.S., 2009. Mineralogy and micromorphology of an Atacama Desert soil ,
 2200 Chile : A model for hyperarid pedogenesis 190.

2201 Jacques-Coper, M., Falvey, M., Muñoz, R.C., 2015. Inter-daily variability of a strong
 2202 thermally-driven wind system over the Atacama Desert of South America:
 2203 synoptic forcing and short-term predictability using the GFS global model.
 2204 *Theor. Appl. Climatol.* 121, 211–223. [https://doi.org/10.1007/s00704-014-1231-](https://doi.org/10.1007/s00704-014-1231-y)
 2205 *y*

2206 Jemmett-Smith, B.C., Marsham, J.H., Knippertz, P., Gilkeson, C.A., 2015.
 2207 Quantifying global dust devil occurrence from meteorological analyses.
 2208 *Geophys. Res. Lett.* 42, 1275–1282. <https://doi.org/10.1002/2015GL063078>

2209 Jiao, L., Wang, X., Li, D., 2018a. Spatial variation in the flux of atmospheric
 2210 deposition and its ecological effects in arid Asia 32, 71–91.
 2211 <https://doi.org/10.1016/j.aeolia.2018.01.008>

2212 Jiao, L., Wang, X., Li, D., 2018b. Spatial variation in the flux of atmospheric
 2213 deposition and its ecological effects in arid Asia. *Aeolian Res.* 32, 71–91.
 2214 <https://doi.org/10.1016/j.aeolia.2018.01.008>

2215 Jickells, T.D., An, Z.S., Andersen, K.K., Baker, A.R., Bergametti, C., Brooks, N., Cao,
 2216 J.J., Boyd, P.W., Duce, R.A., Hunter, K.A., Kawahata, H., Kubilay, N., LaRoche,

2217 J., Liss, P.S., Mahowald, N., Prospero, J.M., Ridgwell, A.J., Tegen, I., Torres,
 2218 R., 2005. Global iron connections between desert dust, ocean biogeochemistry,
 2219 and climate. *Science* (80-.). 308, 67–71.
 2220 <https://doi.org/10.1126/science.1105959>

2221 Jódar, J., Rubio, F.M., Custodio, E., Martos-Rosillo, S., Pey, J., Herrera, C., Turu,
 2222 V., Pérez-Bielsa, C., Ibarra, P., Lambán, L.J., 2020. Hydrogeochemical, isotopic
 2223 and geophysical characterization of saline lake systems in semiarid regions:
 2224 The Salada de Chiprana Lake, Northeastern Spain. *Sci. Total Environ.* 728.
 2225 <https://doi.org/10.1016/j.scitotenv.2020.138848>

2226 Jones, D.L., Olivera-Ardid, S., Klumpp, E., Knief, C., Hill, P.W., Lehdorff, E., Bol,
 2227 R., 2018. Moisture activation and carbon use efficiency of soil microbial
 2228 communities along an aridity gradient in the Atacama Desert. *Soil Biol.*
 2229 *Biochem.* 117, 68–71. <https://doi.org/10.1016/j.soilbio.2017.10.026>

2230 Jordan, T., Riquelme, R., González, G., Herrera, C., Godfrey, L., Colucci, S.,
 2231 Gironás, J., Gamboa, C., Urrutia, J., Tapia, L., Centella, K., Ramos, H., 2015.
 2232 Hydrological and geomorphological consequences of the extreme precipitation
 2233 event of 24–26 March 2015, Chile. *XIV Congr. Geológico Chil. La Serena, Chile*
 2234 2–5.

2235 Jordan, T.E., Herrera L., C., Godfrey, L. V., Colucci, S.J., Gamboa P., C., Urrutia M.,
 2236 J., González L., G., Paul, J.F., 2019. Isotopic characteristics and paleoclimate
 2237 implications of the extreme precipitation event of march 2015 in Northern Chile.
 2238 *Andean Geol.* 46, 1–31. <https://doi.org/10.5027/andgeov46n1-3087>

2239 Jordan, T.E., Kirk-Lawlor, N.E., Nicolás Blanco, P., Rech, J.A., Cosentino, N.J.,
 2240 2014. Landscape modification in response to repeated onset of hyperarid
 2241 paleoclimate states since 14 Ma, Atacama Desert, Chile. *Bull. Geol. Soc. Am.*
 2242 126, 1016–1046. <https://doi.org/10.1130/B30978.1>

2243 Jordan, T.E., Lohman, R.B., Tapia, L., Pfeiffer, M., Scott, C.P., Amundson, R.,
 2244 Godfrey, L., Riquelme, R., 2020. Surface materials and landforms as controls
 2245 on InSAR permanent and transient responses to precipitation events in a
 2246 hyperarid desert, Chile. *Remote Sens. Environ.* 237.
 2247 <https://doi.org/10.1016/j.rse.2019.111544>

2248 Jungers, M.C., Heimsath, A.M., Amundson, R., Balco, G., Shuster, D., Chong, G.,
 2249 2013. Active erosion-deposition cycles in the hyperarid Atacama Desert of
 2250 Northern Chile. *Earth Planet. Sci. Lett.* 371–372, 125–133.
 2251 <https://doi.org/10.1016/j.epsl.2013.04.005>

2252 Kober, F., Ivy-Ochs, S., Schlunegger, F., Baur, H., Kubik, P.W., Wieler, R., 2007.
 2253 Denudation rates and a topography-driven rainfall threshold in northern Chile:
 2254 Multiple cosmogenic nuclide data and sediment yield budgets. *Geomorphology*
 2255 83, 97–120. <https://doi.org/10.1016/j.geomorph.2006.06.029>

2256 Kober, F., Ivy-Ochs, S., Zeilinger, F., Schlunegger, F., Kubik, P.W., Baur, H., Wieler,
 2257 R., 2009. Complex multiple cosmogenic nuclide concentration and histories in
 2258 the arid Rio Lluta catchment, northern Chile. *Earth Surf. Process. Landforms*
 2259 34, 613–628. <https://doi.org/10.1002/esp.1748>

2260 Kohfeld, K.E., Tegen, I., 2007. Record of Mineral Aerosols and Their Role in the
 2261 Earth System, in: Holland, H.D., Turekian, K.K. (Eds.), Treatise On
 2262 Geochemistry. pp. 1–26.

2263 Kohfeld, K.E., Tegen, I., Editors-in-Chief: Heinrich D. Holland, Karl K. Turekian,
 2264 2007. 4.13 - Record of Mineral Aerosols and Their Role in the Earth System 1–
 2265 26.

2266 Kurgansky, M. V., Montecinos, A., Villagran, V., Metzger, S.M., 2011.
 2267 Micrometeorological Conditions for Dust-Devil Occurrence in the Atacama
 2268 Desert. Boundary-Layer Meteorol. 138, 285–298.
 2269 <https://doi.org/10.1007/s10546-010-9549-1>

2270 Lamb, S., Davis, P., 2003. Cenozoic climate change as a possible cause for the rise
 2271 of the Andes. Nature 425, 792–797. <https://doi.org/10.1038/nature02049>

2272 Latorre, C., Betancourt, J.L., Rech, J.A., Quade, J., Holmgren, C., Placzek, C.,
 2273 Maldonado, A.J.C., Vuille, M., Rylander, K., 2005. Late Quaternary history of
 2274 the Atacama Desert, in: Smith, M., Hesse, P. (Eds.), 23°S Archaeology and
 2275 Environmental History of the Southern Deserts. National Museum of Australia
 2276 Press, Canberra, pp. 73–90.

2277 Latorre, C., Betancourt, J.L., Rylander, K.A., Quade, J., 2002. Vegetation invasions
 2278 into absolute desert: A 45 000 yr rodent midden record from the Calama-Salar
 2279 de Atacama basins, northern Chile (lat 22°-24°S). Bull. Geol. Soc. Am. 114,
 2280 349–366. <https://doi.org/10.1130/0016->

2281 7606(2002)114<0349:VIIADA>2.0.CO;2

2282 Latorre, C., González, A.L., Quade, J., Fariña, J.M., Pinto, R., Marquet, P.A., 2011.

2283 Establishment and formation of fog-dependent *Tillandsia landbeckii* dunes in

2284 the Atacama Desert: Evidence from radiocarbon and stable isotopes. *J.*

2285 *Geophys. Res. Biogeosciences* 116, 1–12.

2286 <https://doi.org/10.1029/2010JG001521>

2287 Li, J., Wang, F., Michalski, G., Wilkins, B., 2019. Atmospheric deposition across the

2288 Atacama Desert, Chile: Compositions, source distributions, and interannual

2289 comparisons. *Chem. Geol.* 525, 435–446.

2290 <https://doi.org/10.1016/j.chemgeo.2019.07.037>

2291 Mahowald, N., Albani, S., Kok, J.F., Engelstaeder, S., Scanza, R., Ward, D.S.,

2292 Flanner, M.G., 2014. The size distribution of desert dust aerosols and its impact

2293 on the Earth system. *Aeolian Res.* 15, 53–71.

2294 <https://doi.org/10.1016/j.aeolia.2013.09.002>

2295 Maldonado, A., Betancourt, J.L., Latorre, C., Villagran, C., 2005. Pollen analyses

2296 from a 50 000-yr rodent midden series in the southern Atacama Desert (25° 30'

2297 S). *J. Quat. Sci.* 20, 493–507. <https://doi.org/10.1002/jqs.936>

2298 Marticorena, B., Bergametti, G., 1995. Modeling the atmospheric dust cycle: 1.

2299 Design of a soil-derived dust emission scheme. *J. Geophys. Res.* 100.

2300 <https://doi.org/10.1029/95jd00690>

2301 Marx, S.K., Kamber, B.S., McGowan, H.A., Petherick, L.M., McTainsh, G.H.,

2302 Stromsoe, N., Hooper, J.N., May, J.H., 2018. Palaeo-dust records: A window to
 2303 understanding past environments. *Glob. Planet. Change* 165, 13–43.
 2304 <https://doi.org/10.1016/j.gloplacha.2018.03.001>

2305 Mather, A.E., Hartley, A.J., Griffiths, J.S., 2014. The giant coastal landslides of
 2306 Northern Chile: Tectonic and climate interactions on a classic convergent plate
 2307 margin. *Earth Planet. Sci. Lett.* 388, 249–256.
 2308 <https://doi.org/10.1016/j.epsl.2013.10.019>

2309 Matmon, A., Quade, J., Placzek, C., Fink, D., Copeland, A., Neilson, J.W., 2015.
 2310 Seismic origin of the Atacama Desert boulder fields. *Geomorphology* 231, 28–
 2311 39. <https://doi.org/10.1016/j.geomorph.2014.11.008>

2312 May, M., Hoffmeister, D., 2018. Hourly time-lapse images at weather station 13 -
 2313 Cerros de Calate, Chile from October 2017 to February 2018. CRC1211
 2314 Database (CRC1211DB). [WWW Document].

2315 May, S.M., Hoffmeister, D., Wolf, D., Bubenzer, O., 2019. Zebra stripes in the
 2316 Atacama Desert revisited – Granular fingering as a mechanism for zebra stripe
 2317 formation? *Geomorphology* 344, 46–59.
 2318 <https://doi.org/10.1016/j.geomorph.2019.07.014>

2319 May, S.M., Meine, L., Hoffmeister, D., Brill, D., Medialdea, A., Wennrich, V., Gröbner,
 2320 M., Schulte, P., Steininger, F., Deprez, M., de Kock, T., Bubenzer, O., 2020.
 2321 Origin and timing of past hillslope activity in the hyper-arid core of the Atacama
 2322 Desert – The formation of fine sediment lobes along the Chuculay Fault System,

2323 Northern Chile. Glob. Planet. Change 184, 103057.
 2324 <https://doi.org/10.1016/j.gloplacha.2019.103057>

2325 McFadden, L.; Wells, S.; Jercinovich, M., 1987. Influences of eolian and pedogenic
 2326 processes on the origin and evolution of desert pavements.pdf.pdf. Geology 15,
 2327 504–508. <https://doi.org/10.1039/b110143a>

2328 McKay, C.P., Friedmann, E.I., Gómez-Silva, B., Cáceres-Villanueva, L., Andersen,
 2329 D.T., Landheim, R., 2003a. Temperature and Moisture Conditions for Life in the
 2330 Extreme Arid Region of the Atacama Desert: Four Years of Observations
 2331 Including the El Niño of 1997–1998. Astrobiology 3, 393–406.
 2332 <https://doi.org/10.1089/153110703769016460>

2333 McKay, C.P., Friedmann, E.I., Gomez-Silva, B., Caceres-Villanueva, L., Andersen,
 2334 D.T., Landheim, R., Gomez-Silva, B., Coceres-Villanueva, L., Andersen, D.T.,
 2335 Landheim, R., 2003b. Temperature and Moisture Conditions for Life in the
 2336 Extreme Arid Region of the Atacama Desert: Four Years of Observations
 2337 Including the El Nino of 1997-1998. Astrobiology 3, 393–406.
 2338 <https://doi.org/doi:10.1089/153110703769016460>

2339 McMurry, P.H., 2000. A review of atmospheric aerosol measurements. Atmos.
 2340 Environ. 34, 1959–1999. [https://doi.org/10.1016/S1352-2310\(99\)00455-0](https://doi.org/10.1016/S1352-2310(99)00455-0)

2341 Medialdea, A., May, S.M., Brill, D., King, G., Ritter, B., Wennrich, V., Bartz, M.,
 2342 Zander, A., Kuiper, K., Hurtado, S., Hoffmeister, D., Schulte, P., Gröbner, M.,
 2343 Opitz, S., Brückner, H., Bubenzer, O., 2020. Identification of humid periods in

2344 the Atacama Desert through hillslope activity established by infrared stimulated
 2345 luminescence (IRSL) dating. Glob. Planet. Change 185, 103086.
 2346 <https://doi.org/10.1016/j.gloplacha.2019.103086>

2347 Metzer, S., Kurgansky, M., Montecinos, A., Villagran, V., Verdejo, H., 2010.
 2348 Chasing Dust Devils in Chile's Atacama Desert, in: 41st Lunar and Planetary
 2349 Science Conference. Texas, USA.

2350 Michalski, G., Böhlke, J.K., Thiemens, M., 2004a. Long term atmospheric deposition
 2351 as the source of nitrate and other salts in the Atacama Desert, Chile: New
 2352 evidence from mass-independent oxygen isotopic compositions. Geochim.
 2353 Cosmochim. Acta 68, 4023–4038. <https://doi.org/10.1016/j.gca.2004.04.009>

2354 Michalski, G., Böhlke, J.K., Thiemens, M., 2004b. Long term atmospheric deposition
 2355 as the source of nitrate and other salts in the Atacama Desert, Chile: New
 2356 evidence from mass-independent oxygen isotopic compositions. Geochim.
 2357 Cosmochim. Acta 68, 4023–4038. <https://doi.org/10.1016/j.gca.2004.04.009>

2358 Mintz, Y., Walker, G.K., 1993. Global fields of soil moisture and land surface
 2359 evapotranspiration derived from observed precipitation and surface air
 2360 temperature. J. Appl. Meteorol. [https://doi.org/10.1175/1520-0450\(1993\)032<1305:GFOSMA>2.0.CO;2](https://doi.org/10.1175/1520-0450(1993)032<1305:GFOSMA>2.0.CO;2)
 2361

2362 Moore, R.M., Blough, N. V., 2002. A marine source of methyl nitrate. Geophys. Res.
 2363 Lett. 29, 27-1-27–4. <https://doi.org/10.1029/2002gl014989>

2364 Moran, B.J., Boutt, D.F., Munk, L.A., 2019. Stable and Radioisotope Systematics

2365 Reveal Fossil Water as Fundamental Characteristic of Arid Orogenic-Scale
 2366 Groundwater Systems. *Water Resour. Res.* 55, 11295–11315.
 2367 <https://doi.org/10.1029/2019WR026386>

2368 Moreira-Muñoz, A., 2011. Plant Geography of Chile, *Revista Mexicana de*
 2369 Biodiversidad. <https://doi.org/10.22201/ib.20078706e.2013.1.875>

2370 Morgan, A.M., Howard, A.D., Hobley, D.E.J., Moore, J.M., Dietrich, W.E., Williams,
 2371 R.M.E., Burr, D.M., Grant, J.A., Wilson, S.A., Matsubara, Y., 2014.
 2372 Sedimentology and climatic environment of alluvial fans in the martian Saheki
 2373 crater and a comparison with terrestrial fans in the Atacama Desert. *Icarus* 229,
 2374 131–156. <https://doi.org/10.1016/j.icarus.2013.11.007>

2375 Mostacero, L.J., Coico, F.M., Peláez, F.P., 1996. *Fitogeografía del Norte de Peru.*
 2376 CONYCET.

2377 Mueller, G., 1968. Genetic Histories of Nitrate Deposits from Antarctica and Chole.
 2378 *Nature* 219, 1131–1134.

2379 Muñoz, R.C., Falvey, M.J., Arancibia, M., Astudillo, V.I., Elgueta, J., Ibarra, M.,
 2380 Santana, C., Vásquez, C., 2018. Wind Energy Exploration over the Atacama
 2381 Desert: A Numerical Model–Guided Observational Program. *Bull. Am. Meteorol.*
 2382 *Soc.* 99, 2079–2092. <https://doi.org/10.1175/bams-d-17-0019.1>

2383 Muñoz, R.C., Falvey, M.J., Araya, M., Jacques-Coper, M., 2013. Strong down-valley
 2384 low-level jets over the atacama desert: Observational characterization. *J. Appl.*
 2385 *Meteorol. Climatol.* 52, 2735–2752. <https://doi.org/10.1175/JAMC-D-13-063.1>

2386 Navarro-González, R., Molina, P., De La Rosa, J., Rainey, F.A., Bagaley, D.R.,
 2387 Hollen, B.J., Small, A.M., Quinn, R.C., McKay, C.P., Grunthaner, F.J., Cáceres,
 2388 L., Gomez-Silva, B., 2003. Mars-Like Soils in the Atacama Desert, Chile, and
 2389 the Dry Limit of Microbial Life. *Science* (80-.). 302, 1018–1021.
 2390 <https://doi.org/10.1126/science.1089143>

2391 Nester, P.L., Gayó, E., Latorre, C., Jordan, T.E., Blanco, N., 2007. Perennial stream
 2392 discharge in the hyperarid Atacama Desert of northern Chile during the latest
 2393 Pleistocene Nester, P.L., Gayó, E., Latorre, C., Jordan, T.E., Blanco, N., 2007.
 2394 Perennial stream discharge in the hyperarid Atacama Desert of northern Chile
 2395 dur. *Proc. Natl. Acad. Sci. U. S. A.* 104, 19724–19729.
 2396 <https://doi.org/10.1073/pnas.0705373104>

2397 Nishiizumi, K., Caffee, M.W., Finkel, R.C., Brimhall, G., Mote, T., 2005. Remnants
 2398 of a fossil alluvial fan landscape of Miocene age in the Atacama Desert of
 2399 northern Chile using cosmogenic nuclide exposure age dating. *Earth Planet.*
 2400 *Sci. Lett.* 237, 499–507. <https://doi.org/10.1016/j.epsl.2005.05.032>

2401 Ortlieb, L., 1995. Eventos El Niño y episodios lluviosos en el desierto de Atacama:
 2402 el registro de los últimos dos siglos. *Bull. - Inst. Fr. d'Etudes Andin.* 24, 519–
 2403 537.

2404 Osses, P., Cereceda, P., Schemenauer, R., 1998. Diferencias y similitudes de la
 2405 niebla entre Iquique (Chile) y Mejía (Perú). *Rev. Geogr. Norte Gd.* 7–13.

2406 Osses, P., Escobar, R., del Río, C., García, R., Vargas, C., 2017. El clima desértico

2407 costero con nublados abundantes del desierto de atacama y su relación con los
 2408 recursos naturales energía solar y agua de niebla. Caso de estudio alto patache
 2409 (20,5°S), región de tarapacá, Chile. Rev. Geogr. Norte Gd. 48, 33–48.
 2410 <https://doi.org/10.4067/S0718-34022017000300033>

2411 Owen, J.J., Amundson, R., Dietrich, W.E., Nishiizumi, K., Sutter, B., Chong, G.,
 2412 2011. The sensitivity of hillslope bedrock erosion to precipitation. Earth Surf.
 2413 Process. Landforms 36, 117–135. <https://doi.org/10.1002/esp.2083>

2414 Owen, J.J., Dietrich, W.E., Nishiizumi, K., Chong, G., Amundson, R., 2013. Zebra
 2415 stripes in the Atacama Desert: Fossil evidence of overland flow. Geomorphology
 2416 182, 157–172. <https://doi.org/10.1016/j.geomorph.2012.11.006>

2417 Oyarzun, J., Oyarzun, R., 2007. Massive volcanism in the Altiplano-Puna volcanic
 2418 plateau and formation of the huge atacama desert nitrate deposits: A case for
 2419 thermal and electric fixation of atmospheric nitrogen. Int. Geol. Rev. 49, 962–
 2420 968. <https://doi.org/10.2747/0020-6814.49.10.962>

2421 Parro, V., Sánchez-Román, M., Blanco, Y., Gómez-Elvira, J., Moreno-Paz, M.,
 2422 Gómez, M.J., de Diego-Castilla, G., Rivas, L.A., Postigo, M., Gómez, F., García-
 2423 Villadangos, M., Chong-Díaz, G., Urtuvia, V.N., Fernández-Remolar, D., Cruz-
 2424 Gil, P., Echeverría, A., Rodríguez-Manfredi, J.A., Ruiz-Bermejo, M.,
 2425 Demergasso, C., 2011. A Microbial Oasis in the Hypersaline Atacama
 2426 Subsurface Discovered by a Life Detector Chip: Implications for the Search for
 2427 Life on Mars. Astrobiology 11, 969–996. <https://doi.org/10.1089/ast.2011.0654>

2428 Pfeiffer, M., Latorre, C., Gayo, E., Amundson, R., 2019. Rare calcium chloride-rich
 2429 soil and implications for the existence of liquid water in a hyperarid environment.
 2430 *Geology* 47, 163–166. <https://doi.org/10.1130/G45642.1>

2431 Pfeiffer, M., Latorre, C., Santoro, C.M., Gayo, E.M., Rojas, R., Carrevedo, M.L.,
 2432 McRostie, V.B., Finstad, K.M., Heimsath, A., Jungers, M.C., De Pol-Holz, R.,
 2433 Amundson, R., 2018. Chronology, stratigraphy and hydrological modelling of
 2434 extensive wetlands and paleolakes in the hyperarid core of the Atacama Desert
 2435 during the late quaternary. *Quat. Sci. Rev.* 197, 224–245.
 2436 <https://doi.org/10.1016/j.quascirev.2018.08.001>

2437 Pfeiffer, M., Morgan, A., Heimsath, A., Jordan, T., Howard, A., Amundson, R., 2021.
 2438 Century scale rainfall in the absolute Atacama Desert: Landscape response and
 2439 implications for past and future rainfall. *Quat. Sci. Rev.* 254, 106797.
 2440 <https://doi.org/10.1016/j.quascirev.2021.106797>

2441 Placzek, C., Granger, D.E., Matmon, A., Quade, J., Ryb, U., 2014. Geomorphic
 2442 process rates in the central atacama desert, Chile: Insights from cosmogenic
 2443 nuclides and implications for the onset of hyperaridity. *Am. J. Sci.* 314, 1462–
 2444 1512. <https://doi.org/10.2475/10.2014.03>

2445 Placzek, C.J., Matmon, A., Granger, D.E., Quade, J., Niedermann, S., 2010.
 2446 Evidence for active landscape evolution in the hyperarid Atacama from multiple
 2447 terrestrial cosmogenic nuclides. *Earth Planet. Sci. Lett.* 295, 12–20.
 2448 <https://doi.org/10.1016/j.epsl.2010.03.006>

2449 Pöschl, U., 2005. Atmospheric Aerosols: Composition, Transformation, Climate and
 2450 Health Effects. Atmos. Chem. 7520–7540.
 2451 <https://doi.org/10.1002/anie.200501122>

2452 Prospero, J.M., Bonatti, E., 1969. Continental Dust in the Atmosphere of the Eastern
 2453 Equatorial Pacific. J Geophys Res 74, 3362–3371.
 2454 <https://doi.org/10.1029/jc074i013p03362>

2455 Pueyo, J.J., Chong, G., Vega, M., 1998. Mineralogy and parental brine evolution in
 2456 the Pedro de Valdivia nitrate deposit, Antofagasta, Chile. Andean Geol.

2457 Pye, K., 1987. Dust Entrainment, Transport and Deposition, First. ed, Aeolian Dust
 2458 and Dust Deposits. Harcourt Brace Jovanovich, London.
 2459 <https://doi.org/10.1016/b978-0-12-568690-7.50007-7>

2460 Quade, J., Rech, J.A., Betancourt, J.L., Latorre, C., Quade, B., Rylander, K.A.,
 2461 Fisher, T., 2008. Paleowetlands and regional climate change in the central
 2462 Atacama Desert, northern Chile. Quat. Res. 69, 343–360.
 2463 <https://doi.org/10.1016/j.yqres.2008.01.003>

2464 Quade, J., Reiners, P., Placzek, C., Matmon, A., Pepper, M., Ojha, L., Murray, K.,
 2465 2012. Seismicity and the strange rubbing boulders of the Atacama desert,
 2466 Northern Chile. Geology 40, 851–854. <https://doi.org/10.1130/G33162.1>

2467 Quezada, J., Cerda, J., 2003. Incisiones transversales profundas en la Cordillera de
 2468 la Costa del Norte Grande de Chile : ¿Erosión de un alto topográfico al oeste
 2469 del gran acantilado costero ?, in: 10° Congreso Geológico Chileno.

2470 Quijano, J., 2013. Estudio numerico y observacional de la dinámica de viento
 2471 Paracas, asociado al transporte eólico hacia el océano frente a la costa de Ica-
 2472 Perú. Univ. Peru. Cayetano Hered. Universidad Peruana Cayetano Heredia.

2473 Quinn, R.C., Zent, A.P., Grunthaner, F.J., Ehrenfreund, P., Taylor, C.L., Garry,
 2474 J.R.C., 2005. Detection and characterization of oxidizing acids in the Atacama
 2475 Desert using the Mars Oxidation Instrument. Planet. Space Sci. 53, 1376–1388.
 2476 <https://doi.org/10.1016/j.pss.2005.07.004>

2477 Rech, J.A., Currie, B.S., Jordan, T.E., Riquelme, R., Lehmann, S.B., Kirk-Lawlor,
 2478 N.E., Li, S., Gooley, J.T., 2019. Massive middle Miocene gypsic paleosols in the
 2479 Atacama Desert and the formation of the Central Andean rain-shadow. Earth
 2480 Planet. Sci. Lett. 506, 184–194. <https://doi.org/10.1016/j.epsl.2018.10.040>

2481 Rech, J.A., Quade, J., Betancourt, J.L., 2002. Late Quaternary paleohydrology of
 2482 the central Atacama Desert (lat 22°-24°S), Chile. Bull. Geol. Soc. Am. 114, 334–
 2483 348. [https://doi.org/10.1130/0016-7606\(2002\)114<0334:LQPOTC>2.0.CO;2](https://doi.org/10.1130/0016-7606(2002)114<0334:LQPOTC>2.0.CO;2)

2484 Rech, J.A., Quade, J., Hart, W.S., 2003. Isotopic evidence for the source of Ca and
 2485 S in soil gypsum, anhydrite and calcite in the Atacama Desert, Chile. Geochim.
 2486 Cosmochim. Acta 67, 575–586. [https://doi.org/10.1016/S0016-7037\(02\)01175-](https://doi.org/10.1016/S0016-7037(02)01175-4)
 2487 4

2488 Reich, M., Bao, H., 2018. Nitrate deposits of the atacama desert: A marker of long-
 2489 term hyperaridity. Elements 14, 251–256.
 2490 <https://doi.org/10.2138/gselements.14.4.251>

2491 Reyers, M., Hamidi, M., Shao, Y., 2019. Synoptic analysis and simulation of an
 2492 unusual dust event over the Atacama Desert. *Atmos. Sci. Lett.* 20, 1–9.
 2493 <https://doi.org/10.1002/asl.899>

2494 Reyers, M., Shao, Y., 2019. Cutoff lows off the coast of the Atacama Desert under
 2495 present day conditions and in the Last Glacial Maximum. *Glob. Planet. Change*
 2496 181, 102983. <https://doi.org/10.1016/j.gloplacha.2019.102983>

2497 Riquelme, R., Hérail, G., Martinod, J., Charrier, R., Darrozes, J., 2007. Late
 2498 Cenozoic geomorphologic signal of Andean forearc deformation and tilting
 2499 associated with the uplift and climate changes of the Southern Atacama Desert
 2500 (26°S-28°S). *Geomorphology* 86, 283–306.
 2501 <https://doi.org/10.1016/j.geomorph.2006.09.004>

2502 Ritter, B., Stuart, F.M., Binnie, S.A., Gerdes, A., Wennrich, V., Dunai, T.J., 2018.
 2503 Neogene fluvial landscape evolution in the hyperarid core of the Atacama
 2504 Desert. *Sci. Rep.* 8, 1–16. <https://doi.org/10.1038/s41598-018-32339-9>

2505 Ritter, B., Wennrich, V., Medialdea, A., Brill, D., King, G., Schneiderwind, S.,
 2506 Niemann, K., Fernández-Galego, E., Diederich, J., Rolf, C., Bao, R., Melles, M.,
 2507 Dunai, T.J., 2019. “Climatic fluctuations in the hyperarid core of the Atacama
 2508 Desert during the past 215 ka.” *Sci. Rep.* 9. [https://doi.org/10.1038/s41598-019-](https://doi.org/10.1038/s41598-019-41743-8)
 2509 41743-8

2510 Robinson, C.K., Wierzchos, J., Black, C., Crits-Christoph, A., Ma, B., Ravel, J.,
 2511 Ascaso, C., Artieda, O., Valea, S., Roldán, M., Gómez-Silva, B., Diruggiero, J.,

2512 2015. Microbial diversity and the presence of algae in halite endolithic
2513 communities are correlated to atmospheric moisture in the hyper-arid zone of
2514 the Atacama Desert. *Environ. Microbiol.* 17, 299–315.
2515 <https://doi.org/10.1111/1462-2920.12364>

2516 Ruddiman, W.F., 2013. The anthropocene. *Annu. Rev. Earth Planet. Sci.* 41, 45–68.
2517 <https://doi.org/10.1146/annurev-earth-050212-123944>

2518 Rundel, P.W., Dillon, M.O., Palma, B., Mooney, H.A., Gulmon, S.L., 1991. The
2519 Phytogeography and Ecology of the Coastal Atacama and Peruvian Deserts. *J.*
2520 *Syst. Evol. Bot.* 13.

2521 Rundel, P.W., Mahu, M., 1976. Community Structure and Diversity in a Coastal Fog
2522 Desert in Northern Chile. *Flora* 165, 493–505. [https://doi.org/10.1016/s0367-](https://doi.org/10.1016/s0367-2530(17)31888-1)
2523 [2530\(17\)31888-1](https://doi.org/10.1016/s0367-2530(17)31888-1)

2524 Rutllant, J.A., Muñoz, R.C., Garreaud, R.D., 2013. Meteorological observations on
2525 the northern Chilean coast during VOCALS-REx. *Atmos. Chem. Phys.* 13,
2526 3409–3422. <https://doi.org/10.5194/acp-13-3409-2013>

2527 Sáez, A., Godfrey, L. V., Herrera, C., Chong, G., Pueyo, J.J., 2016. Timing of wet
2528 episodes in Atacama Desert over the last 15 ka. The Groundwater Discharge
2529 Deposits (GWD) from Domeyko Range at 25°S.
2530 <https://doi.org/10.1163/000579510X528224>

2531 Sager, C., Airo, A., Arens, F.L., Rabethge, C., Schulze-Makuch, D., 2020. New types
2532 of boulder accumulations in the hyper-arid Atacama Desert. *Geomorphology*

2533 350. <https://doi.org/10.1016/j.geomorph.2019.106897>

2534 Saukel, C., Lamy, F., Stuut, J.B.W., Tiedemann, R., Vogt, C., 2011. Distribution and
 2535 provenance of wind-blown SE Pacific surface sediments. *Mar. Geol.* 280, 130–
 2536 142. <https://doi.org/10.1016/j.margeo.2010.12.006>

2537 Schemenauer, R.S., Cereceda, P., 1992. The quality of fog water collected for
 2538 domestic and agricultural use in Chile. *J. Appl. Meteorol.* 31, 275–290.
 2539 [https://doi.org/10.1175/1520-0450\(1992\)031<0275:TQOFWC>2.0.CO;2](https://doi.org/10.1175/1520-0450(1992)031<0275:TQOFWC>2.0.CO;2)

2540 Schulz, M., Prospero, J.M., Baker, A.R., Dentener, F., Ickes, L., Liss, P.S.,
 2541 Mahowald, N.M., Nickovic, S., García-Pando, C.P., Rodríguez, S., Sarin, M.,
 2542 Tegen, I., Duce, R.A., 2012. Atmospheric transport and deposition of mineral
 2543 dust to the ocean: Implications for research needs. *Environ. Sci. Technol.* 46,
 2544 10390–10404. <https://doi.org/10.1021/es300073u>

2545 Schulze-Makuch, D., Wagner, D., Kounaves, S.P., Mangelsdorf, K., Devine, K.G.,
 2546 de Vera, J.-P., Schmitt-Kopplin, P., Grossart, H.-P., Parro, V., Kaupenjohann,
 2547 M., Galy, A., Schneider, B., Airo, A., Frösler, J., Davila, A.F., Arens, F.L.,
 2548 Cáceres, L., Cornejo, F.S., Carrizo, D., Dartnell, L., DiRuggiero, J., Flury, M.,
 2549 Ganzert, L., Gessner, M.O., Grathwohl, P., Guan, L., Heinz, J., Hess, M.,
 2550 Keppler, F., Maus, D., McKay, C.P., Meckenstock, R.U., Montgomery, W.,
 2551 Oberlin, E.A., Probst, A.J., Sáenz, J.S., Sattler, T., Schirmack, J., Sephton,
 2552 M.A., Schlöter, M., Uhl, J., Valenzuela, B., Vestergaard, G., Wörmer, L.,
 2553 Zamorano, P., 2018. Transitory microbial habitat in the hyperarid Atacama
 2554 Desert. *Proc. Natl. Acad. Sci.* 115, 2670–2675.

2555 <https://doi.org/10.1073/pnas.1714341115>

2556 Schween, J.H., Hoffmeister, D., Löhnert, U., 2020. Filling the observational gap in
2557 the Atacama Desert with a new network of climate stations. *Glob. Planet.*
2558 *Change* 184, 103034. <https://doi.org/10.1016/j.gloplacha.2019.103034>

2559 Scott, C.P., Lohman, R.B., Jordan, T.E., 2017. InSAR constraints on soil moisture
2560 evolution after the March 2015 extreme precipitation event in Chile. *Sci. Rep.* 7,
2561 1–9. <https://doi.org/10.1038/s41598-017-05123-4>

2562 Sepúlveda, S.A., Rebolledo, S., McPhee, J., Lara, M., Cartes, M., Rubio, E., Silva,
2563 D., Correia, N., Vásquez, J.P., 2014. Catastrophic, rainfall-induced debris flows
2564 in Andean villages of Tarapacá, Atacama Desert, northern Chile. *Landslides* 11,
2565 481–491. <https://doi.org/10.1007/s10346-014-0480-2>

2566 Shao, Y., Wyrwoll, K.H., Chappell, A., Huang, J., Lin, Z., McTainsh, G.H., Mikami,
2567 M., Tanaka, T.Y., Wang, X., Yoon, S., 2011. Dust cycle: An emerging core
2568 theme in Earth system science. *Aeolian Res.* 2, 181–204.
2569 <https://doi.org/10.1016/j.aeolia.2011.02.001>

2570 Shen, J., Shirey, T.B., Wyness, A.J., Claire, M.W., Zerkle, A.L., 2020. Spatial and
2571 temporal variability of microbial communities and salt distributions across an
2572 aridity gradient before and after heavy rains in the Atacama Desert.
2573 <https://doi.org/10.20944/preprints202002.0433.v1>

2574 Sinclair, K.E., MacDonell, S., 2016. Seasonal evolution of penitente glaciochemistry
2575 at Tapado Glacier, Northern Chile. *Hydrol. Process.* 30, 176–186.

2576 <https://doi.org/10.1002/hyp.10531>

2577 Squeo, F.A., Warner, B.G., Aravena, R., Espinoza, D., 2006. Bofedales: High
2578 altitude peatlands of the central Andes. *Rev. Chil. Hist. Nat.* 79, 245–255.
2579 <https://doi.org/10.4067/S0716-078X2006000200010>

2580 Stern, J.C., Sutter, B., Jackson, W.A., Navarro-González, R., McKay, C.P., Ming,
2581 D.W., Archer, P.D., Mahaffy, P.R., 2017. The nitrate/(per)chlorate relationship
2582 on Mars. *Geophys. Res. Lett.* 44, 2643–2651.
2583 <https://doi.org/10.1002/2016GL072199>

2584 Sträter, E., Westbeld, A., Klemm, O., 2010. Pollution in coastal fog at Alto Patache,
2585 Northern Chile. *Environ. Sci. Pollut. Res.* 17, 1563–1573.
2586 <https://doi.org/10.1007/s11356-010-0343-x>

2587 Stuut, J.B.W., Lamy, F., 2004. Climate variability at the southern boundaries of the
2588 Namib (southwestern Africa) and Atacama (northern Chile) coastal deserts
2589 during the last 120,000 yr. *Quat. Res.* 62, 301–309.
2590 <https://doi.org/10.1016/j.yqres.2004.08.001>

2591 Tapia, J., González, R., Townley, B., Oliveros, V., Álvarez, F., Aguilar, G., Menzies,
2592 A., Calderón, M., 2018. Geology and geochemistry of the Atacama Desert.
2593 *Antonie van Leeuwenhoek, Int. J. Gen. Mol. Microbiol.* 111, 1273–1291.
2594 <https://doi.org/10.1007/s10482-018-1024-x>

2595 Tully, C.D., Rech, J.A., Workman, T.R., Santoro, C.M., Capriles, J.M., Gayo, E.M.,
2596 Latorre, C., 2019. In-stream wetland deposits, megadroughts, and cultural

2597 change in the northern Atacama Desert, Chile. *Quat. Res. (United States)* 91,
 2598 63–80. <https://doi.org/10.1017/qua.2018.122>

2599 UNEP, 2011. *Global Drylands : a UN system-wide responde.*

2600 Urrutia, J., Herrera, C., Custodio, E., Jódar, J., Medina, A., 2019. Groundwater
 2601 recharge and hydrodynamics of complex volcanic aquifers with a shallow saline
 2602 lake: Laguna Tuyajto, Andean Cordillera of northern Chile. *Sci. Total Environ.*
 2603 697, 134116. <https://doi.org/10.1016/j.scitotenv.2019.134116>

2604 Valdivia-Silva, J.E., Navarro-González, R., Fletcher, L., Perez-Montaña, S., Condori-
 2605 Apaza, R., McKay, C.P., 2012. Soil carbon distribution and site characteristics
 2606 in hyper-arid soils of the Atacama Desert: A site with Mars-like soils. *Adv. Sp.*
 2607 *Res.* 50, 108–122. <https://doi.org/10.1016/j.asr.2012.03.003>

2608 Valdivieso, S., Vázquez-Suñé, E., Custodio, E., 2020. Origin and variability of
 2609 oxygen and hydrogen isotopic composition of precipitation in the Central Andes:
 2610 A review. *J. Hydrol.* 587, 124899. <https://doi.org/10.1016/j.jhydrol.2020.124899>

2611 Vargas, G., 1995. Late holocene alluvial sedimentation in the Antofagasta coastal
 2612 area, Chile L, 115–117.

2613 Vargas, G., Rutllant, J., Ortlieb, L., 2006. ENSO tropical-extratropical climate
 2614 teleconnections and mechanisms for Holocene debris flows along the hyperarid
 2615 coast of western South America (17°-24°S). *Earth Planet. Sci. Lett.* 249, 467–
 2616 483. <https://doi.org/10.1016/j.epsl.2006.07.022>

2617 Vázquez, P., Sepúlveda, F.A., Quezada, A. A., Guilef, S., Franco, C., N, B., 2018.
 2618 Cartas Guanillos del Norte y Salar de Llamara, Regiones de Tarapacá y
 2619 Antofagasta.

2620 Voigt, C., Klipsch, S., Herwartz, D., Chong, G., Staubwasser, M., 2020. The spatial
 2621 distribution of soluble salts in the surface soil of the Atacama Desert and their
 2622 relationship to hyperaridity. Glob. Planet. Change 184.
 2623 <https://doi.org/10.1016/j.gloplacha.2019.103077>

2624 Wang, F., 2013. The Mechanism and Timescales of Soil Formation in the Hyper-arid
 2625 Atacama Desert , Chile.

2626 Wang, F., Michalski, G., Luo, H., Caffee, M., 2017. Role of biological soil crusts in
 2627 affecting soil evolution and salt geochemistry in hyper-arid Atacama Desert,
 2628 Chile. Geoderma 307, 54–64. <https://doi.org/10.1016/j.geoderma.2017.07.035>

2629 Wang, F., Michalski, G., Seo, J. hye, Ge, W., 2014. Geochemical, isotopic, and
 2630 mineralogical constraints on atmospheric deposition in the hyper-arid Atacama
 2631 Desert, Chile. Geochim. Cosmochim. Acta 135, 29–48.
 2632 <https://doi.org/10.1016/j.gca.2014.03.017>

2633 Warren-Rhodes, K.A., Lee, K.C., Archer, S.D.J., Cabrol, N., Ng-Boyle, L.,
 2634 Wettergreen, D., Zacny, K., Pointing, S.B., 2019. Subsurface microbial habitats
 2635 in an extreme desert Mars-analog environment. Front. Microbiol. 10.
 2636 <https://doi.org/10.3389/fmicb.2019.00069>

2637 Warren-Rhodes, K.A., Rhodes, K.L., Pointing, S.B., Ewing, S.A., Lacap, D.C.,

2638 Gómez-Silva, B., Amundson, R., Friedmann, E.I., McKay, C.P., 2006. Hypolithic
 2639 cyanobacteria, dry limit of photosynthesis, and microbial ecology in the
 2640 hyperarid Atacama Desert. *Microb. Ecol.* 52, 389–398.
 2641 <https://doi.org/10.1007/s00248-006-9055-7>

2642 Watts, D., Durán, P., Flores, Y., 2017. How does El Niño Southern Oscillation impact
 2643 the wind resource in Chile? A techno-economical assessment of the influence
 2644 of El Niño and La Niña on the wind power. *Renew. Energy* 103, 128–142.
 2645 <https://doi.org/10.1016/j.renene.2016.10.031>

2646 Webb, N.P., Strong, C.L., 2011. Soil erodibility dynamics and its representation for
 2647 wind erosion and dust emission models. *Aeolian Res.* 3, 165–179.
 2648 <https://doi.org/10.1016/j.aeolia.2011.03.002>

2649 Wierzchos, J., Cámara, B., De los ríos, A., Davila, A.F., sánchez almazo, I.M.,
 2650 Artieda, O., Wierzchos, K., Gómez-silva, B., Mckay, C., Ascaso, C., 2011.
 2651 Microbial colonization of Ca-sulfate crusts in the hyperarid core of the Atacama
 2652 Desert: Implications for the search for life on Mars. *Geobiology* 9, 44–60.
 2653 <https://doi.org/10.1111/j.1472-4669.2010.00254.x>

2654 Workman, T.R., Rech, J.A., Gayó, E.M., Santoro, C.M., Ugalde, P.C., De Pol-Holz,
 2655 R., Capriles, J.M., Latorre, C., 2020. Landscape evolution and the
 2656 environmental context of human occupation of the southern pampa del
 2657 tamarugal, Atacama Desert, Chile. *Quat. Sci. Rev.* 243.
 2658 <https://doi.org/10.1016/j.quascirev.2020.106502>

2659 Yu, H., Chin, M., Yuan, T., Bian, H., Remer, L.A., Prospero, J.M., Omar, A., Winker,
2660 D., Yang, Y., Zhang, Y., Zhang, Z., Zhao, C., 2015. The fertilizing role of African
2661 dust in the Amazon rainforest: A first multiyear assessment based on data from
2662 Cloud-Aerosol Lidar and Infrared Pathfinder Satellite Observations. *Geophys.*
2663 *Res. Lett.* 42, 1984–1991. <https://doi.org/10.1002/2015GL063040>

2664 Zhang, X., Sharratt, B., Chen, X., Wang, Z., Liu, L., Guo, Y., Li, J., Chen, H., Yang,
2665 W., 2017. Dust deposition and ambient PM10 concentration in northwest China:
2666 spatial and temporal variability. *Atmos. Chem. Phys.*, 17, 1699–1711.
2667 <https://doi.org/10.5194/acp-17-1699-2017>

2668

2669